PRODUCTION AND ASSESMENT OF COMPACTED GRAPHITE IRON DIESEL ENGINE BLOCKS

A THESIS SUBMITTED TO
THE GRADUATE SCHOOL OF NATURAL AND APPLIED SCIENCES
OF
MIDDLE EAST TECHNICAL UNIVERSITY

BY

ANIL ALKAN

IN PARTIAL FULFILLMENT OF THE REQUIREMENTS
FOR
THE DEGREE OF MASTER OF SCIENCE
IN
METALLURGICAL AND MATERIALS ENGINEERING

OCTOBER 2011

Approval of the thesis:

PRODUCTION AND ASSESMENT OF COMPACTED GRAPHITE IRON DIESEL ENGINE BLOCKS

submitted by **ANIL ALKAN** in partial fulfillment of the requirements for the degree of **Master of Science in Metallurgical and Materials Engineering Department, Middle East Technical University** by,

Prof. Dr. Canan Özgen _____
Dean, Graduate School of **Natural and Applied Sciences**

Prof. Dr. Tayfur Öztürk _____
Head of Department, **Metallurgical and Materials Engineering**

Prof. Dr. Ali Kalkanlı _____
Supervisor, **Metallurgical and Materials Engineering Dept., METU**

Examining Committee Members:

Prof. Dr. Ekrem Selçuk _____
Metallurgical and Materials Engineering Dept., METU

Prof. Dr. Naci Sevinç _____
Metallurgical and Materials Engineering Dept., METU

Prof. Dr. Haluk Atala _____
Metallurgical and Materials Engineering Dept., METU

Prof. Dr Ali Kalkanlı _____
Metallurgical and Materials Engineering Dept., METU

Prof. Dr Engin Kılıç. _____
Mechanical Engineering Dept., METU

Date: 07.10.2011

I hereby declare that all information in this document has been obtained and presented accordance with the academic rules and ethical conduct. I also declare that, as required by these rules and conduct, I have fully cited and referenced all material and results that are not original to this work.

Name, Last name : Anıl ALKAN

Signature :

ABSTRACT

PRODUCTION AND ASSESMENT OF COMPACTED GRAPHITE IRON DIESEL ENGINE BLOCKS

Alkan, Anıl

M.Sc., Department of Metallurgical and Materials Engineering

Supervisor: Prof. Dr. Ali Kalkanlı

October 2011, 150 pages

In Diesel engine blocks properties such as tensile strength, heat conductivity, sound damping, engine vibration and noise are strongly influenced by graphite shape and volume percent in the matrix microstructure. In this study, the engine blocks were produced at ELBA Basınçlı Döküm Odöksan Cast iron foundry in Osmaneli Turkey by performing casting into furan resin sand and preparing cast iron liquid alloy in induction furnace that were treated with Mg by using ladle method. The main purpose of this study is to achive 0 – 25% volume nodularity and remaining is compacted graphite in the produced engine blocks. The shape and volume percent of graphite particles were characterized by an image analyze system.

In the first part of this work, after the diesel engine blocks were produced at ELBA Basınçlı Döküm Odöksan Cast iron foundry in Osmaneli Turkey, the blocks were cut and samples were obtained from 14 different thicknesses of diesel engine blocks. Afterwards, the samples were examined under optical microscope, Soif XJP-6A. The nodularity and compacted graphite values were obtained numerically with the help of Materials Plus image analyzer systems, which is attached to the optical microscope.

In the second part of the study, the diesel engine blocks which are produced at Odöksan were examined by ultrasonic test that was done by using USM 35 flaw detector test machine. Solidification – time and temperature – time simulations were also done by using NovaCast NovaFlow simulation code. Finally mathematical formulas for 13 different thickness of diesel engine blocks were obtained by using excel linest code.

The compacted graphite volume percent observed at different sections of the diesel engine blocks were found to be a function of cooling rate and chemical composition. Best results were obtained when chemical Mg/S ratio was approximately 1 and C.E.V. was between 4.40 – 4.50.

Keywords: Compacted graphite iron, diesel engine block, Mg:S ratio, solidification simulation, ultrasonic test.

ÖZ

KOMPAKT GRAFİTLİ DİZEL MOTOR BLOKLARININ ÜRETİLMESİ VE DEĞERLENDİRİLMESİ

Alkan, Anıl

Yüksek Lisans, Metalurji ve Malzeme Mühendisliği Bölümü

Tez Yöneticisi: Prof. Dr. Ali Kalkanlı

Ekim 2011, 150 sayfa

Micro yapıda ki grafit şekli ve volume oranı dizel motor bloklarında ki çekme dayanımı, ısı iletkenliği, ses titreşimi ve motor vibrasyonu gibi özellikleri güçlü bir şekilde etkiler. Grafit parçacıklarının şekil ve hacim oranı imaj analiz sistemleri ile ölçülür. Bu çalışmada motor blokları furan reçineli kum kalıp ve pota içerisinde Mg alaşımı ile işlemden geçmiş sıvı metal kullanılarak ELBA Basınçlı Döküm Odöksan Osmaneli Türkiye de bulunan Döküm fabrikasında üretildi. Bu çalışmanın ana amacı 0 ile %25 arası küresel grafit ve kalan kısmının kompak grafitlerden oluşmuş motor blokları elde etmektir.

Bu tezin ilk bölümünde dizel motor blokları ELBA Basınçlı Döküm Odöksan Osmaneli Türkiye de bulunan Döküm fabrikasında üretildikten sonra kesildi ve dizel motor bloklarının 14 farklı kalınlığından numuneler alındı. Daha sonra Soif XJP – 6A optik mikroskobu altında numuneler incelendi. Material Plus 4.1 imaj analiz programı yardımıyla küreselik değerleri elde edildi.

Çalışmanın ikinci bölümünde Odöksan da üretilen dizel motor blokları USM 35 tarama dedektörü test makinası kullanılarak yapılan ultrasonik test ile incelendi. Katılaşma – zaman ve sıcaklık – zaman similasyonları NovaCast – Novaflow

similasyon programı kullanılarak yapıldı. Sonuç olarak dizel motor bloklarının 13 farklı kalınlığı için excel linest codu kullanılarak matematiksel formüller geliştirildi.

Motor bloklarını farklı kalınlıklarından alınmış olan numunelerin küresel grafit oranın katılaşma hızına ve kimyasal komposisyona bağlı olduğu anlaşılmıştır. En iyi sonuçlar Mg/S oranın yaklaşık olarak 1 eşit olduğu ve karbon eşiğinin 4.40 – 4.50 arası olduğu durumlardır.

Anahtar kelimeler: kompakt grafitli demir, dizel motor bloğu, Mg/S oranı, katılaşma similasyonu, ultrasonic test.

To my family;
Halit, and Sultan Alkan

ACKNOWLEDGEMENTS

I would like to express my deepest gratitude to my supervisor Prof. Dr. Ali Kalkanlı for his guidance, continuous support and encouragement throughout this study.

My special thanks go to Prof. Dr. Ekrem Selçuk for his helps and supports.

I am also thankful to Ece Alat for her invaluable helps, supports and friendship in all parts of the study.

I would like to thank to the technical staff of the Department of Metallurgical and Materials Engineering, METU, especially Birnur Doyum and Salih Türe for their contributions to this study.

I would also like to thank to Seda Sayılgan and Gökhan TürkYılmaz for their helps and supports.

Thanks are also extended to Sema Bahsi and Seçil Yücel Avkar from Odöksan Osmaneli A.Ş. and Tarel A.Ş. for kindly providing the facility of casting.

Finally, I want to express my great thanks to my family for supporting, encouraging, and loving me all through my life. It would not have been possible to complete this study without their love.

Authors would like to acknowledge the financial support provided by TUBİTAK under the framework of Teydeb Project Number: 3070136

TABLE OF CONTENTS

LIST OF TABLES

TABLES

LIST OF FIGURES

FIGURES

CHAPTER 1

INTRODUCTION

Compacted graphite diesel engine blocks contain an amount of spheroidal graphite iron due to the nature of compacted graphite iron formation. Spheroidal graphite iron engine blocks have lower thermal conductivity, thermal expansion, noise and vibration properties than compacted graphite iron diesel engine bocks although they include higher mechanical properties than compacted graphite iron blocks. Although an increase in a volume fraction of spheroidal graphite iron leads to increase in ultimate tensile strength and elastic modulus to meet engine producers' requirements, diesel engine blocks should contain maximum 25% volume of spheroidal graphite iron and remaining structure must be fully compacted graphite iron. The ratio of 25% volume of compacted graphite / spheroidal graphite iron was determined by means of performance requirement such as torque, noise, peak firing pressure of the diesel engine blocks considered [1].

Even though flake graphite iron diesel engine blocks have higher thermal conductivity, thermal expansion than compacted graphite iron diesel engine blocks, compacted graphite iron diesel engine blocks are preferred due to the fact that flake graphite iron diesel engine blocks do not have enough mechanical strength especially for thin sections of diesel engine blocks. Compacted graphite iron has perfect mechanical properties such as 70% higher UTS and 35% higher elastic modulus compared to gray cast iron including flake patch microstructure with respect to the increase in tensile and elastic modulus, which leads to advanced working performance and diminished weight of the products. Diesel engine blocks that were

designed for compacted graphite iron can be produced with approximately 16% weight reduction with respect to conventional gray cast iron diesel engine blocks [2, 3, 4].

According to the literature published, high quality compacted graphite iron should include approximately 0 – 25% nodularity, and then the remaining is compacted graphite iron in the produced engine blocks. In other words, flake type graphite must not exist in the iron matrix. Due to the fact that presence of flake type graphite in iron matrix leads to a decrease in tensile strength and elastic modulus. This decrease ratio is approximately 30% and 70% of Ultimate Tensile Strength [5, 3, 6].

The aim of the study is to achieve maximum 25% volume of spheroidal graphite iron in thin sections having 7 mm. The remaining matrix structure is fully compacted graphite. During production of diesel engine blocks, step block castings representing cooling rate difference in various thicknesses of diesel engine blocks were placed side by side of diesel engine block casting. However, step block castings having various thicknesses did not have the same volume percentage of compacted graphite iron compare to the same section thickness of the diesel engine blocks produced. To correlate the effect of filling sequence and local undercooling on the percentage of compacted graphite rather than section thickness, flow and solidification simulation in engine block cavity were simulated by Novacast – Novaflow simulation program.

Alloy characteristics such as carbon equivalent (C.E.V.), Mg/S ratio, O(ppm) and temperature were optimized in order to determine compacted graphite/ spheroidal graphite iron ratio. Therefore, Excel linear regression code was used to reveal the effect of alloy and casting parameters such as Carbon equivalent (C.E.V.), Mg/S ratio, O(ppm) and temperature on volume percentage of compacted graphite/ spheroidal graphite iron ratio.

Ultrasonic test is also applied, which is a non-destructive testing method used for obtaining nodularity values without damaging CGI diesel engine blocks.

CHAPTER 2

LITERATURE SURVEY

2.1 Graphite Formation in Cast Iron

Graphite formation has attracted a great deal of attention because it provides wide range of opportunities for material science and engineering. Properties of cast irons are largely affected by means of chemical composition. Especially, two alloying elements that are C and Si also affect graphite formation in cast irons. An increase in carbon concentration leads to promote graphite formation. Carbon can be found in cast iron as a cementite or graphite form that is free form of carbon. If carbon content in the cast iron is above 2.0%, tendency of graphite formation will increase. Since Si content make graphite to be more stable than cementite, Si content in cast iron helps to promote formation of graphite. Figure 2.1 exhibits different type of cast irons that include approximately the same chemical composition, but have different properties [7, 8, 9].

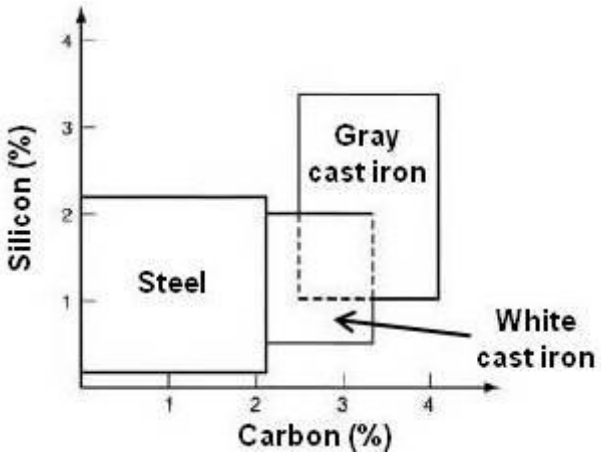

Figure 2.1 Effect of Si and C content on cast irons can be noticed [10]

The best way to show graphite formation in cast iron is that Fe – C binary phase system can easily exhibit stages of graphite formation [11, 12].

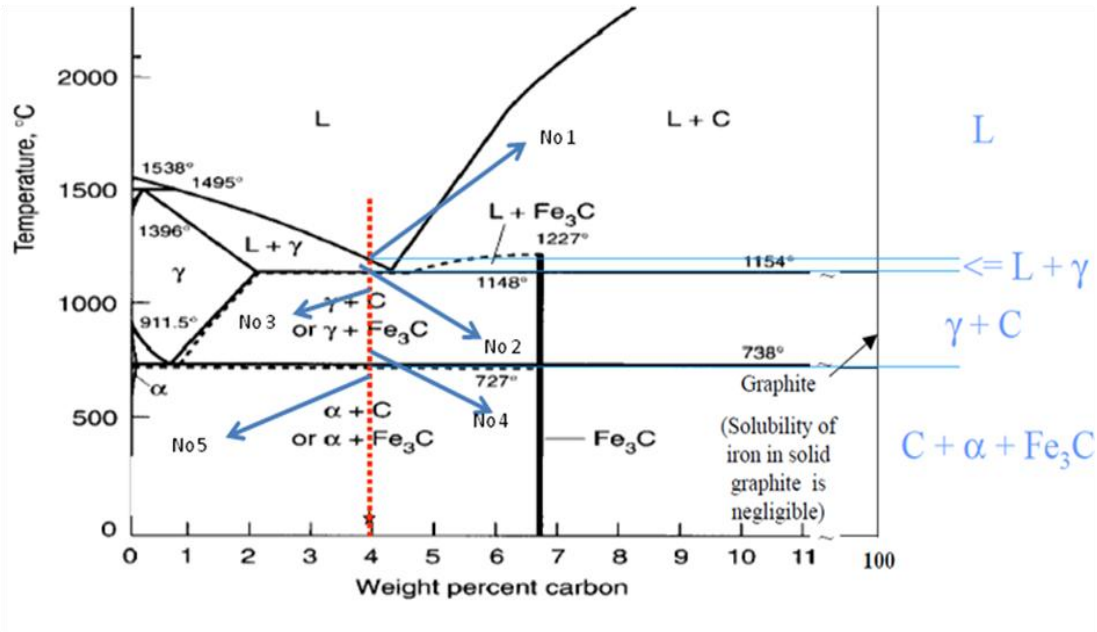

Figure 2.2 Shows solidification and graphitization of cast iron [13].

Fallowing steps can be helpful to understand graphite formation in cast iron;

- When the area at point 1 is entered with decreasing temperature, austenite dendrites start to form and grow. Afterwards, growth of the austenite will

stop as temperature of liquid iron falls to the point 2.

- Eutectic solidification starts when temperature reaches to the point 2. Eutectic solid consists of austenite plus Fe_3C or austenite plus graphite. If carbon is found to be in cast iron as Fe_3C, this is white cast iron. If carbon is present in cast iron as graphite, it can be named as gray, spheroidal or compacted graphite iron. Slow cooling rate and graphite stabilizer elements must be supplemented so as to achieve graphite formation in cast iron. And finally, while temperature reaches to the point 3, there will be no liquid phase in the system.
- After freezing is completed, microstructure of cast iron will be composed of solid phases that are developed during initial two steps. Graphite plus austenite can be formed in gray, spheroidal and compacted graphite iron.
- Precipitation of carbon is expected between point 3 and 4 since solubility of carbon decreased from 2.0% to 0.6 – 0.8% C in austenite phase as the area at point 4 was entered with decreasing temperature. These excessive carbon atoms cause compacted, gray or spheroidal graphite iron to develop graphite formation, while formation of Fe_3C is expected to be seen in white cast iron.
- Austenite transforms to pearlite and ferrite between point 4 and 5. This is one of the quite complex changes due to the fact that there are just a few approximations. If cooling is very slow, only ferrite formation can be obtained. If cooling conditions is severe, pearlite plus ferrite or only pearlite can be seen depending on how quickly cooled.
- After cooling below point 5 to room temperature, there will not be an important change in cast iron microstructure [14, 15].

2.1.2 Microstructures of Compacted Graphite Iron in Cast Iron

Graphite particles consist of the thick rounded edges and worm shaped that can be seen when it is observed in two dimensions. Due to morphology of graphite formation, crack initiation and growth are interrupted by presence of the compacted graphite in the iron matrix [5, 16, 17].

Compacted graphite iron has been utilized as industrial product since 1975. However, compacted graphite iron production is restricted by shape and morphology of the product on account of very narrow range of compacted graphite iron stability [2].

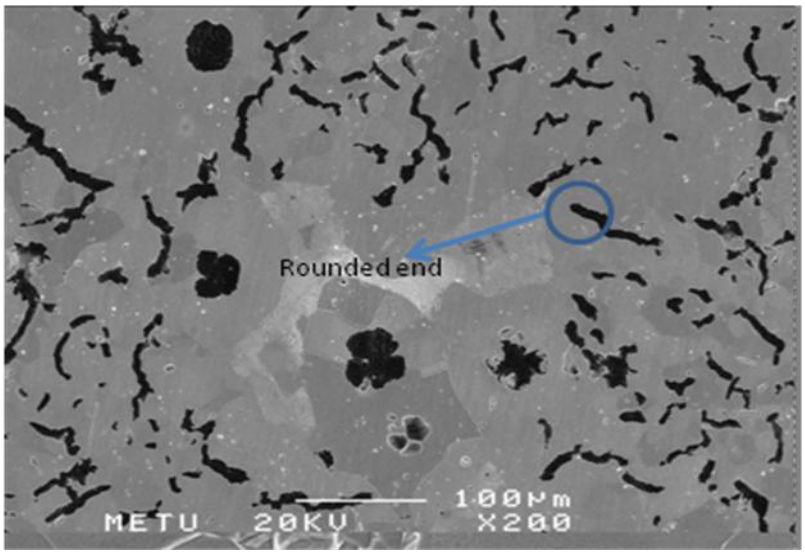

Figure 2.3 Thick and worm shaped graphite particles can be noticed in this SEM figure.

Compacted graphite particles are linked to other particles within the eutectic phase, so there is a powerful adhesion force between the iron matrix and particles of which the mechanism cannot be exactly understood. However, graphite particles own a strong influence on elastic modulus for product that is produced as cast iron [16, 18].

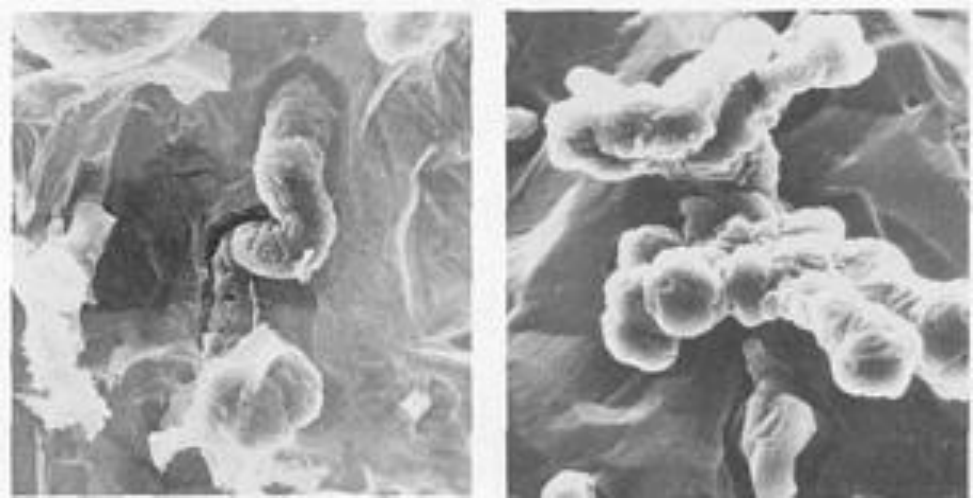

Figure 2.4 A fine sample of compacted graphite iron microstructure. Full deep etch. SEM, 395X [11].

When compacted graphite is confronted with flake graphite particles, the first particles are seen to be shorter, thicker and worm shaped than the second ones. Moreover, compacted graphite particles lead to improve mechanical properties. In contrast, flake graphite particles cause formation of crack initiation [16].

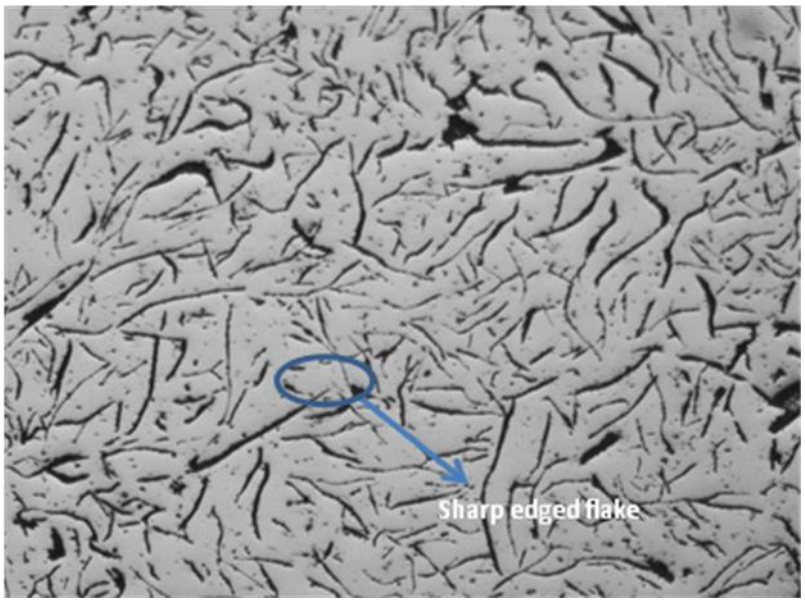

Figure 2.5 Sharp edges of flake graphite iron leads to increase stress concentration. This simplifies crack initiation under mechanical loads [9]

2.1.2.1 Formation and Growth of Compacted Graphite Iron

Compacted graphite solidification morphology includes both spheroidal and gray iron solidification morphology. The first stage of solidification is similar in spheroidal graphite iron (SG) in that mushy zone enlarges from solid skin to completely liquid center. Afterwards, solidification of compacted graphite iron akin to that of gray iron. To illustrate, liquid iron percent at the center of the casting rises sharply, which can be associated with gray iron solidification morphology. Moreover, growth of compacted graphite iron is not similar to that of nodular and flake graphite due to the fact that compacted graphite iron growth mechanism includes both of them. To illustrate, the ends of the worm shaped graphite grows like nodular graphite of which growth goes on c – axis direction. This type of growth causes formation of ferrite during eutectoid transformation in the matrix [19, 20, 21].

Nodular graphite is formed as long as proeutectic solidification occurs at high temperatures. In this case, nodular graphite is surrounded with liquid phase. Some experiments indicate that compacted graphite iron owns its worm-shape by means of

degeneration of nodular graphite during eutectic solidification. If Mg or inoculants that are present in molten iron is sufficient to nodulize or compact the graphite iron, the proeutectic graphite which is developed in high temperature area will form as nodular particles [6, 21].

After proeutectic solidification process is concluded at approximately 1147 ^{o}C, eutectic solidification process began. During this process, nodular graphite starts to change their shapes from nodular graphite to compacted graphite. When nodular graphite starts to change its shape from nodular graphite to compacted graphite, graphite particles are surrounded by austenite cells. In the meantime, compacted graphite irons in contact with the molten iron which occurs due to segregation of some elements are not decomposed in eutectic as long as solidification process occurs. This causes the formation of enriched liquid area containing elements reacting with some elements [6].

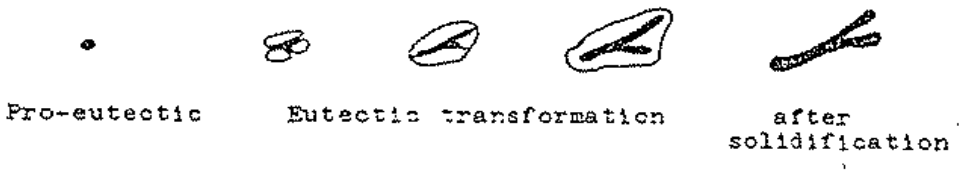

Figure 2.6 This figure reveals that most of the nodular graphite starts to change their shapes from nodular to compacted when graphite particles are enclosed within austenite cells at high temperatures such as 1150 ^{o}C [4].

When growth of compacted graphite is considered, it can be realized that graphite particles grow along a-axis direction as compacted graphites connect with liquid phase of channels. Then, compacted graphite particles are completely surrounded by austenite and then compacted graphite begins to grow along c – axis direction. Diffusion of carbon begins relatively slow in this direction, and thicker austenite cell can be seen in this condition. Hence, Segregation of elements that has a strong effect

on the growth of the compacted graphite iron is caused by transformation of austenite during solidification process. [6, 19, 21].

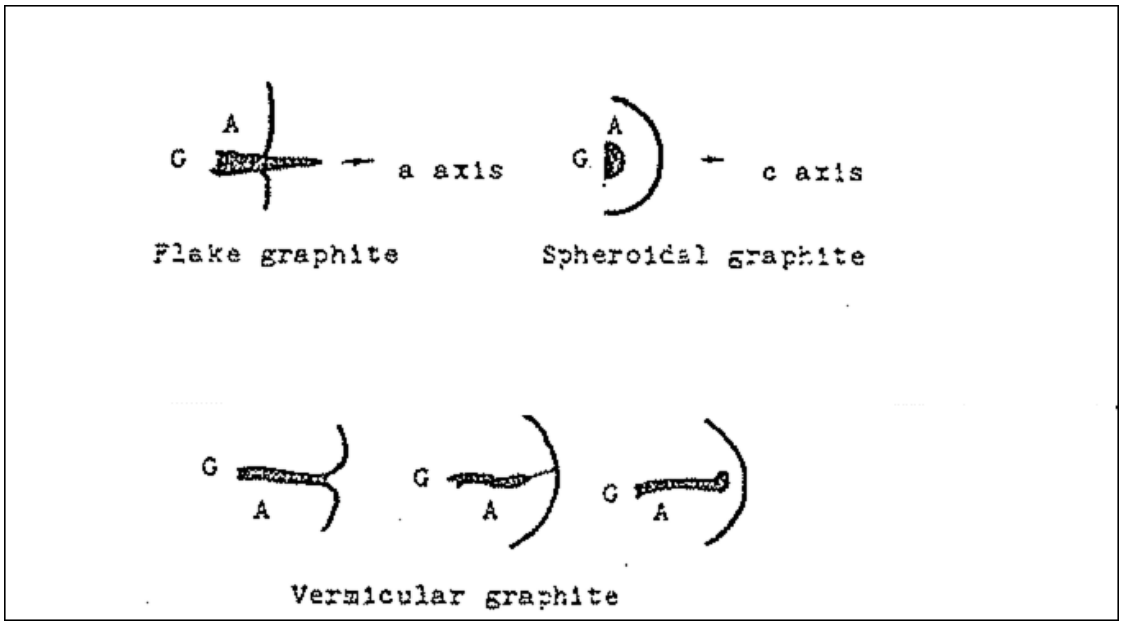

Figure 2.7 As compacted graphite connects with liquid phase of channels, graphite particles grow along a – axis direction [1010]. Afterwards, compacted graphite particles are completely surrounded by austenite and then compacted graphite begins to grow along c – axis direction [0001] [6, 21].

2.1.2.2 Properties of Compacted Graphite Iron

Compacted graphite particles are thicker, shorter and consist of the rounded edges, while flake graphite posses sharper edges that cause crack initiation. If these graphite particles are viewed in deep-etched scanning electron micrographs, these worm shaped graphite particles can be noticed to be connecting with each other in iron matrix, which causes strong adhesion between matrix and graphite and also enhanced thermal conductivity [2, 5, 17].

Mechanical properties of compacted graphite iron are similar to those of flake

graphite with regards to conductivity and expansion. And it is also similar to spheroidal graphite in respect to tensile strength. [11].

In contrast to gray iron, compacted graphite iron is preferred with respect to better mechanical properties and weight reduction in the auto engine block industry. To illustrate, new Opel Ag is using the compacted graphite iron diesel engine technology and Opel has acquired approximately 20.4% weight reduction. BMW 3 – 9 lt V8d and Audis 3.3 lt V8 TDI engine blocks can be given as the other examples [20].

2.1.2.3 Thermal Conductivity of Compacted Graphite Iron

Graphite particles present in compacted graphite iron have three times greater thermal conductivity than ferrite and pearlite phases. Shape of graphite also owns a great influence on thermal conductivity [22].

Thermal conductivity of compacted graphite iron is greater than that of nodular graphite iron due to worm shape and interconnection. However, the thermal conductivity of compacted graphite iron is about 25% less than that of pearlitic flake graphite iron at room temperature. A decrease in thermal conductivity of flake graphite can be noticed when temperature of stage where gray cast iron is present increases, but when thermal conductivity of compacted and nodular graphite iron are discussed, this is not the case that happens. Thermal conductivity increases with an increase in temperature. According to some articles, compacted graphite iron with ferritic iron matrix has higher thermal conductivity than pearlitic one [22].

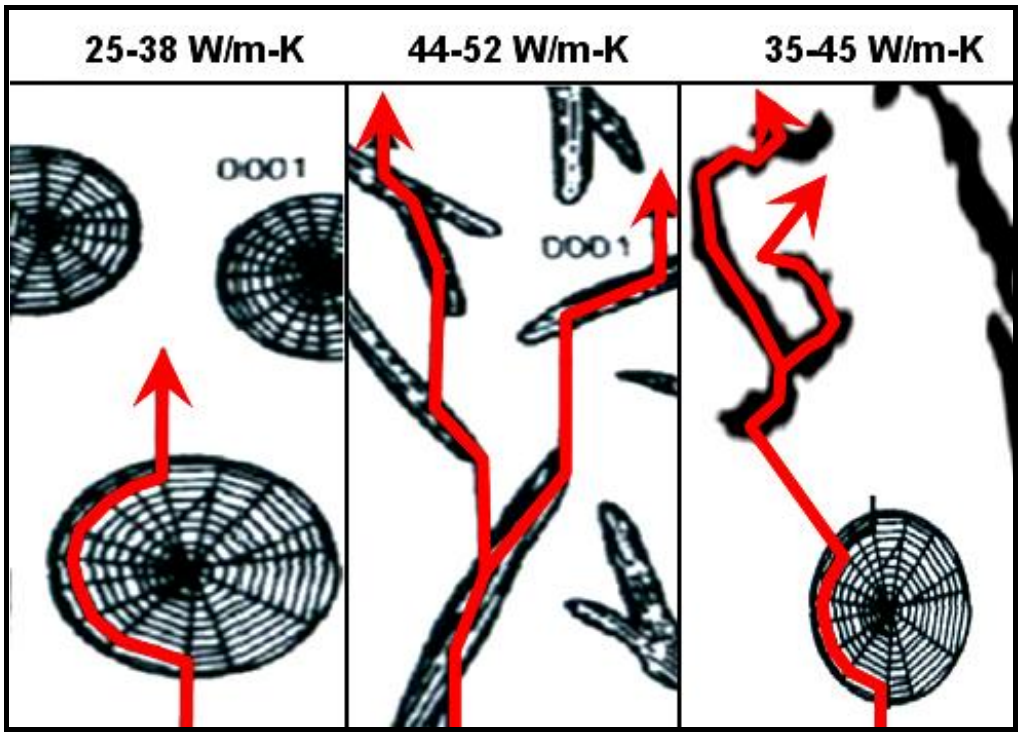

Figure 2.8 Red colored arrows are used to show thermal conduction in microstructure. It can be noticed that thermal conductivity is the highest when microstructure consists of kish or flake graphite iron. Thermal conductivity decreases as graphite shape changes from flake graphite to nodular graphite [12].

Thermal conductivity can also be influenced by carbon content and volume percent of nodularity. To illustrate, an increase in carbon level from 3.5 to 3.8 promote approximately a 10% increase in thermal conductivity. If nodularity% of engine block increases from 10 to 30%, a 10% decrease in thermal conductivity is expected to be seen [22].

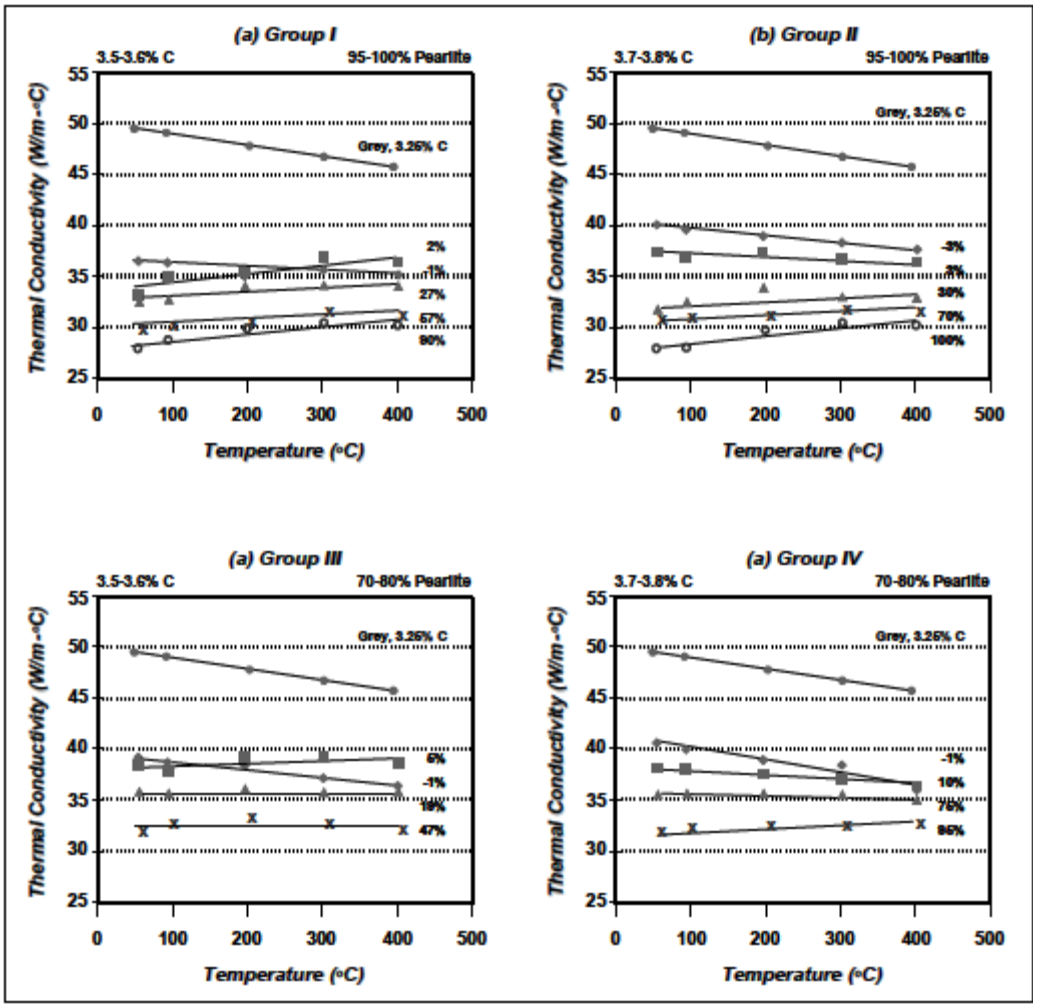

Figure 2.9 Thermal conductivity of gray iron is the highest in all conditions. Negative numbers mean that flake graphite iron is present in microstructure. An increase in nodularity percentage promotes a decrease in thermal conductivity [22].

2.1.2.4 Impact of Nodularity% on Properties

The matrix structure and the percent of compacted graphite together governs mechanical properties such as tensile strength, 0.2 % yield strength, elastic modulus, percent elongation and thermal conductivity. An increase in % nodularity directly increases tensile strength, 0.2 % yield strength, elastic modulus, percent elongation but decreases thermal conductivity as can be seen in Table 2.1

Table 2.1 Properties of pearlitic compacted graphite iron as a function of nodularity [16].

Property 25 ^{o}C	**% Nodularity**				
	10	30	50	70	90
Tensile strength (MPa)	450	520	590	640	700
0.2% yield Strength (MPa)	370	390	410	440	490
Elastic Modulus (GPa)	145	150	155	155	160
Elongation (%)	1-2	1-3	2-4	2-5	3-6
Thermal Conductivity (W/m^{o}C)	36	33	31	30	28

Diesel engine blocks which include different thickness are expected to possess nodularity values that are between 0 to 25%. However, thin sections of the diesel engine blocks that are approximately 7 mm may contain 30 – 50% nodularity and remaining is compacted graphite iron due to fast cooling rate. High nodularity values yields an increase in strength and stiffness [16].

Diesel engine blocks are expected to work under high thermal and mechanical loading. Therefore, diesel engine blocks are supposed to include 0 – 25% volume spheroidal graphite and remaining is compacted graphite in the produced engine blocks. Cu, Sn and some alloying elements are necessary to promote an increase in mechanical properties reported by references [5, 16].

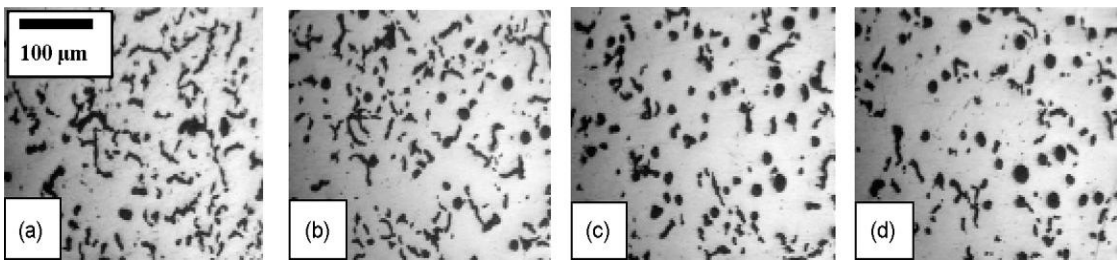

Figure 2.10 Samples were taken from the parts that include different chemical

composition but same thickness of step block castings. (a) 5% nodularity, (b) 15% nodularity, (c) 20% nodularity, (d) 30% nodularity [23].

Compacted graphite iron has perfect mechanical properties such as 70% higher Ultimate tensile strength and elastic modulus compared to gray iron. This leads to advanced working performance and diminished weight of the products that is approximately 16% depending on engine design. In addition, the compacted graphite iron can also be recycled similar to cast iron [2, 16].

Due to shrinkage difference in gray, spheroidal and compacted graphite iron. Spheroidal graphite iron parts require risers but gray and compacted graphite do not require risering. Shrinkage defects can be prevented in diesel engine blocks without excessive risers and runners usage if the product includes lower nodularity% value. [29].

2.1.2.5 Ferrite to Pearlite Ratio

As the temperature of casting alloy having C.E.V (carbon equivalent) values less than 4.3 between 1175 and 1200 ^{o}C drops slowly, iron matrix consists of austenite and liquid phase. When temperature of the alloy at solid state metal reaches just below approximately 725 ^{o}C, austenite phase transforms into either pearlite or ferrite. If cooling is fast enough, carbon atoms present in austenite phase cannot diffuse to graphite particles. Therefore, excessive carbon atoms will form cementite that is Fe_3C plates within the ferrite. Growth of pearlite phase starts from the area that is far away from the graphite particles and this growth continues until the austenite phase is diminished. Tensile strength and hardness of engine block will increase due to reinforcements of hard cementite plates, but unfortunately, this ferrite plus Fe_3C phase mixture reduces machinabilty. If cooling is slow enough and chemical composition of engine block is not available for pearlite formation, carbon atoms will diffuse to graphite particles, which causes formation of ferritic matrix [17, 19].

Since CGI particles have wide surface area in the iron matrix, and there is no obstacle to reduce or stop carbon atoms diffusion from iron matrix to graphite particles, graphite particles can, therefore, grow easily, so formation of ferrite is

expected to be seen in the compacted graphite iron matrix. For this reason, strong pearlite – stabilizing elements are required to achieve approximately 60 – 70 % pearlite content in the iron matrix. Copper is generally preferred on account of the fact that carbide formation is not seen and it can distribute uniformly through the iron matrix [24].

According to references, fully pearlitic microstructures are obtained by adding Cu that is between 1 and 1.5%. The amount of copper and tin added to the ladle simply changes the amount of pearlite present in the cast iron. If copper and tin are not added to the alloy in the furnace more ferrite phase appears and less pearlite is expected since these elements are strongly pearlite stabilizers. The addition of these elements does not affect the nodule count or volume percent graphite [18].

Metallography is of a significant importance to evaluate the nodularity percentage and pearlite/ferrite content for a metallurgist by the help of optical microscopy [25].

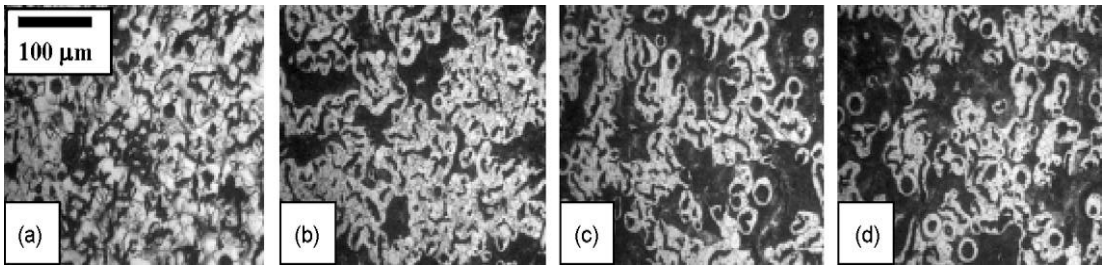

Figure 2.11 Each microstructure include same 0.012% Mg but different Cu% ratio (a) 25% pearlite (0.2% Cu), (b) 45% pearlite (0.4% Cu), (c) 60% pearlite (0.6% Cu) and (d) 75% pearlite (0.8% Cu). It can be seen that increase in wt% Cu yields higher percent of pearlite in the matrix appears on more gray areas [23].

Cu and Sn increase the proportion of the pearlite, since these elements decrease the carbon diffusion coefficient; thus, carbon cannot attain a graphite region and is expected to react with iron. Consequently, carbon reacts with iron and they produce

cementite. Approximately 0.45 – 0.60% Cu and 0.05 – 0.08% Sn are added in order to achieve minimum 70 -90% pearlitic matrix. Amount of added Cu and Sn are based on the weight and geometry of the product [5, 26, 27].

Chromium is stronger pearlite stabilizer than Mn. Cr stabilizes pearlite in the same way as Mn by means of increasing the solubility of carbon in austenite phase. Cr causes the formation of finer pearlite structure, so pearlite phase is composed of more cementite plate than pearlite produced by Mn addition. It also reduces nuclei of graphite formation. For this reason, possibility of chill formation at fast cooled areas will increase. However, another important property of chromium is that it causes pearlite to be stabilized at elevated temperatures that are higher than 400 ^{o}C [17, 22].

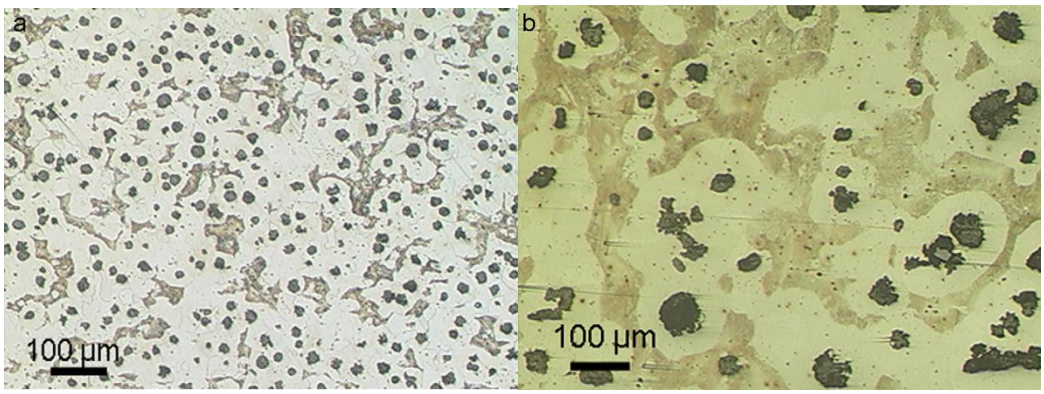

Figure 2.12 (a) 5 mm (b) 30 mm samples. It can be realized that amount of graphite particles are increased with decreasing thickness sections of step block castings due to fast cooling rate [28].

The silicon content of CGI alloys are generally in the range of 2.0 – 2.4 % wt to obtain optimum C.E.V. values. To achieve higher pearlite phase volume fraction Cu. Sn, Sb and Mn concentration can be increased to improve strength and hardness. However, according to some references, Cu Sn, Sb and Mn are reduced to trace element level or not added at all. In the meantime, Si presence in the molten iron is arranged as 3.0% or more. This makes the microstructure to be fully ferritic. Ferrite phase is generally expected to be soft, but ferritic compacted graphite iron has the

same hardness and UTS values can be increased as high as pearlitic gray iron when ferrite phase is hardened by means of increased Si concentration, which is a result of solid – solution hardening mechanism [17].

2.2 Production of Compacted Graphite Iron

Compacted graphite iron production process is a hard task on account of the fact that compacted graphite iron is stable within a very narrow processing window and also temperature of furnace, Mg content in FeSiMg alloy, used type of inoculants, furnace holding time, ladle holding, transport and pouring times can easily alter the obtainable percentage of high quality compacted graphite iron [16].

It is true that requirement of improved performance of the engine block at higher peak firing pressure that is approximately 200 bar causes engineers to work on improving new diesel engine block. Despite the fact that compacted graphite iron with enhanced mechanical properties can be used for diesel engine design of which geometry is complex, obtaining of high quality compacted graphite iron that can be stable within a very narrow processing window is the main difficulty to produce high quality compacted graphite iron diesel engine blocks whose production volume and shrinkage tendency are high [22, 29].

Due to high performance requirements and zero tolerance of the geometric complexity and desired compacted graphite iron ratio that can be just stable for some restricted conditions, it requires laborious work to achieve engine blocks without problem [4].

Application of compacted graphite iron to diesel engine block that is composed of complex components is difficult when restriction of chemical composition is considered. Magnesium fade that is approximately 0.003% can be encountered at any part of the diesel engine block, which causes these parts of the diesel engine block to introduce flake patch microstructure contains [4].

Especially when engine block faces with a fast cooling condition at thin sections, chemical composition has to be close to compacted graphite iron to ductile iron transition condition to avoid formation of flake graphite [4].

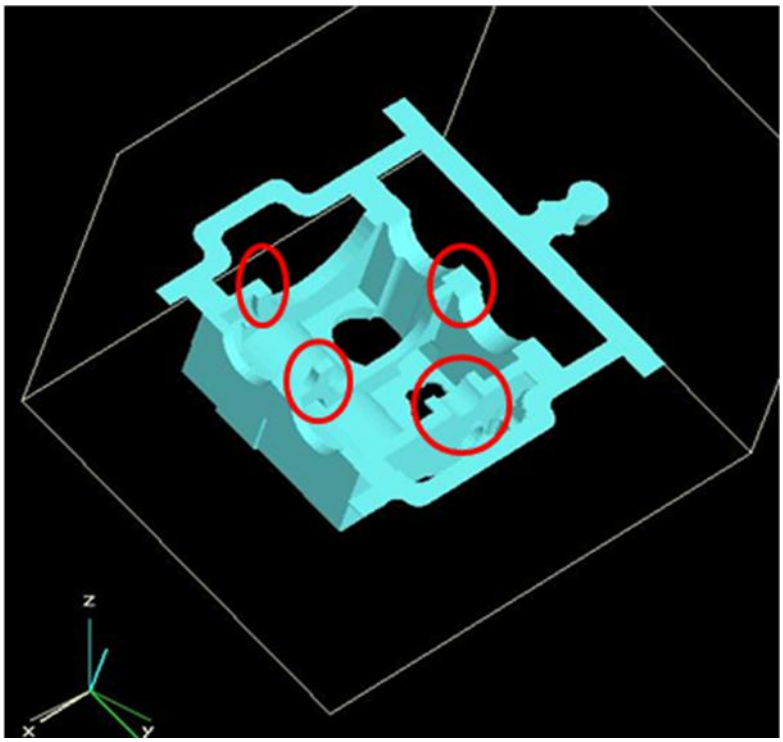

Figure 2.13 Diesel engine blocks include complex shapes and parts that have different thickness from each other.

2.2.1 Production of CGI by Ladle Treatment Method

2.2.1.1 Titanium Containing Alloys

Compacted graphite iron provides benefits to designers due to their useful combination of strength, thermal conductivity and other properties. Compacted graphite iron can also be produced with the help of Ti. To illustrate, chemical compositions that are given at Table 2.2 can be used to obtain high quality of compacted graphite iron. Addition of Ti that is about 0.1 – 0.15% is also beneficial in order to obtain compacted graphite iron at higher Magnesium contents. The higher Magnesium contents are desired so as to prevent formation of flakes graphite since the addition of Ti prevents excess formation of spheroidalidal graphite but increases the frequency of formation of worm shape graphites [5, 24, 25, 30].

Table 2.2 Required residual Mg ranges for various Sulphur and Titanium contents and desired nodularity values. Titanium is a perfect denodulizer and even a small amount of Ti such as 0.01% is of importance for denodulizing [24].

Base S Content	**Base Ti Content**	**Acceptable Mg Range for 25% max nodularity**	**Acceptable Mg Range for 30% max nodularity**	**Acceptable Mg Range for 35% max nodularity**
≤0.007%	≤0.06%	0.01-0.013%	0.01-0.013%	0.01-0.014%
≤0.007%	0.07-0.11%	ND	ND	ND
≤0.007%	0.15-0.20%	0.01-0.019%	0.01-0.023%	0.01-0.027%
0.008-0.013%	≤0.06%	0.01-0.014%	0.01-0.014%	0.01-0.016%
0.008-0.013%	0.07-0.11%	0.01-0.017%	0.01-0.020%	0.01-0.023%
0.008-0.013%	0.15-.20%	0.01-0.023%	0.01-0.026%	0.01-0.030%
0.014-0.015%	≤0.06%	0.011-0.014%	0.011-0.015%	0.011-0.017%
0.014-0.015%	0.07-0.11%	0.011-0.019%	0.011-0.021%	0.011-0.024%
0.014-0.015%	0.15-.20%	0.011-0.022%	0.011-0.025%	0.011-0.028%

Ti is added to the molten iron as alloy that includes 8.0 – 10% Ti, 4.5 – 5.5% Mg and 0.3 – 0.4% Ce [25].

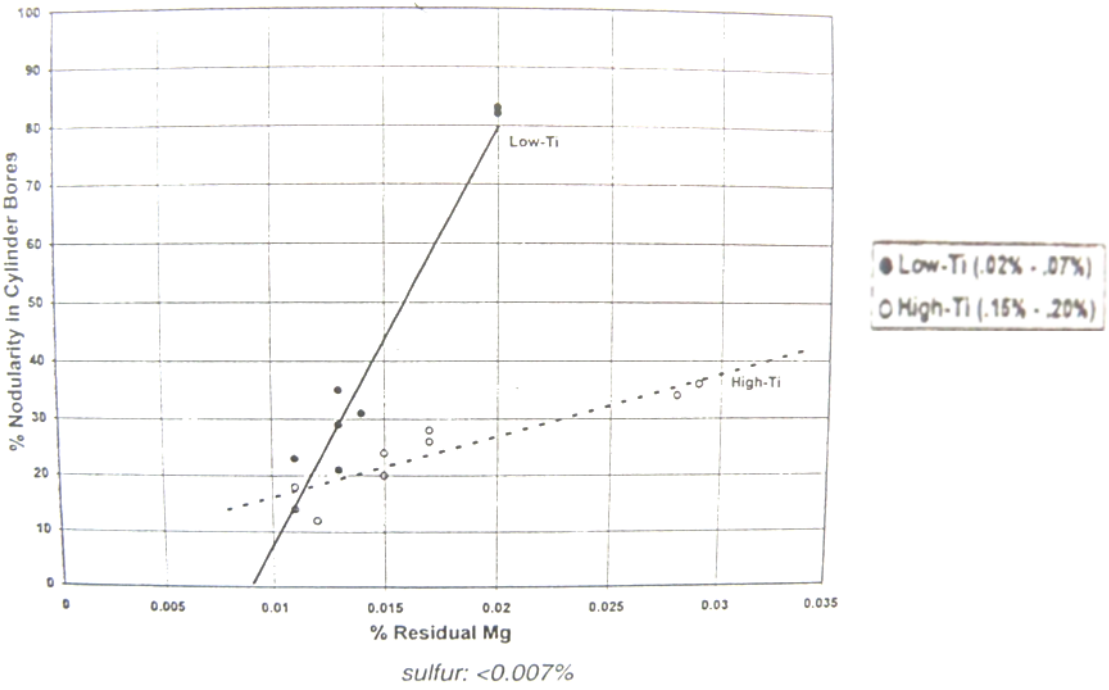

Figure 2.14 It can be recognized that, as S level of the base iron is low, nodularity percentage values is highly dependent on Mg content, especially when Ti content is low. The high quality compacted graphite iron contains approximately 25% nodularity. It can be achieved in the range of 0.010 and 0.013% Mg. An increase in Ti content causes the range of high quality compacted graphite iron to extend from 0.010 to 0.020% Mg without increasing the nodule percent in the alloy matrix [24, 30].

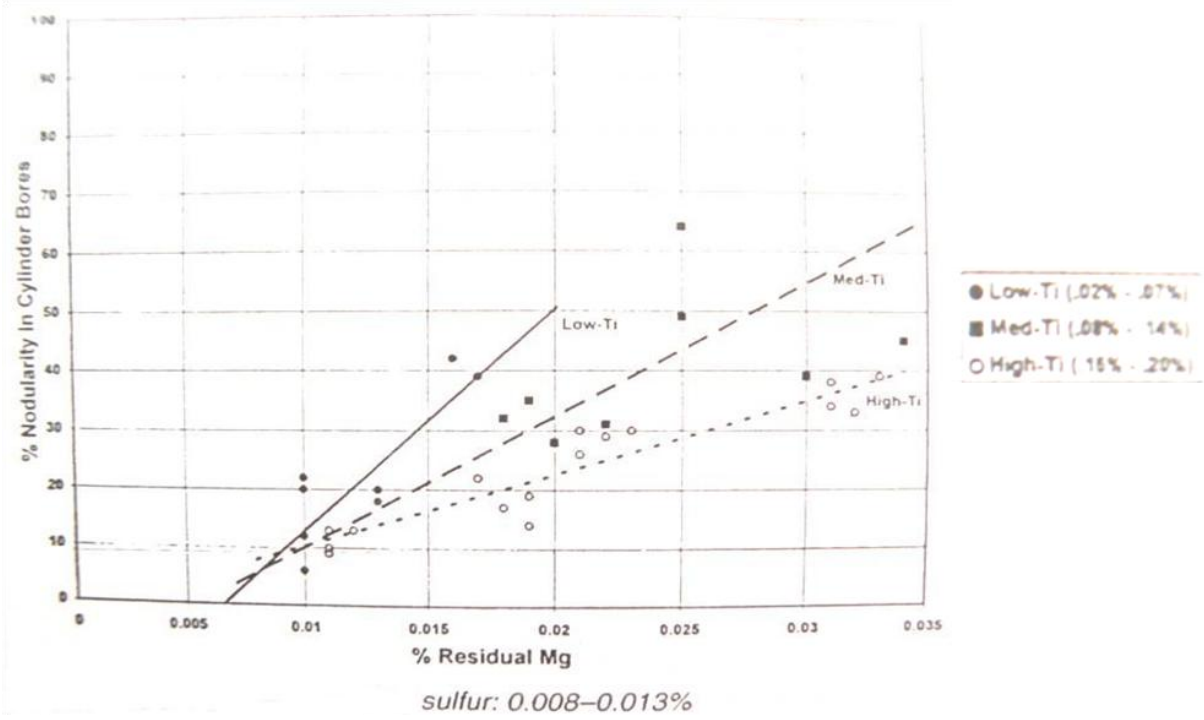

Figure 2.15 The range of high quality compacted graphite iron is less sensitive to sulphur level. High quality compacted graphite iron can be obtained as magnesium content is between 0.010 and 0.023% at low Ti content [24, 30].

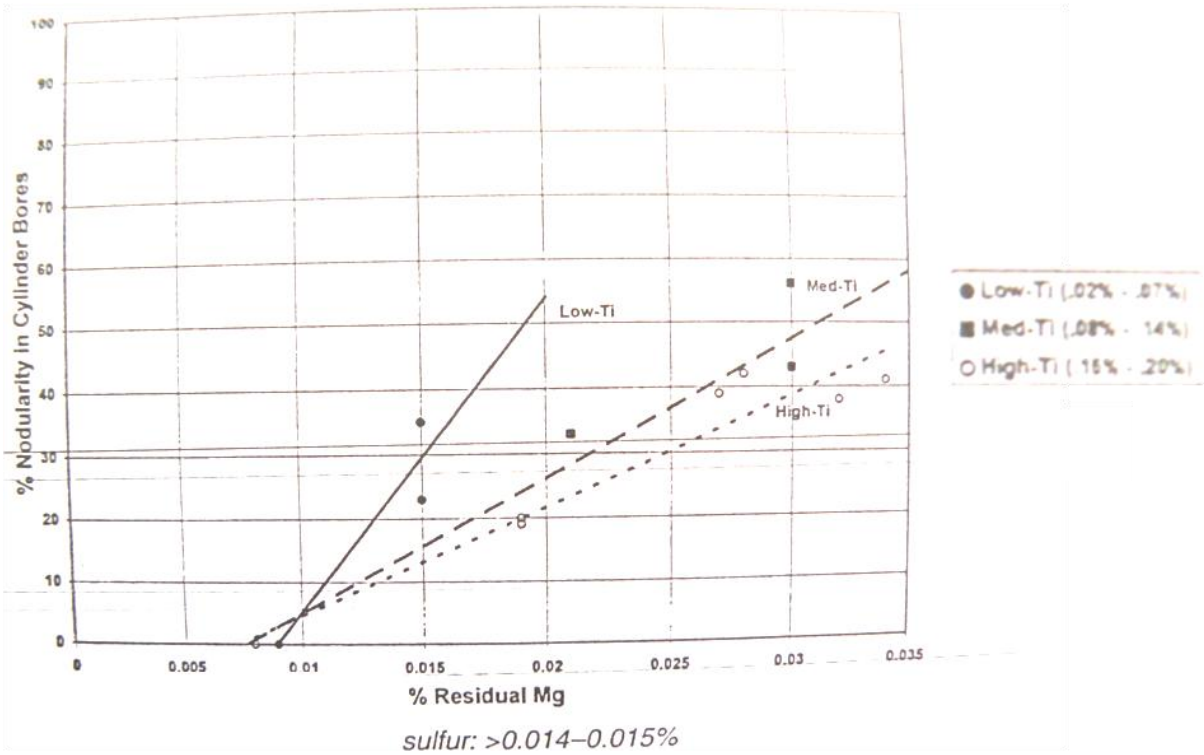

Figure 2.16 Nodularity in cylindrical bones is a function of both residual %Mg and %Ti in alloy composition in the presence of both %Mg and %Ti the amount of Ti markedly reduces the % of nodularity for sulphur level higher than 0.015%. for particular case 0.015% Mg is sufficient to keep nodularity in the range of 0 – 25 % when medium amount of Ti is added together with Mg. [24].

Approximately 0.1 -0.25% Ti is added to achieve high quality compacted graphite iron. The main purpose of Ti addition to the compacted graphite iron is that higher stable Mg ranges for compacted graphite iron production. Although Titanium has such a beneficial property to control graphite shape, this method is not recommended in many cases since even a small amount of Ti that is 0,005 – 0,02% Ti is sufficient to act in response to (Ti(C, N)) inclusions by means of carbon and nitrogen in the liquid metal. These (Ti(C, N)) inclusions are too hard particles and also cause D type graphite in the iron matrix. Titanium carbonitride inclusions have an opposite influence in the iron matrix when they are compared with MnS. Therefore, serious deterioration in machinability is caused by Ti additions [1, 17].

Engineers should avoid formation of carbides and Ti usage that is added to control

spheroidal graphite formation to obtain optimal machinability due to very hard TiCN particles. These inclusions may form in the cast alloy matrix structure, and their angular shapes can be realized as these inclusions are examined under optical microscope [11, 29, 31].

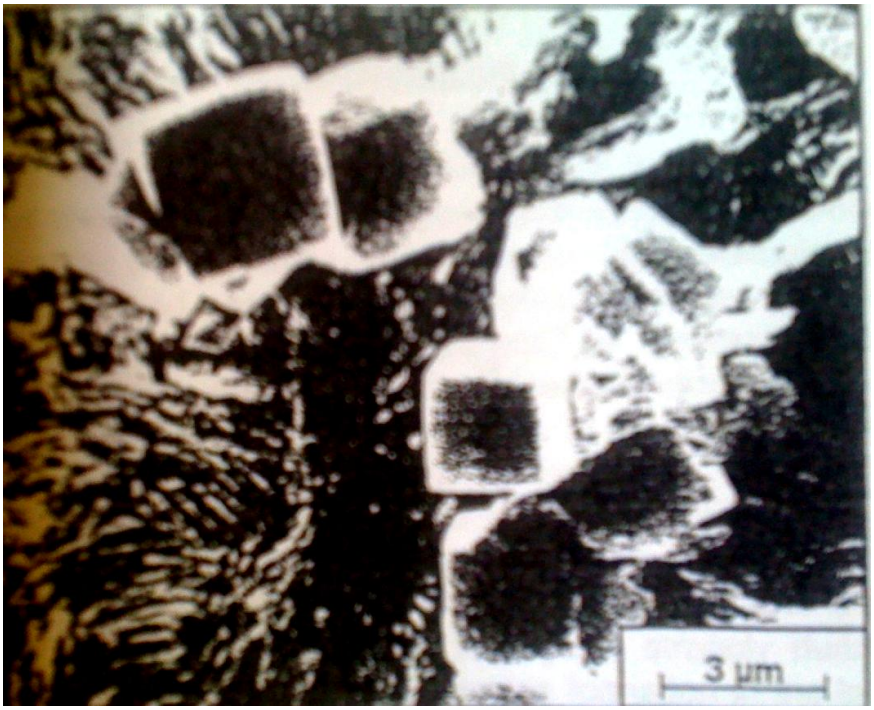

Figure 2.17 These titanium carbonitride inclusions are formed in cubic shapes and their sizes are approximately between 1 and 5 µm. These hard inclusions significantly reduce the tool life because of harmful effects of (Ti (CN)) inclusions. If (Ti (CN)) inclusions are regularly separated in the iron matrix, they increase wear resistance of the product. [17].

2.2.1.2 Mg Treatment

The melting operation for the production of compacted graphite iron in principle is similar to the production of spheroidal graphite iron. Induction furnace is used for adequate melting in the experiments. Alloying elements such as Mg and Ce are used

less than those in spheroidal graphite iron production [11].

Production of diesel engine blocks whose nodularity range is from 0 to 25% depends on the process control. Liquid metal is treated with magnesium and inoculant, which is called initial base treatment. Rare earth treatment has some advantages unless reaction time is critical, since section thickness which is lower than 6 mm has high chilling tendency. Magnesium treatment is safer in this case than rare earth treatment. Required chemical composition such as the added amount of magnesium depends on solidification time and size of the engine blocks. After initial base treatment process is accomplished, thermal analysis of liquid metal can be studied in order to determine the process variations [5, 11, 20].

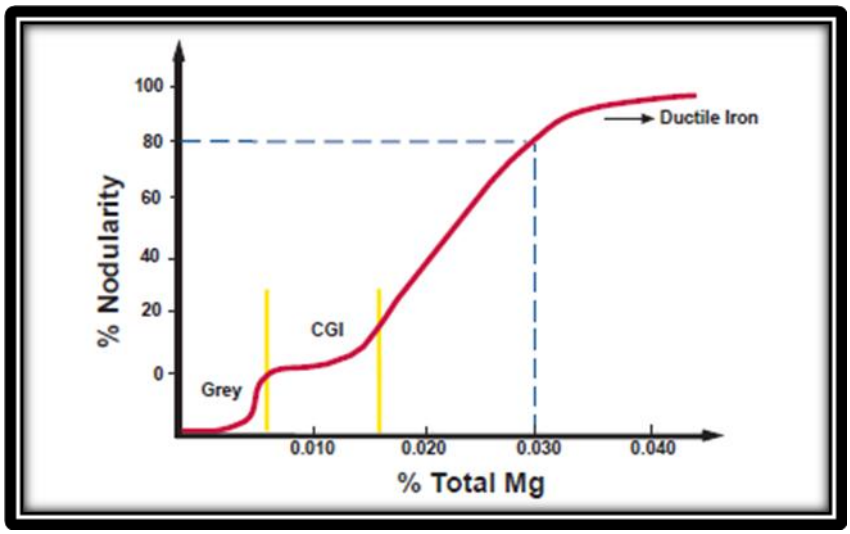

Figure 2.18 Stable range of compacted graphite iron can be noticed between yellow lines. If total Mg value is less than it should be, flake graphite formation will be seen. This promotes a decrease in UTS approximately 20%. High nodularity percentage value will be obtained if excessive total Mg is present in the molten iron [4, 16].

Since total Mg content directly affects the graphite shape of the products and compacted graphite iron is stable within a restricted Mg range that can be seen from figure 2.18, an amount of magnesium that is added to the liquid iron during the base

treatment is so important in order to convert gray iron microstructure into high quality compacted graphite microstructure. Moreover, production of nodular graphite iron is based on that of magnesium [2, 32].

Effect of additional 0.001% active Mg on the number of nuclei can also be present in figure 2.19 [4].

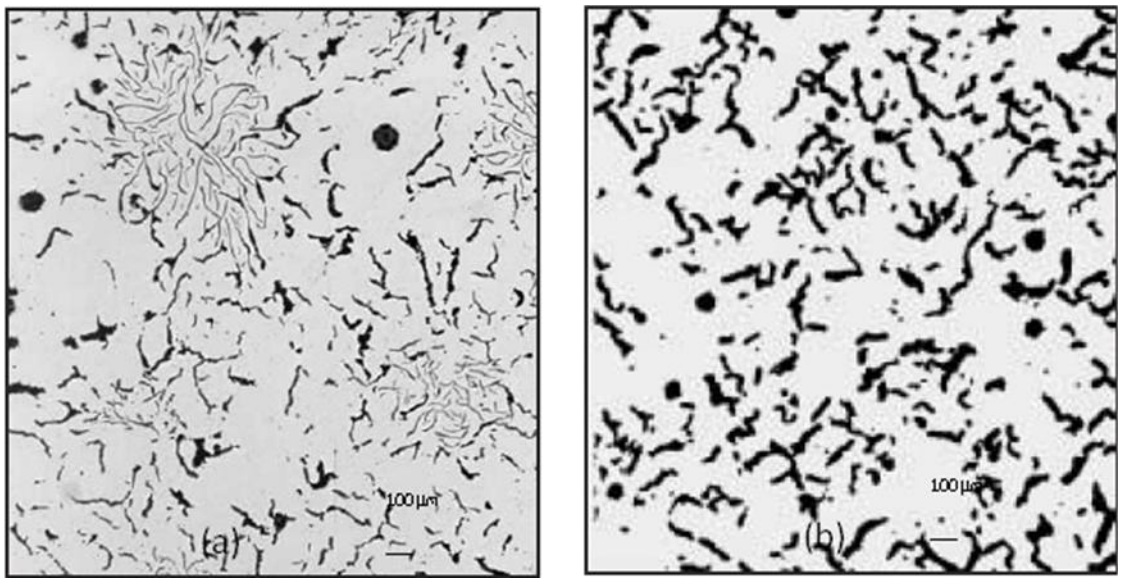

Figure 2.19 Additional 0.001% active Mg can convert alloy (having 300 MPa UTS) flake patch microstructure into a high quality compacted graphite iron microstructure with 450 MPa Ultimate tensile strength [25].

After magnesium and inoculants are added to the liquid iron, amount of dissolved magnesium present in the molten iron is too difficult to determine since magnesium can react with sulphur and oxygen which are present in the molten iron. Namely, about 0,003% magnesium might be lost because of fading during approximately 10 minutes from end of the base treatment until end of the pouring. For this reason, D type flake graphite can be seen due to magnesium deficiency. Even a small amount of flake graphite which is present in iron matrix can easily reduce approximately 20 – 30% in UTS and elastic modulus [2, 5, 16].

If excessive amount of magnesium is added to the molten iron, more – nodularity can be faced. This causes microstructure of engine blocks to have excess nodularity%. Over – nodularity can also be seen in the case of the high magnesium recovery [2].

Oxides, nitrides, complex intermetallics and/or other non – metallic inclusions that can be found in compacted graphite iron engine block are usually in the size range of 0.1 – 10 μm. One diesel engine block whose weight is approximately 125 kg can include 10^9 inclusions. Chemical composition of molten iron determines type of inclusions that can be hard such as Ti(C, N) or be soft such as MnS. When gray cast iron production is considered, the possibility to generate favorable inclusions is a more difficult process for compacted graphite iron production since Mg, whose addition is required to form compacted graphite iron is a predominant element with regard to thermodynamic strength [17].

2.2.1.3 Inoculation

Inoculants that can be found to be several different master alloy forms with different chemical compositions such as Foundrysil and Wastly are added to the molten iron to achieve high quality compacted graphite iron microstructure at each desired thickness of diesel engine block because formation of high quality compacted graphite iron which is not a simple magnesium plateau requires simultaneous control of Mg and inoculants throughout the whole production process. Effect of inoculation on the number of nuclei can be seen in figure 2.20 [4, 16, 19, 25].

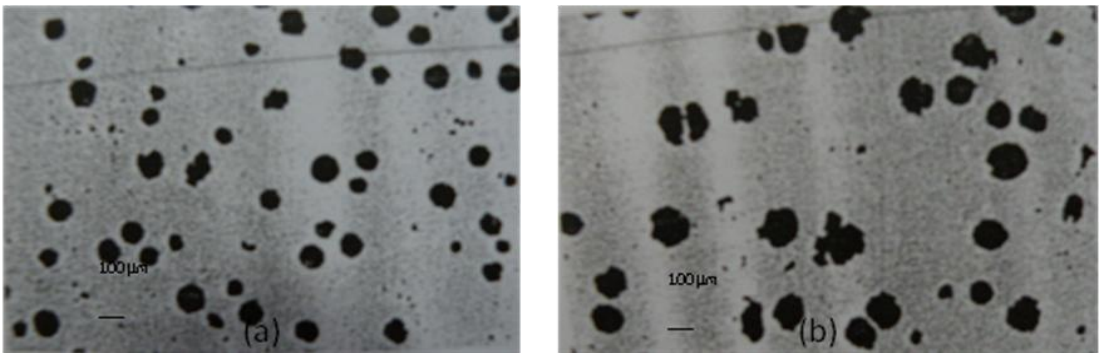

Figure 2.20 (a) inoculated sample and (b) uninoculated sample. An increased nodule

count can be seen in this figure [25]

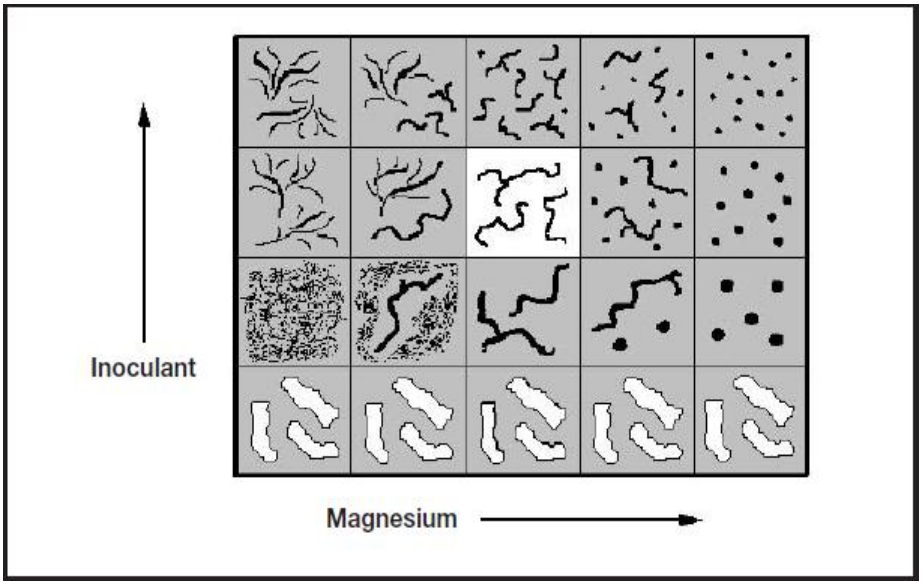

Figure 2.21 High quality compacted graphite iron is just stable within a four sided window and both Mg and inoculations have approximately the same degree of importance to achieve the desired result [4].

Although Al, Ti, Ba, Mg, and rare earth elements that come from inoculation increase formation of dross on account of the fact that these alloying elements react with S and O_2 which are present in the molten iron, an advantage of inoculation is that inoculated compacted graphite iron includes more cell counts and less chill depth than uninoculated compacted graphite iron samples. However, the amount of inoculants that is added to the molten iron during ladle method should be chosen carefully to avoid excessive inoculant present. If inoculants level in the molten iron is higher than it should be, an increase in spheroidal graphite ratio is expected to be seen due to presence of more nuclei [11, 4].

In contrast to spheroidal graphite iron, post inoculation is not recommended to produce diesel engine blocks with high quality compacted graphite iron due to the fact that high rise in nodularity percentage values are noticed after post inoculation.

To illustrate this event, a change in spheroidal ratio can be seen in figure 2.25 after 80 gr additional inoculant to a one tone ladle [16, 4, 22]

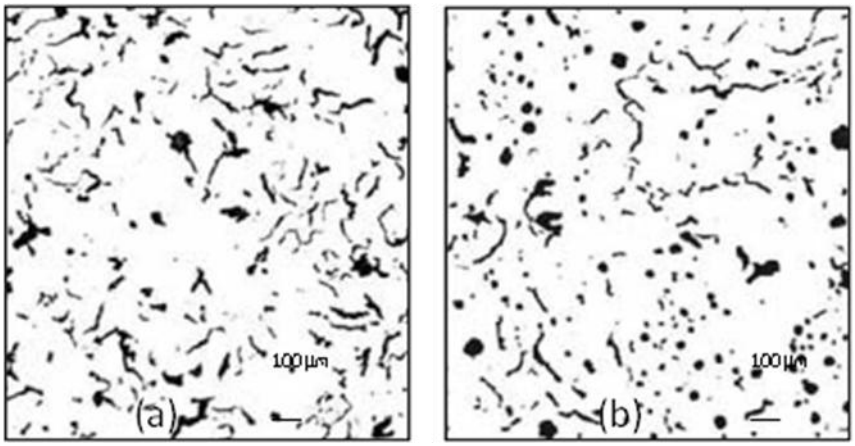

Figure 2.22 (a) before inoculant addition, there is 3% nodularity and remaining is compacted graphite iron. (b) After 80 gr inoculant addition, nodularity of test bar with 25 mm thickness increases from 3 to 21% [16, 4].

2.2.1.4 Cooling Rate

It is assumed that the main factor is chemical composition of compacted graphite iron so as to determine nodularity percentage values. However, cooling rate is as important as chemical composition to form microstructure of products. This is the reason that different sections of the product which have different thicknesses and different locations in mold cavity have the same chemical composition although they have different cooling rates. This difference in cooling rate can induce to have totally different microstructure within the same product or diesel engine block [33].

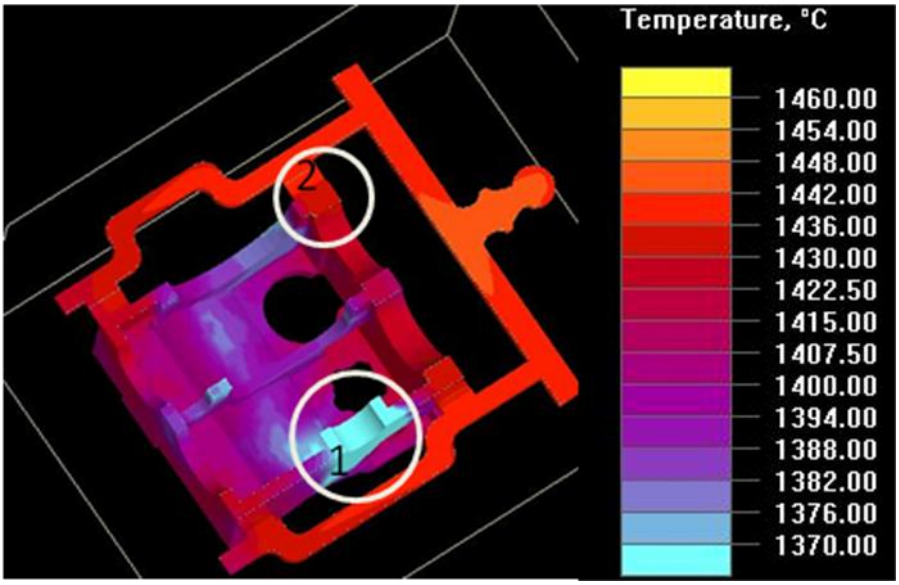

Figure 2.23 Temperature differences can be noticed by means of colors. Section 1 has approximately 1370 ^{o}C and section number 2 owns about 1440 ^{o}C.

Some thin sections that are approximately ≤ 7 mm might include nodularity percentage values larger than 30% which are based on gating system, their location and cooling rate. Low compacted graphite iron proportion is generally present in thin sections due to natural tendency of compacted graphite formation. This leads to inhomogeneous graphite distribution in the diesel engine block. Patents are available where high nodularity sections are located in the mechanically loaded areas. Mazda and Ford use this technique in their engine designs [22].

2.2.1.5 Alloying Elements in Compacted Graphite Iron

Iron has such a chemical composition that, after solidification, a large amount of its carbon is distributed throughout the casting as free carbon. However, before pouring molten iron, it should be specially prepared by treating with a small amount of Mg, Ce or other agents. This will make a large amount of its carbon to form as compacted graphite iron rather than as nodular or flake [7].

Table 2.3 Chemical compositions of compacted graphite iron specimens with different nodularity% and pearlite content were located in this table [22].

Group Number	Nodularity%	Pearlite %	Chemical Analysis %									
			C	Si	Mn	S	Mg	Cu	Sn	Cr	Al	P
1	4	25	3.63	2.49	0.42	0.014	0.007	0.42	0.039	0.02	0.008	0.010
2	4	45	3.54	2.49	0.41	0.010	0.007	0.40	0.040	0.02	0.003	0.011
3	8	50	3.54	2.50	0.41	0.012	0.010	0.41	0.040	0.02	0.003	0.011
4	7	75	3.61	2.49	0.40	0.014	0.008	0.45	0.053	0.03	0.004	0.011
5	6	94	3.59	2.48	0.39	0.013	0.011	0.71	0.094	0.03	0.007	0.011
6	-3	86	3.60	2.45	0.40	0.014	0.008	0.45	0.051	0.03	0.004	0.010
7	-2	93	3.57	2.48	0.39	0.014	0.006	0.72	0.094	0.03	0.008	0.010
8	0	99	3.58	2.48	0.39	0.016	0.010	0.71	0.094	0.03	0.008	0.010
9	33	87	3.57	2.50	0.40	0.011	0.023	0.41	0.039	0.03	0.003	0.011
10	67	90	3.50	2.47	0.41	0.010	0.027	0.44	0.052	0.02	0.003	0.011
11	80	90	3.58	2.50	0.39	0.012	0.030	0.72	0.095	0.03	0.007	0.011

2.2.1.5.1 Effects of Carbon and Silicon

The amount of added carbon and silicon is used to maintain carbon equivalent that is desired between 4.30 and 4.45% in order to obtain high quality liquid metal fluidity and to decrease formation of austenite dendrites. These dendrites enhance level of segregation. Moreover, carbon equivalent level that is approximately 4.40% is acceptable in order to decrease nodularity% due to diminished proeutectic graphite [24].

It can be realized that Si is the main element in order to encourage formation of graphite during cast iron production; thereby it can be estimated when analyzing Fe – C – Si (2% Si) phase diagram. That is the best way to explain effect of carbon and silicon on compacted graphite iron formation [14].

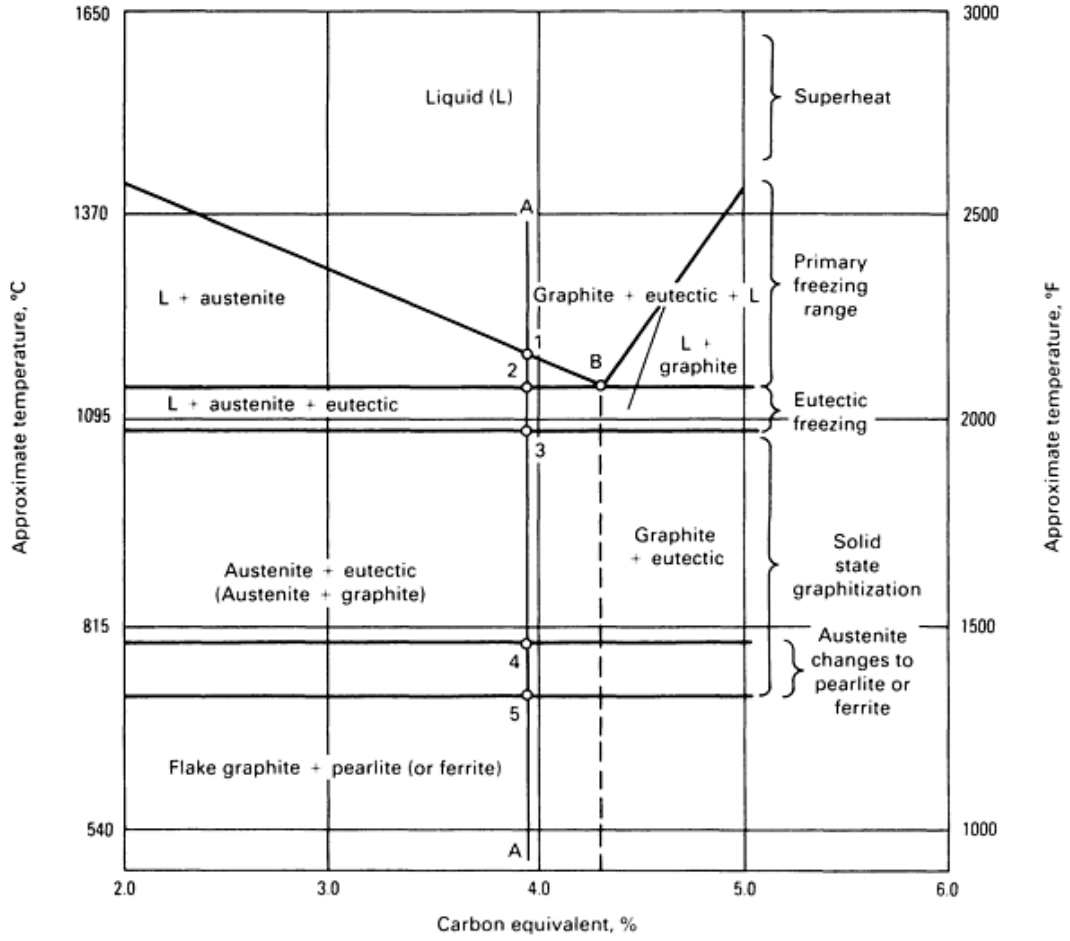

Figure 2.24 Silicon which is added to the molten iron not only decreases the carbon solution in the austenite but also raises the point on which ferrite and graphite are formed by the transformation of austenite phase as temperature decreases. Moreover, if eutectic area that is about 1147 ^{o}C is inspected, there are two lines, the first one is graphite – liquidus line and the second one is austenite – liquidus line. The first one is approximately three times sharper than the second [19, 11, 21].

Prior to the first point, metal is completely liquid due to high temperature. After temperature drops to the bottom of liquidus line, development of proeutectic austenite dendrites are seen due to primary freezing. There are two important factors when determining dendrite sizes (that is C.E.V and cooling rate). If cooling rate increases, the area that is between point 1 and 2 will be passed quickly, so finer

dendrites will form. C.E.V, which is $C + \frac{Si}{3} + \frac{P}{3}$, is also responsible for formation of austenite dendrite sizes. To illustrate, if C.E.V. increases, temperature interval will be closer to eutectic point. Hence, austenite dendrites will be finer [11].

Carbon atoms diffuse from austenite to remaining liquid phase as austenite dendrites grow in the molten iron. Carbon atoms can continue to diffuse from austenite dendrites to remaining liquid as long as carbon level attains 4.3%. Afterwards, eutectic reaction that is L (4.3%C)$\rightarrow \gamma\ (2.08\%C) + C$ is seen. Now, all remaining liquid phase is disappeared during eutectic reaction yielding two different solid phases which are graphite and austenite phases during the stable solidification process [11, 14].

Austenite phase that includes high carbon level at high temperature region of the phase diagram tries to release excessive carbon atoms when temperature starts to get closer to the eutectoid phase transformation reaction temperature. With the help of these processes, eutectoid reaction can be achieved. Austenite phase can transform to pearlite or pearlite and ferrite phases according to alloying elements and solidification rate [11].

Carbon equivalent level ought to be determined carefully in order to obtain high quality compacted graphite iron. This is the reason that, if C.E.V level is too low, white iron can be seen at thin sections of engine block or if C.E.V level is high, excessive graphite flotation that cause kish graphite formation will occur. High quality compacted graphite iron is achieved as carbon equivalent ratio is approximately 4.40% [7, 11].

The first formation of graphite particles leads to an expansion as long as eutectic transformation occurs. This expansion is related to carbon equivalent. During solidification of engine block, requirement of feeding is not required when carbon equivalent increases, since more graphite particles will occur due to high carbon equivalent during eutectic transformation [11].

A decrease in the silicon requirement that is an important element in order to increase graphitization leads to a decrease in the production of compacted graphite because less carbon is used for on the graphite nodules that are produced before.

Also, strengthening of the ferrite phase occurs as a result of solid solution which is promoted by silicon present in the molten iron. For this reason, a decrease in the silicon content will lead to a decrease in strengthening.

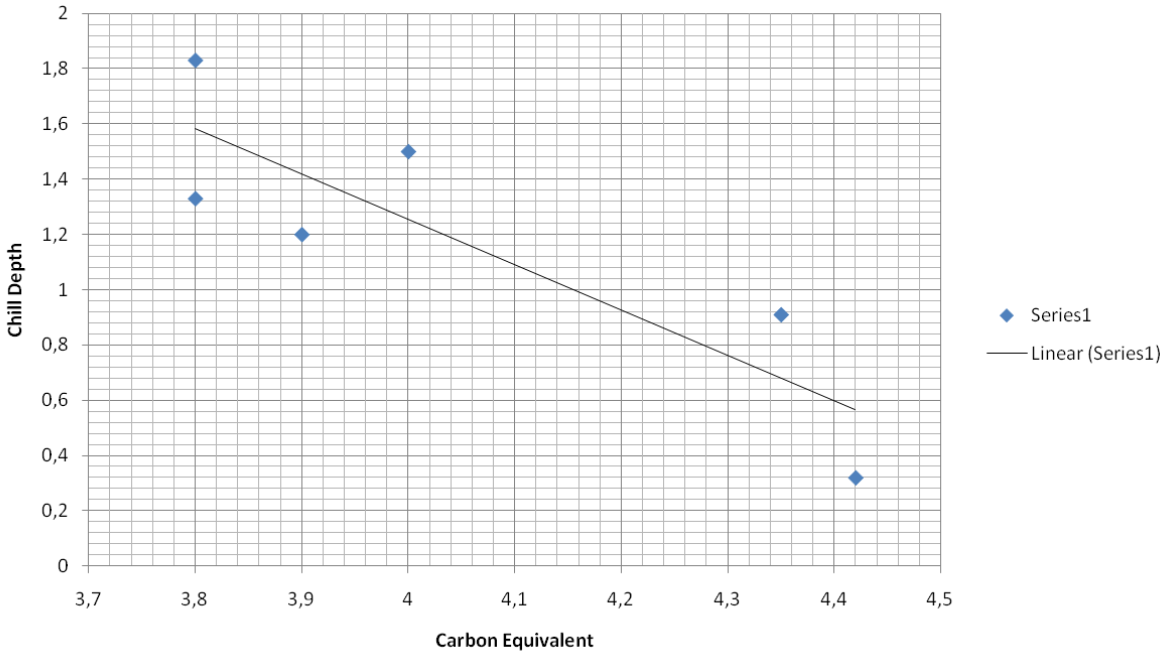

Figure 2.25 Chill depth is also affected by carbon and Si content if carbon equivalent value is low. Chill depth is expected to reach closer to centre of the casting as hypoeutectic cast iron is investigated [18, 14].

The iron matrix containing compacted graphite iron has high thermal conductivity that is an important factor for diesel engine blocks. And ferritic matrix has more advantages than pearlitic matrix in this regard. High Si content helps to encourage ferritic matrix content [25].

2.2.1.5.2 Effects of Magnesium and Sulfur

Magnesium treatment for producing compacted graphite iron involves the addition of Mg so as to alter the graphite morphology. Silicon content in the molten iron should be increased in order to avoid carbide formation in thin sections, so Mg treatment is

combined with FeSi inoculation. The molten iron should generally be at a temperature of 1450 to 1510 ^{o}C so as to be prepared for Mg treatment [11].

Sulphur content in molten iron that can be between 0.008 and 0.018% (this ratio is acceptable when sulphur content is coming from base iron) owns another important characteristic so as to detect variations in active magnesium in molten iron due to the fact that these variations are chiefly affected by sulphur content, used type of ladle to treatment and oxygen level. According to the references; desulfurization can be achieved by means of pure magnesium usage in order to reduce slag formation and furnace cleaning process [34, 4].

Required magnesium content that should be added to produce vermicular iron is mainly based on sulphur content of molten metal and geometry of casting that affect the cooling rate. Excessive Mg will encourage the formation of nodular graphite in the iron matrix. In addition, added magnesium level must be carefully selected to prevent flake graphite formation due to fading [4, 25, 34].

Nodular and compacted graphite content are mainly influenced by the presence of free magnesium content in the cast iron. Even though magnesium addition that is between 0,04 – 0,06% leads to achieve approximately fully nodular graphites, even a small amount of Mg that is 0,025% is sufficient to obtain high ratio of nodularity% that is also based on cooling rate. For this reason, diesel engine blocks that contain some thin sections such as 7.99 and 7.25 mm may have approximately 30% nodularity [25, 35].

After treatment process, magnesium efficiency can change from ladle to ladle since magnesium efficiency can shift from 55 to 77 % according to the changes of factore mentioned above. [34]

The main differences in magnesium efficiency can be faced due to the variations in oxygen contents in molten iron and sulphur; meanwhile, that dissolved sulphur level is another important factor to determine nodularity%. As excessive dissolution causes formation of flake patch microstructure, too low dissolution will encourage formation of nodularity that is higher than expected. Hence, additional amount of FeSiMg alloy should be added to the ladle so as to tolerate excessive sulphur and oxygen content in the molten iron [11, 34].

2.2.1.5.3 Effects of Oxygen (ppm)

Oxygen levels in the molten iron are influenced by three main determiners that are furnace type, iron type and molten iron temperature. An increase in molten iron temperature increases the oxygen content. The thing which is meant by the iron type is that what type of cast iron, such as gray iron, spheroidal cast iron and compacted graphite iron, is desired to produce [36, 37].

As reported in the reference [38], the presence of high amount of oxygen and S in the liquid iron causes the graphite particles to grow usually in the length and width. In order words, the growth of graphite particles is seen throughout the basal planes by means of extending the surface edges. This type of growth is seen in flake graphite formation. Removal of oxygen by means of Mg or Ce treatment or Mn addition results in restricted growth of graphite particles in basal plane direction. The growth of graphite particles of which basal planes are aligned parallel to the surface of the nodule occurs c – axis radially [38, 39].

Oxygen content in the molten iron is expected to reduce with an increase in Mg/S ratio. Too low oxygen content such as 0.034 ppm promotes formation of nodular graphite iron by increasing liquid vapor surface energy. On the contrary, flake graphite formation occurs as oxygen level of molten iron is too high. Based upon oxygen content, growth of graphite particles are illustrated with this approach; that is removal of oxygen and sulphur get graphite particles that are greater than one micron to grow c – axis direction [39].

Mischmetal includes cerium and magnesium as a nodulizing element while FeSiMg has only magnesium as a nodulizing element. The equations of oxygen level reduction in molten metal are given below;

$$\underline{Mg} + \underline{O} = (MgO) \qquad (2.1)$$

$$\underline{Mg} + \underline{Si} + \underline{3O} = (MgSiO_3) \qquad (2.2)$$

$$\underline{2Mg} + \underline{Si} + \underline{4O} = (Mg_2SiO_2) \qquad (2.3)$$

If mishmetal is used to remove sulphur and oxygen in the molten iron, cerium also

reacts with sulphur and oxygen present in the molten iron [39].

$$\underline{2O} + \underline{S} + \underline{2Ce} = (Ce_2O_2S) \quad (2.4)$$

$$\underline{3S} + \underline{2Ce} = (Ce_2S_3) \quad (2.5)$$

$$\underline{S} + \underline{Mg} = (MgS) \quad (2.6)$$

Active oxygen content that is measured by means of Celox foundry cell in the experiments measures a small part of the total oxygen content which is called active oxygen in the molten iron since oxygen level is reduced by means of magnesium which is present in the molten iron. Active oxygen level has an important effect on compacted graphite stable size similar to sulphur [34, 40]

2.2.1.5.3 Effects of Cerium

Cerium is used to achieve high quality compacted graphite iron with the same purpose of magnesium. However, treatment of compacted graphite iron is generally realized by using Mg treatment alloy due to being cheaper than Cerium treatment alloy. Cerium that is added to the molten iron by means of addition of some master alloys such as Misch metal or CompacMag TM during ladle operation neutralizes some elements that have harmful effects on the production of compacted graphite iron diesel engine blocks. These elements are Pb and Sn [7, 25].

Cerium which is present in the molten iron can encourage the formation of chunky type graphite that reduces tensile strength and elongation [25].

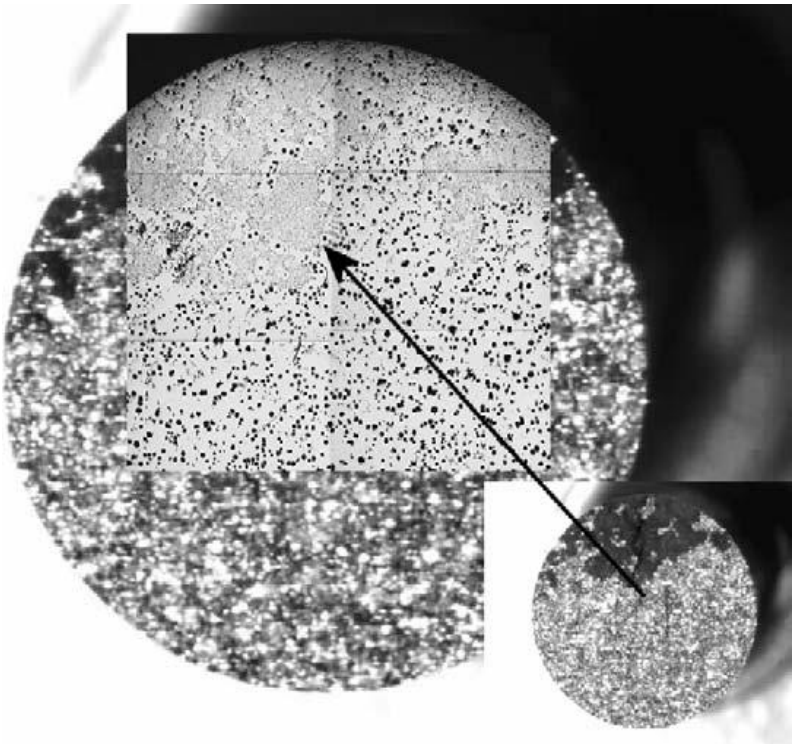

Figure 2.26 Dark areas in fracture surface of test bar (Ø 14 mm) corresponding to the amount of chunky graphite [30].

2.2.1.5.5 Effects of Aluminum

Aluminum is added with the same purpose of titanium, and aluminum usage gives roughly the same results with titanium usage. If Aluminum is added to the molten cast iron, aluminum oxide – based inclusions are expected to be seen on the microstructure of cast iron on account of the fact that these small inclusions act as nucleation areas for graphite production [41].

Al and Zr yield a tendency to promote A type graphite. Otherwise, Ti has a tendency to promote D type graphite in gray cast iron. Aluminum that can cause a formation of hydrogen pinhole defects is useful to neutralize nitrogen. In the experiments, added inoculants are source of aluminum [11, 41].

2.2.1.5.6 Effects of Phosphor

Phosphor content should be lower than 0.15% in order to achieve high quality machinability. In addition, carbon equivalent is also affected by phosphor present; boundry is given below; [14].

$$C.E.V = C\% + \frac{(Si\% + P\%)}{3} \qquad (2.7)$$

Especially phosphor that increases fluidity of molten metal and other trace alloying elements are responsible for presence of liquid channels by segregation process. This occurrence has a great significance when spheroidal graphite particles that are formed during proeutectic reaction transforms from nodular shape to worm shaped compacted graphite iron [6, 11].

When phosphor is present in the cast iron, phosphor and iron can form steatite phase of which temperature is approximately 954 – 982 ^{o}C. Steatite phase that is composed of 10.2% phosphor appears last solidified part of casting. Moreover, steatite phase is as hard as Fe_3C (cementite) [14].

P level is prefered to be lower than 0.06% so as to obtain enhanced ductility of compacted graphite iron. During production of compacted graphite iron approximately 0.04% phosphorus is always present in chemical composition of all of the experiments so as to increase ductility [11].

2.2.1.5.7 Effects of Manganese

Harmful effects of sulphur can be prevented by means of Mn (Manganese) addition. After addition of manganese, manganese will form manganese sulfides; hereby, sulphur present in the molten iron has been stabilized by forming of mangane sulfides [11].

$$Mn\% \geq S\% + 0.2\% \qquad (2.8)$$

Manganese sulfides that are generally round shaped inclusions are produced by means of Mn addition to the molten iron in order to avoid formation of brittle Fe – S [11].

S present in the gray cast iron is consumed by Mn to form small inclusions that are approximately 10 μm in size and soft (MnS) inclusions, but as production of compacted graphite iron is examined, Mg addition to the molten iron is used to react with sulphur and oxygen. Magnesium sulfide (MgS) inclusions are preferentially formed as (MnS) since Mg is a stronger sulfide former than Mn. It also has a deoxidizing property so (MgO) and magnesium silicate ($_xMgO._ySiO_2$) inclusions can be present in compacted graphite iron diesel engine blocks. These inclusions are stronger and harder than manganese sulfide inclusions that are found in gray cast iron [17].

2.2.1.5.8 Mold Material

Mold material selection ought to be made carefully for compacted graphite production process since molten iron can simply pick up sulphur when touching with mold material. For this reason, selection of mold material and its hardening catalyst for compacted graphite iron is not simple as that of spheroidal graphite iron that can be bentonite, cementite or resin sand mold. High quality compacted graphite iron can be achieved by using resin sand mold. During this process, paratolusulfonic acid (PTS) that leads to an increase sulphur level in the molten iron is not used as catalyst. Mold material used in our experiments consisted of Furan resin and Silica sand [11].

CHAPTER 3

EXPERIMENTAL PROCEDURE

3.1 Production of Compacted Graphite iron

3.1.1 Induction Furnace

Diesel engine blocks were produced at Odöksan Osmaneli A.Ş. by using medium frequency induction furnace operated at 500 to 5000 Hz frequency current. Approximately 3500 kg spheroidal pig iron, 1000 kg steel scrap, 42 kg spheroidal carbon and 120 kg FeSi was used as the basic charge materials that were melted inside rammed silica refractory lining. Induction furnace coil is made of copper tubing and a high frequency magnetic field is generated by current passing through this coil which is cooled by intense water cooling inside.

During base iron alloy preparation stage, the sulphur content is kept low. Base iron that will be used to achieve high quality compacted graphite iron should have low sulphur such as 0.02%. C.E.V level for compacted graphite iron is approximately 4.3%. This ratio is higher than that for gray cast iron [16].

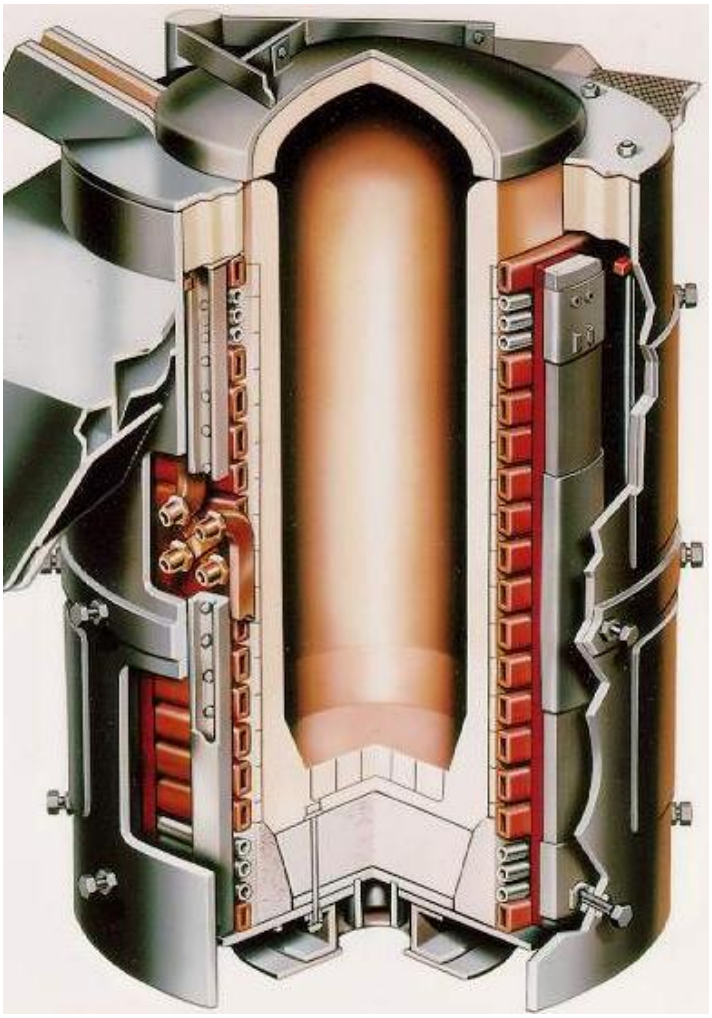

Figure 3.1 Induction furnace used for melting of the charge [10].

3.1.2 Mg Treatment and Inoculation with Ladle Process

Compacted graphite iron diesel engine blocks were produced by using ladle treatment technique in our experiments. This method is one of the most important techniques in respect to alloying elements that are added to the molten iron during production [24].

Required metal to achieve diesel engine blocks, each one weighs about 125 kg, were prepared in induction furnace by melting steel scrap, SG iron returns, FeSi alloy. A base treatment alloy packed should be placed in the pouring ladle in order to keep in under sufficient hydrostatic pressure of coming liquid cast iron alloy during melt

delivery into the ladle to have sufficient Magnesium recovery. (In addition, variation in time during ladle operation such as holding, transport and pouring can easily alter the ratio of magnesium fading). Afterwards, the liquid alloy was poured into furan binder silica sand moulds. Total treatment operation took approximately 2 – 3 minutes and pouring was completed in about 12 – 15 seconds. After allowing sufficient time, diesel engine block was removed and obtained by shakeout process after 150 minutes [5, 4, 41].

Charges that were consisted of Sorel white iron and steel scrap and different master alloys. The MgFeSi, Ce Mischmetal and other base treatment alloys for production of compacted graphite iron were less required than those which were required to treat spheroidal graphite iron. Due to small quantity of Mg, when molten iron was treated with base alloys such as the MgFeSi, excessive Mg vapor flame was not seen above the pouring ladles [5].

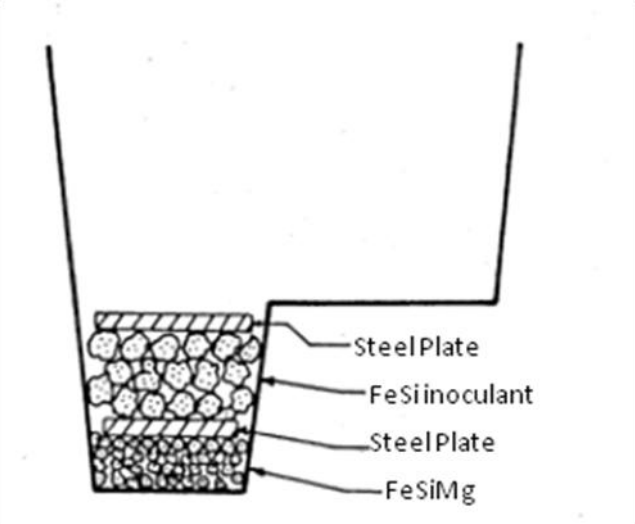

Figure 3.2 A simple sample of ladle pocket method was used to change the form of graphite in all our experiments. A base treatment alloy packed should be placed in the pouring ladles in order to keep in good condition of sufficient magnesium recovery [5].

Inoculants and magnesium and/or cerium treatment alloy were added to the Ladle pocket in a sequence that is FeSi inoculants were placed on top and had a steel plate on itself. Then, Mg – Ce treatment master alloy having finer particle size than FeSi inoculant was placed at the bottom of the pocket. Before Mg treatment, 350 gr Mn was added to ladle in order to increase Mn content in the molten iron from 0.1% to 0.21%.

Surface of liquid metal should be cleaned from dross in order to remove dross inclusions before pouring. In addition, the liquid metal was heated between liquid and molten iron temperature in order to keep fluidity high enough to fill thin sections of casting cavity. The liquid metal temperature was kept to sufficiently higher when filling the thin sections of mold. Time from ladle to pouring is also another important factor. If this time is increased, effectiveness of inoculants will be slightly lost due to fading [11].

3.1.3 Master Alloys

During casting trials, four different master alloys with different chemical composition were placed into ladle cavity during production of different diesel engine blocks.

About 52 gr Mischmetal was used so as to produce engine block for each ladle until production of diesel engine blocks 6 to 9. Mischmetal is also called Cerium Mischmetal or Rare earth Mischmetal. Chemical composition of it can be seen at Table 3.1.

Table 3.1 Chemical composition of Cerium Mischmetal.

Cerium	50 %
Lanthanum	25 %
Neodymium	15%

Rare – earth metals	10%
Iron	Balance

Mischmetal has been applied on relatively large scale in foundry technology in order to make FeSiMg alloy since the early 1990. Mischmetal is also used to remove free oxygen and sulphur which are present in the molten iron by stable oxysulfide formation [41].

600 gr Snam (FeSi base alloy) was used as inoculant for each ladle of our all experiments except for diesel engine blocks 12 to 19 because Snam master alloy is ideally suitable in order to produce high quality of compacted graphite iron.

Table 3.2 Chemical composition of Snam

Silicon	50 – 60%
Calcium	1.8 – 2.5%
Aluminium	0.80 – 1.25%
Lanthanum	1.75 – 2.25%
Iron	45 – 33%

Size of the snam inoculant can be changed between 12 and 0.20 mm with regards to orders. Diesel engine blocks 6 to 9 Diesel engine blocks were produced by using Snam and its size was changed between 2 and 6 mm [18].

After production of Diesel engine block 4 was completed with Mischmetal used as inoculant, diesel engine blocks were produced with addition of CompactMag TM alloy [3, 42].

Table 3.3 Chemical composition of CompactMag TM alloy.

Silicon	44 – 48%
Magnesium	5.0 – 6.0%
Calcium	1.8 – 2.3%
Rare – earth metals	5.5 – 6.5%
Aluminum	max 1.0%
Iron	Balance

Foundrysil that is used as an inoculant instead of Snam with the same ratio at the two castings, which are diesel engine blocks 12 to 19, is a (Elkems) commercial product [36].

Table 3.4 Chemical composition of Foundrysil

Silicon	73 – 78%
Calcium	0.75 – 1.25%
Barium	0.75 – 1.25%
Aluminum	0.75 – 1.25
Iron	Balance

3.1.4 Oxygen Measurement in Liquid Cast Iron

Measurement principles of the celox foundry sensor are presented by Heraeus Electro – Nite. “The measurement of active oxygen is based on the use of an electro – chemical cell in combination with a thermocouple. The cell consists of a solid electrolyte in the form of a closed end tube, filled with oxygen reference material. When immersed in liquid metal, the cell will produce an EMF as a result of different oxygen activities at both sides of the solid electrolyte” [35].

Celox foundry sensor that was developed by Heraeus Elektro – Nite is a new model as for CE10910600 which is generally used to determine low oxygen level in steel. Celox foundry sensor is developed to be a sensor that can determine ultra low oxygen level in cast iron. Therefore, this foundry sensor can evaluate active oxygen content until 0.01 ppm. The Celox Foundry sensor calculate active oxygen (ppm) level by means of following formula derived from Nernst's law [35, 40].

$$\log a(O) = 8.62 - \frac{13580 - 10.08(E+24)}{T} \qquad (3.1)$$

Where E is EMF (in mV) value, O is oxygen ppm value in the molten iron and T is temperature (in ^{o}K) value of molten iron that is obtained after treatment process [35].

Production of compacted graphite iron is too difficult process due to the fact that vermicular iron is stable within a very narrow area, so active oxygen results that were achieved by means of Celox foundry sensor were very helpful to obtain high quality compacted graphite diesel engine blocks.

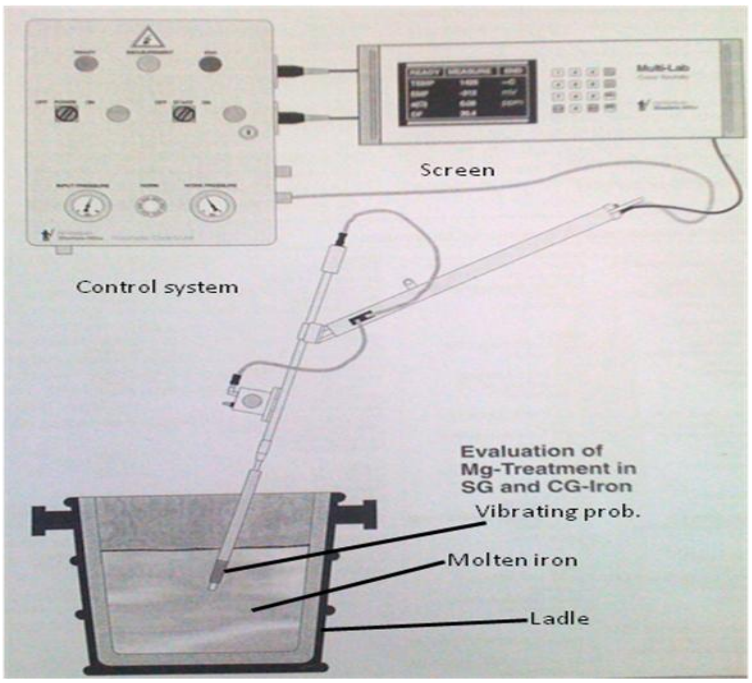

Figure 3.3 The Celox foundry sensor not only measures active oxygen content but

also measures temperature of the molten iron. Vibrating lance is an important part of the test specimen in order to achieve correct datum from the molten iron [35].

3.1.5 Diesel Engine Block

44 diesel engine blocks were produced at Odöksan by casting into furane binded silica sand moulds in this work and each one was approximately 125 kg in weight. After casting, 14 different points with different section thicknesses are examined. They are given in Table 3.5 and marked on the diesel engine blocks.

Table 3.5 Different thicknesses of diesel engine block

Samples	Average Thicknesses (mm)
No 1	32.72
No 2	36.26
No 3	35.86
No 4	9.82
No 5	40.85
No 6	7.99
No 7	11.08
No 8	7.25
No 9	13.94
No 10	16.30
No 11	10.95
No 12	12.71
No 13	10.39
No 14	9.48

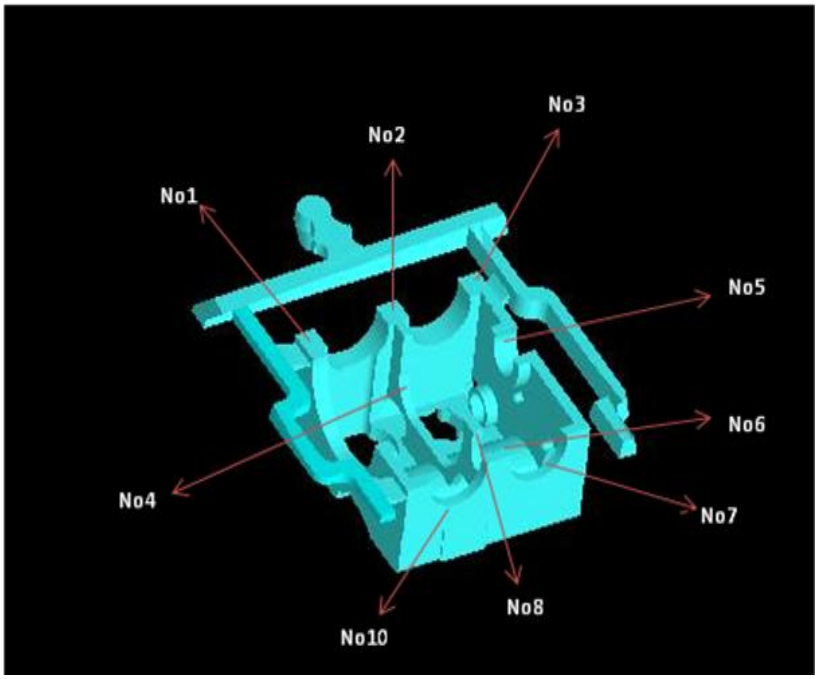

Figure 3.4 First five samples and samples 6 – 7 – 8 – 9 can be seen on the figure above.

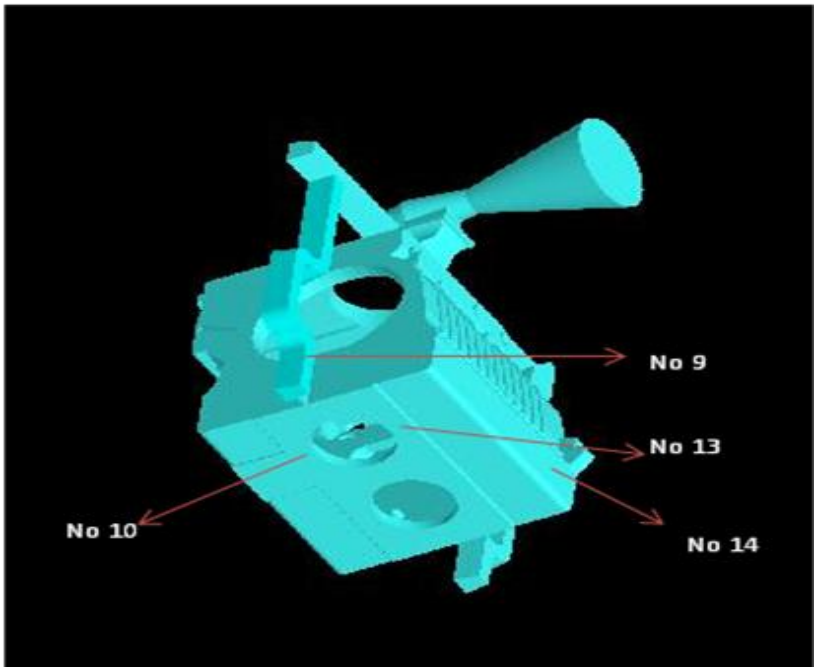

Figure 3.5 Samples 9 – 10 – 13 – 14 were taken from the points marked on the figure

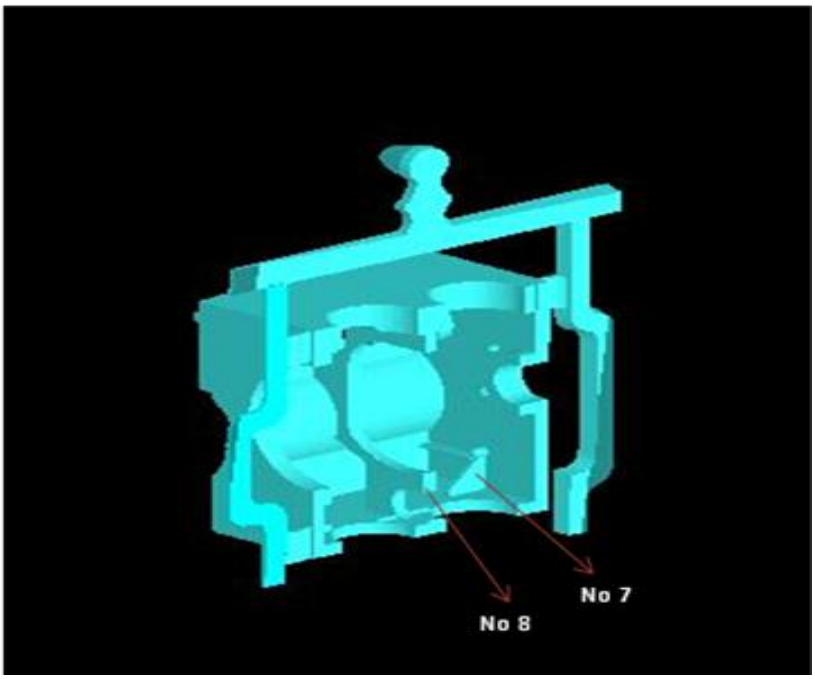

Figure 3.6 Samples 8 and 7 can be easily seen in this figure

3.1.6 Step Block Casting

Step block castings were produced side by side during engine block casting. Then they were used to represent different thickness of diesel engine blocks. Moreover, step block castings were designed to consist of different thicknesses with 5 – 9 – 14 – 26 mm to reveal the effect of treatment and inoculation on the section thickness.

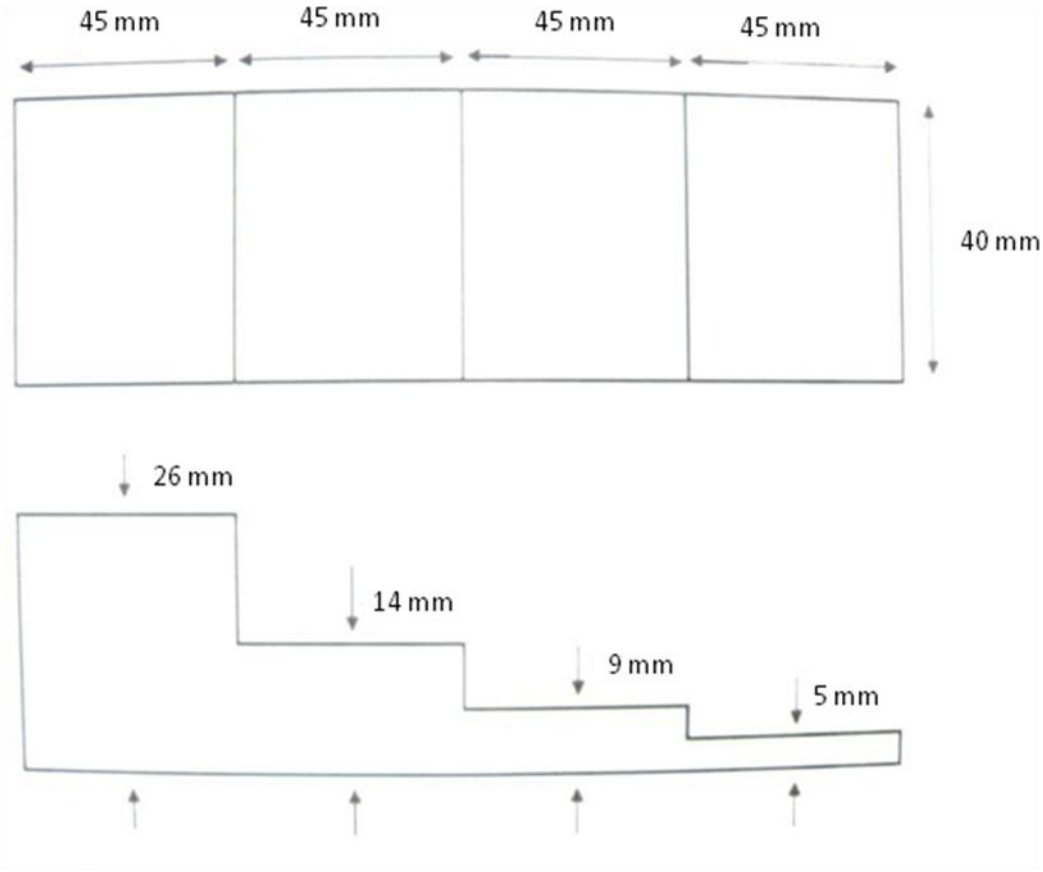

Figure 3.7 A sample of step block cast with 5 – 9 – 14 – 26 thick steps [33].

Mold of step block castings were placed near mold side by side of diesel engine block to have the same chemical composition with diesel engine block. Each step block has been produced with different pouring temperatures, chemical composition which has different Mg/S ratios and treated with different commercial FeMgSi master alloys and inoculants. Microstructure differences of each different thick step can be seen in figure 3.8 through figure 3.11.

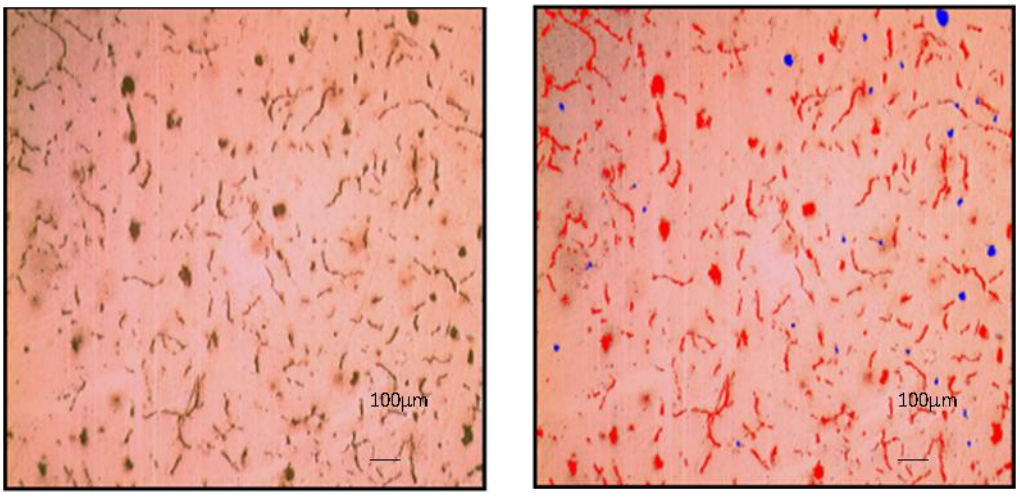

Figure 3.8 A section of step block casting has 5 mm thickness.

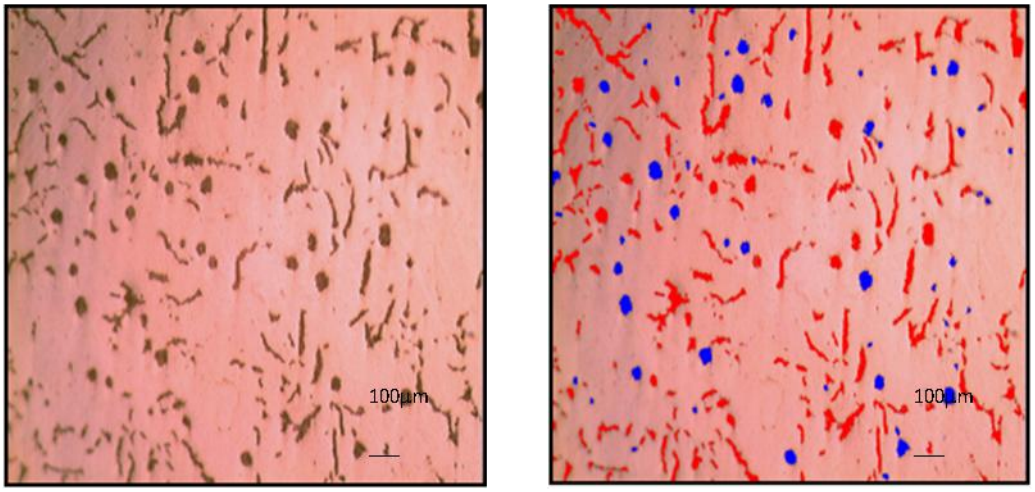

Figure 3.9 A section of step block casting has 9 mm thickness.

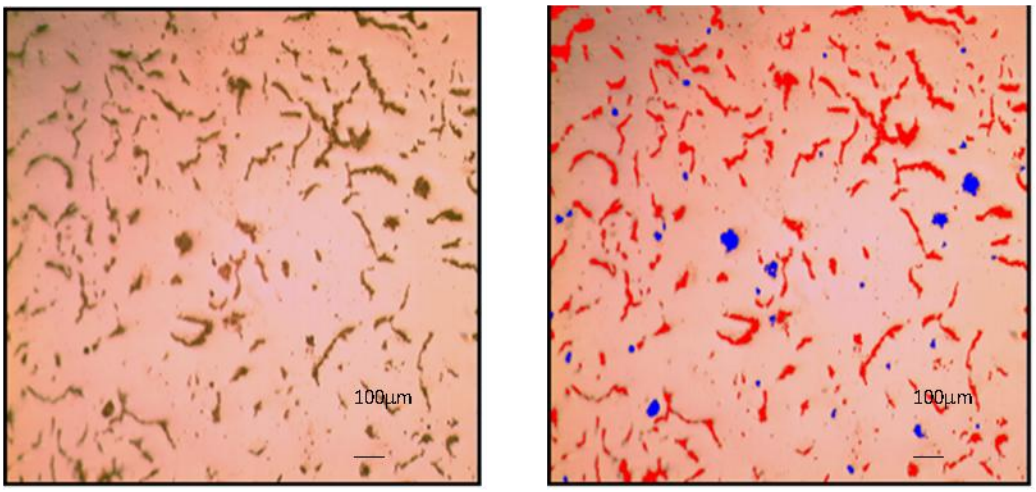

Figure 3.10 A section of step block cast has 14 mm thickness.

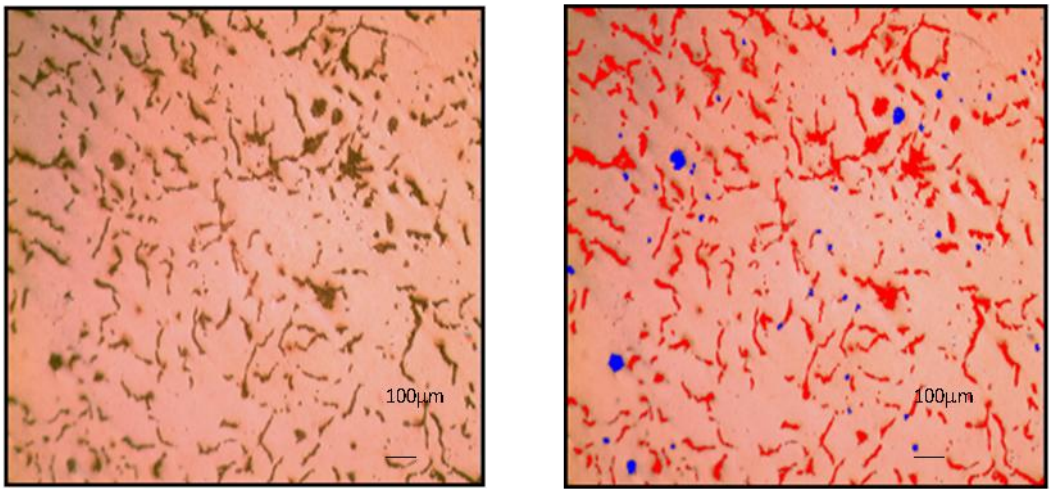

Figure 3.11 A section of step block cast has with 26 mm thickness.

3.2 Characterization

3.2.1 Optical Microscopy

Microstructures of diesel engine blocks were examined by means of optical microscopy. The samples were prepared following standard metallographic procedures. The samples were always cut from the same 14 different sections of the

diesel engine block parts with different thicknesses and then some of them were mounted in bakalite. After that, samples were grinded automatically or manually with 180X, 300X, 600X, 1000X and polished with diamond suspension with 1μm particle size. Then, the samples were etched in 2% Nital solution. This method is chosen due to its reliability and consistency. An SOIF XJP – 6A optical microscope was used for taking the representative photographs of the resulting samples.

Figure 3.12 SOIF XJP – 6A optical microscope

3.2.2 Image Analysis

While examining each diesel engine block, four or nine different sections from the same sample were evaluated in order to measure all local sections of the same sample. In addition to that, during this process, nodularity percentage values were determined by using optical metallography and an image analysis program.

Nodular graphite that is present in cast iron is analyzed by Material plus 4.1 image analysis software. The nodules were separated from compacted graphite by means of

ASTM A 247 in the micro structure on predefined spheroidalid nodulus with blue color and others which are colored with red color in the image.

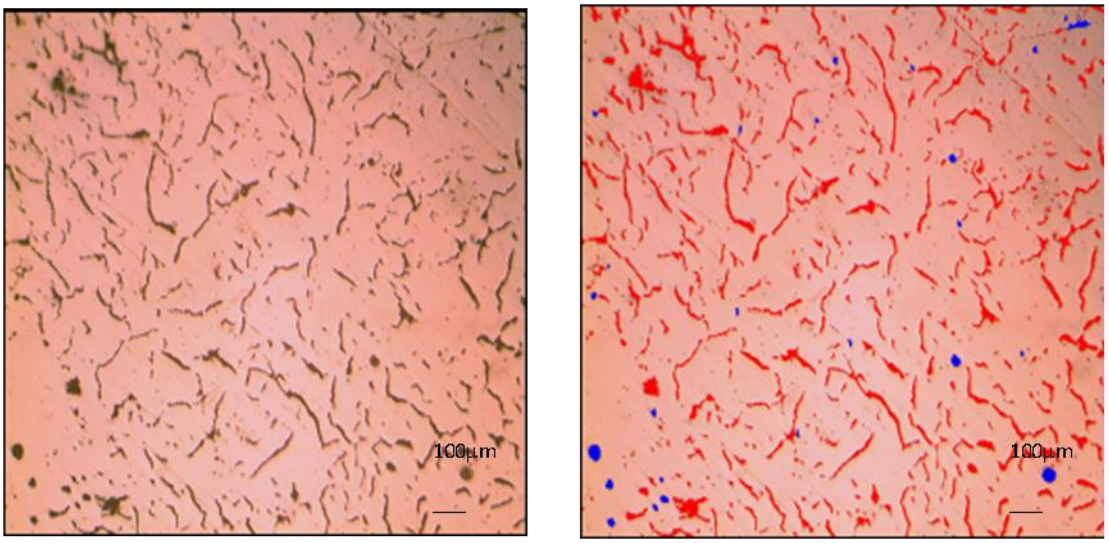

Figure 3.13 Nodularity measurement of the sample that was obtained by means of Material plus 4.1 image analysis code is approximately 19% nodularity and remaining is compacted graphite iron.

ASTM A 247 is selected to be used in our experiments, because ASTM A 247 is used for assessment of the classification of graphite in cast irons on account of graphite types and distribution. According to the ASTM, ASTM A 247 can be simply used for gray irons and spheroidalidal graphite irons. Since compacted graphite iron has properties between gray and ductile iron [4, 43].

3.2.3 Solidification Simulation

NovaCast NovaFlow code was used for simulation of instantaneous solidification in different section thicknesses with different time steps of diesel engine blocks. During solidification simulation input parameters were introduced and were performed, boundary conditions, mold material selection, pouring rate and mesh building were numerically determined.

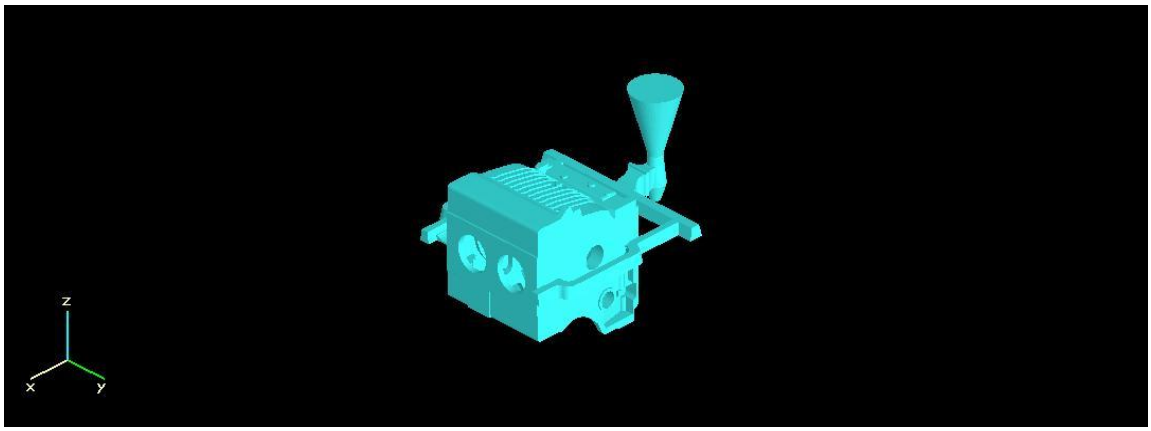

Figure 3.14 3D drawing of the diesel engine block model was composed of approximately one million meshes. Therefore, one solidification simulation lasted about 5 hours.

Inputs that represent the process variations should be carefully selected to attain the best results from simulation. Otherwise, simulation results do not give the true results and these results can also be misleading.

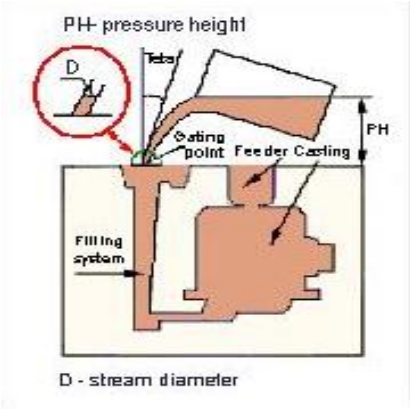

Figure 3.15 A simple sample of ladle pouring technique was used in our experiments

Liquid metal that was present in the ladle was poured into the mold cavity from approximately 200 mm high and liquid metal was poured with and its flow rate is about 6.297 kg/s. Afterwards, castings were allowed to cool to room temperature of approximately 25 ^{o}C. If stream diameter and stream area are calculated before casting, results will be 25.900 mm and 526.855 mm^2 respectively.

3.2.4 Linest Code

Linear regression analysis was performed to correlate the variables of engine block castings. Depending on some variables in diesel engine block production, the nodularity percentage values that belong to the same thickness of the diesel engine blocks were studied with the help of excel Linest code. The effect of variations on compacted graphite iron (vermicular iron) was tried to be seen by means of Linest code.

3.2.5 Ultrasonic Test

The main reason why this study was conducted is to examine the values of diesel engine blocks produced - Nodularity % without cutting the engine blocks. As a consequence, engine blocks might be used after testing. After testing, using the velocity versus nodularity percentage values that were achieved by ultrasonic testing were obtained as a result.

CHAPTER 4

RESULTS AND DISCUSSION

Since the target value of different sections of the engine blocks studied in this work is to achieve maximum 25% volume of nodular graphite structure with the remaining matrix containing compacted graphite, engine blocks were produced by furan resin binded silica sand moulds after carefully treating the liquid cast iron alloy by optimum Mg in special master alloy based on FeSi – Rare earths by using ladle method via at ELBA Basınçlı Döküm Odöksan Cast Iron Foundry in Osmaneli, Turkey. Chemical composition such as Mg/S, O (ppm), carbon equivalent, and cooling rate of diesel engine blocks were investigated in order to achieve high quality compacted graphite iron because chemical composition and cooling rate of various thickness and filling sequence of different thickness in mold cavity have a great influence on microstructure of vermicular iron products. Influence of chemical composition and cooling rate were determined by means of image analysis software and NovaCast NovaFlow simulation code. The amount of 26 diesel engine blocks were produced and approximately 550 sample that were taken from diesel engine blocks or step block castings were investigated in this study.

4.1 Compacted Graphite Iron Casting

Casting of compacted graphite iron product is a hard issue when spheroidal and flake graphite iron casting is considered because formation of worm shaped graphite particles are stable for some restricted conditions. Moreover, difficulties to produce diesel engine blocks can be listed as interrelation between alloy chemistry, cooling

conditions and physical characteristics such as weight, volume and geometric complexity of casting which require almost minimum tolerance or without any type of mistake. Therefore, chemical composition of casting is to be prepared very carefully such as sufficient Mg level, free oxygen and inoculation requirement. As a matter of fact, chemical composition that allowed for the formation of compacted graphite iron in a particular foundry might not work for another foundry [4].

Solidification simulation of diesel engine block was carried out to reveal cooling conditions of different section, the effect of alloying elements and the ultrasonic test were studied to understand compacted graphite iron formation in different section thickness of the particular diesel engine block studied in this work. The chemical compositions and pouring temperature of each heat were tabulated in Table 4.1.

Table 4.1 Descriptions of the diesel engine blocks that were produced at Odöksan A.Ş.

Diesel Engine Code	**C.E.V**	**O_2(ppm)**	**Mg/S**	**Pouring Temperature ^oC**
1	4.61	0.2181	1.07	1410
2	4.47	0.2162	1.33	1394
3	4.38	0.3926	1	1417
4	4.41	0.2286	0.81	1421
5	4.39	0.1839	0.82	1418
6	4.52	0.3127	1.05	1441
7	4.29	0.4522	1	1445
8	4.36	0.405	1.15	1437
9	4.36	0.369	0.93	1437
10	4.31	0.4654	0.68	1431
11	4.29	0.5148	0.76	1449
12	4.27	0.1965	0.65	1410
13	4.45	0.1686	1	1392

14	4.42	0.1109	1	1393
15	4.43	0.384	0.8	1424
16	4.27	0.17	1.54	1404
17	4.20	0.272	0.92	1413
18	4.26	0.2652	1.1	1426
19	4.28	0.3196	0.76	1424

4.1.1 Solidification Features of Diesel Engine Block

Solidification behavior of the molten metal was examined to obtain best results by means of reducing the degree of process variations.Cooling rate has a great influence on formation of compacted graphite iron. The pouring temperature was in the range of 1379 to 1450 ^{o}C. Temperature of liquid metal was around 1480 ^{o}C and below 1510 ^{o}C in our experiments since possibility of undercooling raises during solidification process as temperature of molten iron was heated above 1510 ^{o}C. [4, 11, 14].

Compacted graphite iron percentage values presented in this thesis were acquired from 19 different diesel engine blocks. The data changed from section number 1 to 14 in a diesel engine block. In other words, compacted graphite iron percentage value was not constant in all sections of the diesel engine block. The effect of cooling rate and undercooling in various section thicknesses were studied by means of NovaCast – NovaFlow simulation code.

16 different diesel engine blocks have been simulated so far. Simulation of the diesel engine block 7 that was poured at 1445 ^{o}C was compared with number 13 diesel engine block simulation that was poured at 1392 ^{o}C. In the meantime, temperature differences between 13 different section thicknesses can be also noticed with the help of figures below in the fallowing pages. And Table 4.2 shows nodularity percentage values of 14 different section thicknesses of diesel engine block number 7 and 13.

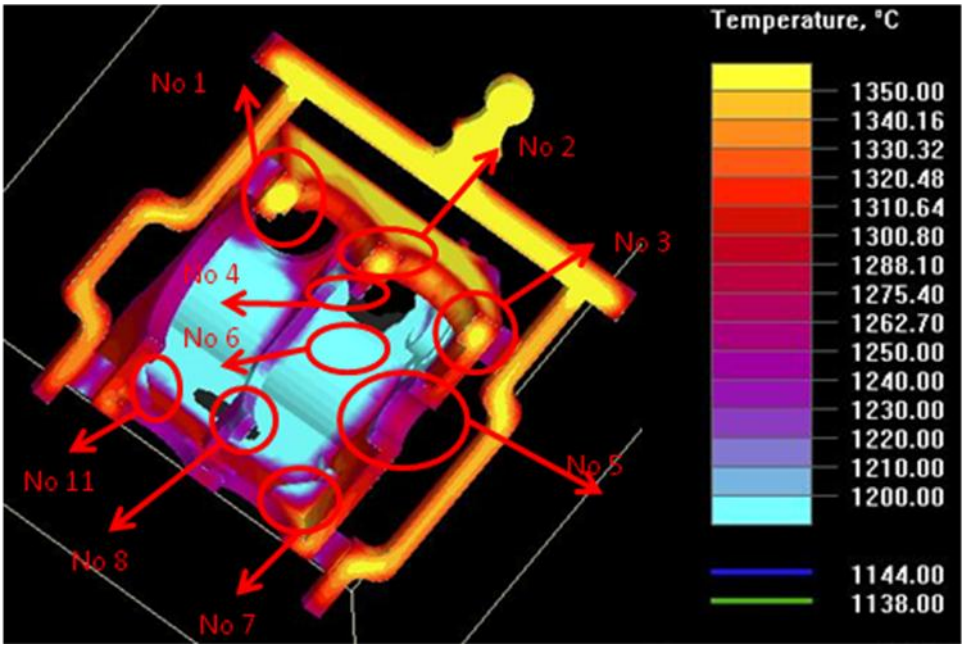

Figure 4.1 Blue areas are low temperature regions. Moreover, yellow and red areas are high temperature regions. Temperature differences of sample engine block 7 can be seen around the whole engine block and in some thickness sections. To illustrate, when section number 7 that consisted of rectangular shape was examined, remote parts of the corner had low temperature that was approximately 1216 ^{o}C, but parts closer to the corner had higher temperature. This temperature could change from 1228 to 1321 ^{o}C for diesel engine block 7. For this reason, sample that was taken from section number 7 could include high or low nodularity percentage value according to the sample which was taken from remote or close to part of the corner.

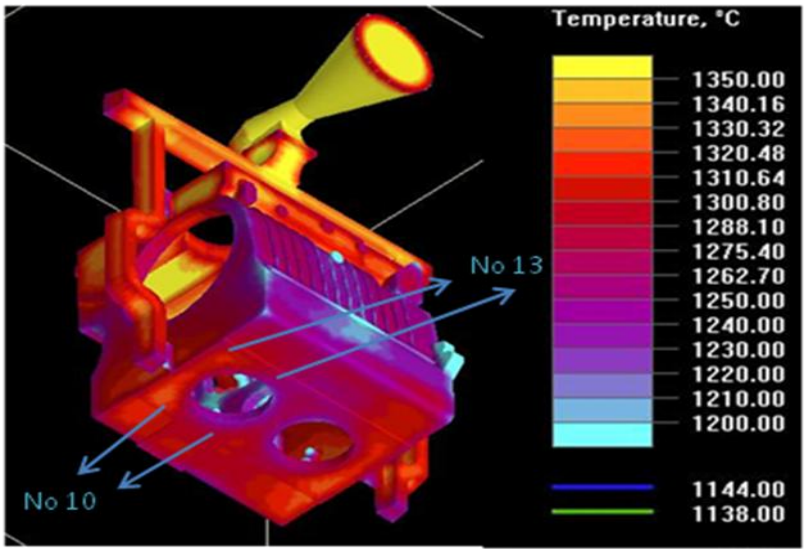

Figure 4.2 Section numbers 10 and 13 are marked in this figure. These two section included parts that were close to the runner, so these parts were hotter than the other parts that were remote from the runner. Hot sections of the number 10 and 13 could change from 1287 to 1313 ^{o}C and those sections also had cold parts that were remote from the runner and its temperature could change from 1232 to 1277 ^{o}C. For this reason, nodularity% value could alter in the same thickness depending on where the sample was taken.

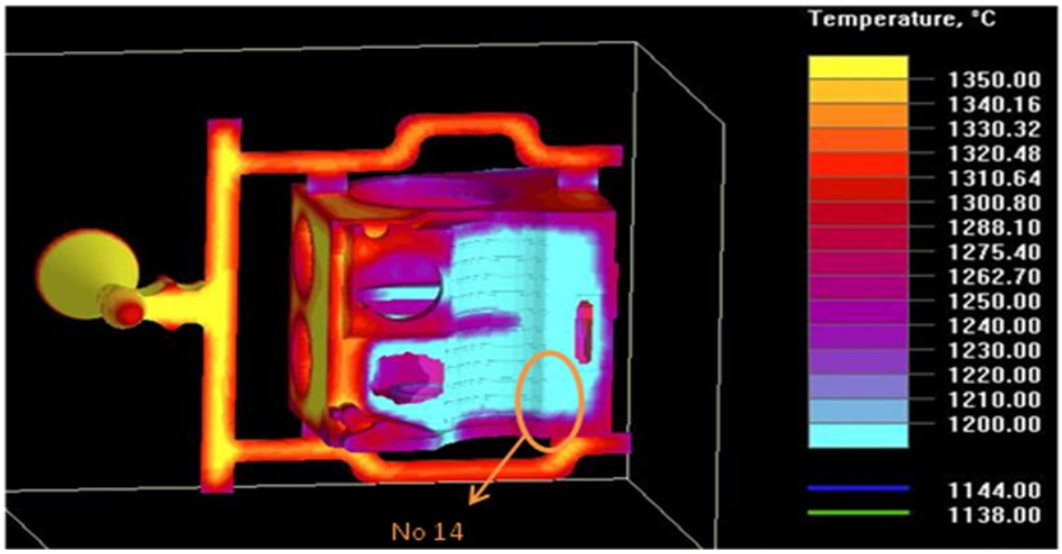

Figure 4.3 Temperature of section number 14 was variable depending on where the

sample was taken. Temperature could change from 1151 to 1262 ^{o}C for diesel engine block 7. Therefore, nodularity% is a function of cooling rate and undercooling.

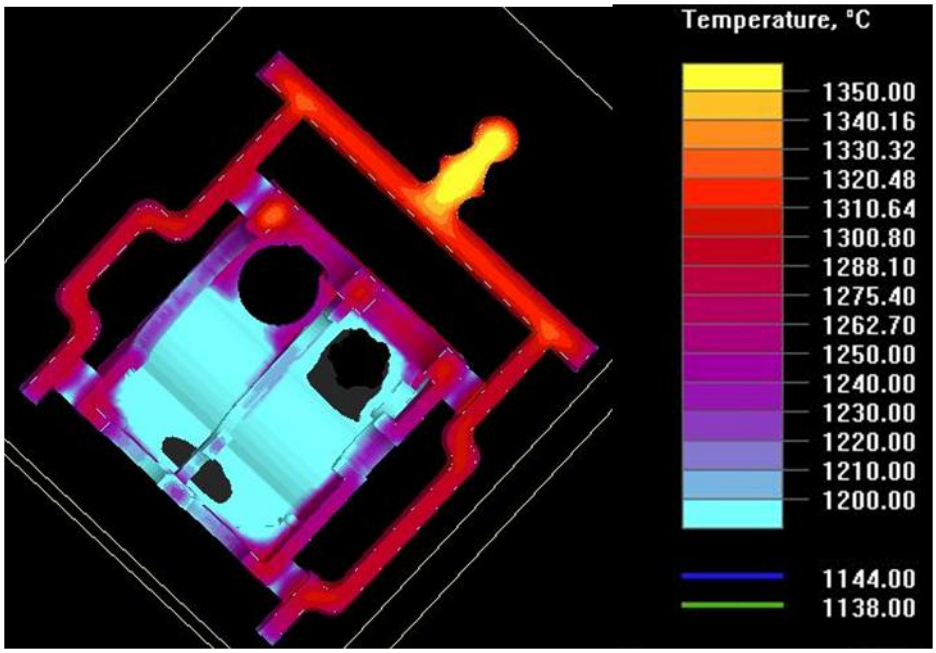

Figure 4.4 Simulation results of diesel engine block 13 of which description was given in Table 4.1 can be noticed in this figure. Due to its low pouring temperature, 1392 ^{o}C, different sections of the diesel engine block resulted in low temperature when it is compared to other heats of the same thicknesses of diesel engine block 7. Even though chemical compositions of engine blocks were close to each other, nodularity percentage values were determined to be different due to different cooling rates. Diesel engine block 7 which had high pouring temperature posses lower nodularity% value than diesel engine block 13 having slow cooling rate. In the case of slow cooling conditions graphite nucleation and growth in worm shape graphite which is called compacted graphite is expected if chemical conditions are satisfied. Otherwise, nodularity percentage values would be quite different although liquid iron had the same temperature in the ladle before pouring. To illustrate; diesel engine block 2 that was poured at 1394 ^{o}C could contain 27 – 39 % nodularity values depending on section thicknesses.

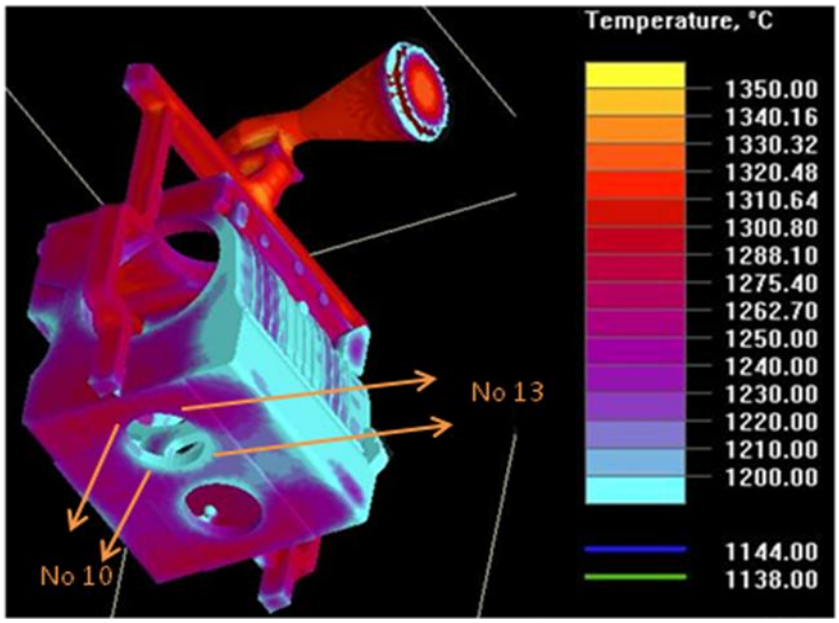

Figure 4.5 Temperature differences within the same thickness can be easily noticed in this figure. Blue area of section number 13 of diesel engine block 13 represents the cold region. In this section temperature changes from 1186 to 1208 ^{o}C. Red area of section number 13 of the same engine block represents relatively hot region whose temperature changes from 1222 to 1264 ^{o}C.

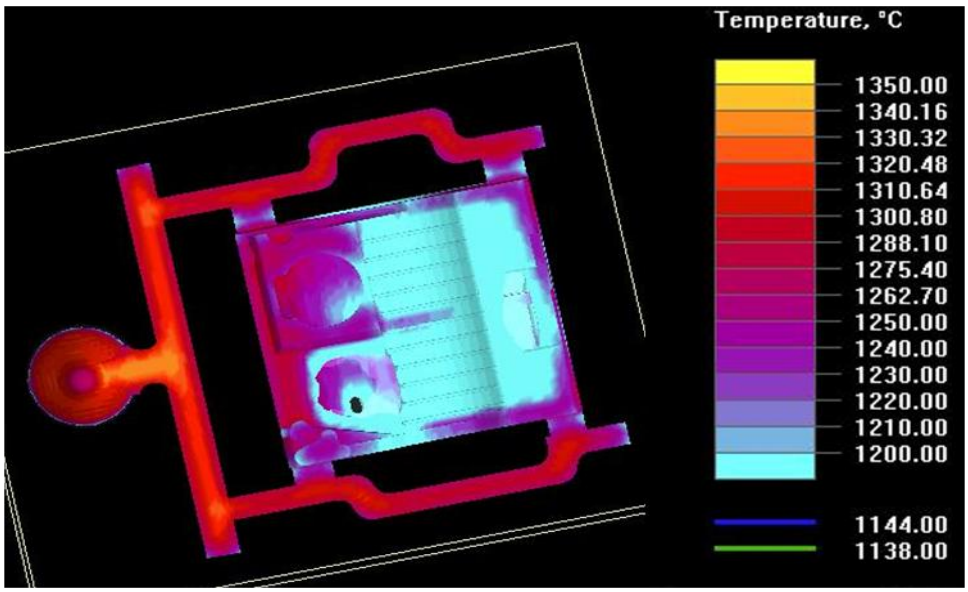

Figure 4.6 Section number 14 can be easily noticed in this figure. Its highest temperature was 1234 ^{o}C and this region is close to the runner and gating system.

Other section thicknesses can be compared to their own diesel engine block since every engine block was produced with different chemical composition. In other words, each one had different Mg/S ratio, accordingly different Oxygen (ppm) ratio and also different carbon equivalent.

Table 4.2 Nodularity percentage values against section thicknesses of diesel engine block 7 and 13 are given in this table.

Section Number	Section thickness (mm)	Diesel Engine Block 7 Nodularity%	Diesel Engine Block 13 Nodularity%	Diesel Engine Block 2 Nodularity %
1	32.72	22	26	35
2	36.26	23	25	28
3	35.86	25	17	27
4	9.82	34	25	35
5	40.85	20	23	39
6	7.99	27	22	33
7	11.08	34	38	34
8	7.25	40	32	35
9	13.94	21	32	27
10	16.30	36	21	31
11	10.95	32	26	33
12	12.71	25	27	28
13	10.39	22	30	39
14	9.48	30	23	32

Section number 1, 2, 3 and 5 belong to the thickest part of the diesel engine block, so these sections were expected to have lower nodularity percentage values than the other thin sections. This case is usually true but in some cases, thick parts may

contain higher nodularity% value. If the region where the sample is cut is found to be in cold part of the section to be selected, values of nodularity percentage have to be higher than expected. To illustrate, the section 5 with 40.85 mm thickness which is the thickest section of the diesel engine block was expected to contain higher compacted graphite iron. Although section number 5 had low nodilarity percentage value in most cases, it could also contain 27 – 41% nodularity according to chemical composition and region temperature where the sample was taken.

Section number 1 with 32.72 mm thickness and section number 3 with 35.86 mm thickness were one of the thickest parts of the diesel engine block. Moreover, these two sections were placed very near the gating, which helped them to have higher local temperature ratio than the other sections in the diesel engine block. Therefore, after samples which were obtained from section number 1 and 2 were examined by means of image analysis, it revealed that these two sections generally contained 0 – 20% nodularity.

Section number 2 that had 36.26 mm thickness was another hot and thick section of diesel engine block. As predicted, this section had also low noduarity% value and was suitable for our purpose.

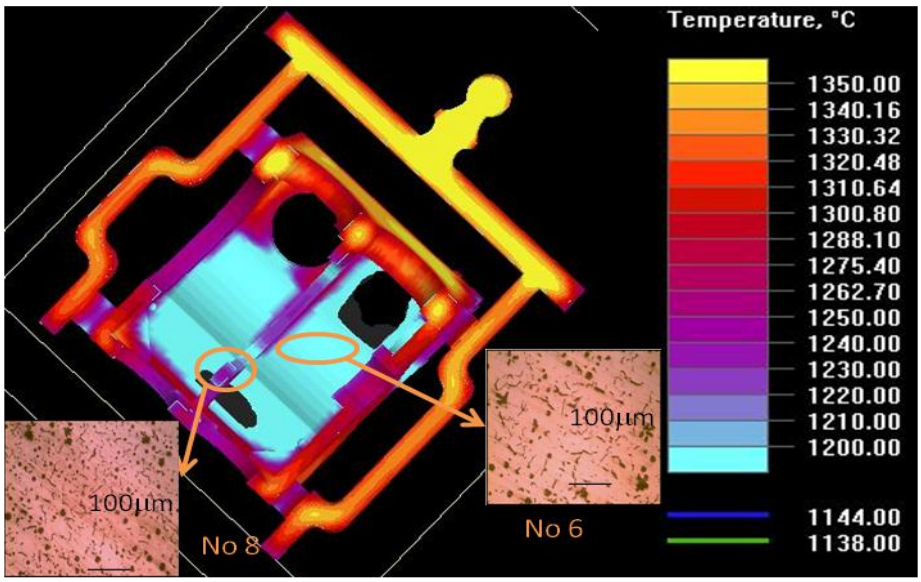

Figure 4.7 As it can be seen in the figure of diesel engine block 9, they contained

different solidification time due to temperature differences although section number 8 and 6 has approximately the same thickness.

An approach that temperature is only based on thickness of the sections is not true since temperature of section can vary depending on position in the mold cavity. If section is placed below the mold cavity, it is expected to have low temperature due to the fact that mold cavity will be cool when first liquid metal filling the mold cavity is undercooled. Therefore, mould can be designed to place thin section in upper part of the diesel engine block to achieve high quality compacted graphite iron.

Results that were obtained from simulation code were consistent with experimental results when they were compared. High cooling rate was encountered as thin sections of diesel engine block were cooled to room temperature. Approximately 0 – 25% nodularity could be achieved in thick sections that are about higher than 10 mm. Thin sections that were approximately lower than 10 mm were consisted of 30 – 41 % nodular graphite due to the high cooling rate. On the other hand, graphite morphology was also highly influenced by means of design of mould, and gating design. To illustrate, if the sample belonging to section number 9 is taken from part of the region close to the runner, section No 9 that was one of the thickest part of the diesel engine block may have higher compacted graphite ratio than section No 5 that was thicker than No 9. On account of the fact that the area in which No 9 was close to the runner of the casting was exposed to hotter liquid metal flow [16].

Shrinkage is expected to be seen during solidification of compacted graphite iron casting that has a eutectic composition due to shrinkage of solidifying austenite. However, this is not the case that happened since precipitation of graphite particles will cause a volume enlargement which can offset the shrinkage. That is the main reason for expansion of compacted graphite iron castings [21].

4.1.2 Chemical Composition of Diesel Engine Block

Magnesium, sulphur, oxygen (ppm) ratio and carbon equivalent were selected to be as decisive factors. Mg and S ratios were evaluated together because required amount of Mg was strongly dependent on S present in the molten iron. Diesel engine blocks that were produced at Odöksan Osmaneli A.Ş. were expected to have Magnesium ratio that is between 0.013 and 0.019% so as to achieve 0 – 25% nodularity. However, production of compacted graphite iron (vermicular iron) depends on not only magnesium ratio, but also strongly depends on Magnesium/Sulphur ratio. For this reason, Magnesium/Sulphur ratio values were selected to handle data for linear regression work in our experimental study. Cerium that came from master alloy used for Mg treatment alloys was not evaluated as a decisive factor due to the presence of low amount.

Sulphur level that came from pig iron is between 0.01 and 0.021% in our experiments. For this reason, due to high sulphur level, more alloying elements such as magnesium was added.

Oxygen (ppm) ratio was another important factor to control compacted graphite content. Optimum value for our experiments was between 0.31 and 0.40 ppm. Oxygen level of the molten iron could be estimated by means of knowing the rate of magnesium and sulphur in the molten iron. The reaction between Mg and S can be given as

$$\underline{Mg} + \underline{S} = (MgS) \qquad (4.1)$$

Atomic weight of Mg is 24 gram and that of S is 32 gram, so MgS is 56 gram. Mg/S ratio can be given as

$$\frac{Mg}{S} = 0.75 \qquad (4.2)$$

$$\underline{Mg} + \underline{O} = (MgO) \qquad (4.3)$$

Free sulphur content in the molten iron will be a very small percentage if weight ratio of magnesium / sulphur is equal to 0.75. It can be understood from this equation that

oxygen level of the molten iron is expected to be low when equation is higher than 0.75 since a large amount of sulphur content is bounded with magnesium and there is still excessive magnesium in the system. This excessive magnesium that reacts with oxygen present in the molten iron will form MgO. Therefore, decrease of active oxygen content in the molten iron is expected.

Manganese is also sufficient to react with free sulphur in the molten iron. If the value of Mn had been increased in the molten iron, free sulphur level would have decrease, so low oxygen (ppm) level would have been encountered because more Mg would have reacted with oxygen present in the molten iron. Oxygen levels in the molten irons were measured by using Celox foundry device and its sensor during our experiments. To illustrate, oxygen (ppm) ratio of diesel engine block 11 can be calculated by formula that is derived from Nernst's law [35, 40].

$$\log a(O) = 8.62 - \frac{13580 - 10.08\,(E+24)}{T} \qquad (4.4)$$

$$\log a(O) = 8.62 - \frac{13580 - 10.08\,(-199.5+24)}{(1449+273)} \qquad (4.5)$$

$$a(O) = 0.5087 \text{ ppm} \qquad (4.6)$$

Here E value was obtained directly from the Celox Foundry sensor. According to the results, when temperature of molten iron increased, oxygen level in the molten iron increased with an increase in temperature as well. Negative EMF values were obtained by Celox Foundry sensor during all our engine blocks production study since oxygen values in the molten iron were too close to zero point as the result in the example above [40].

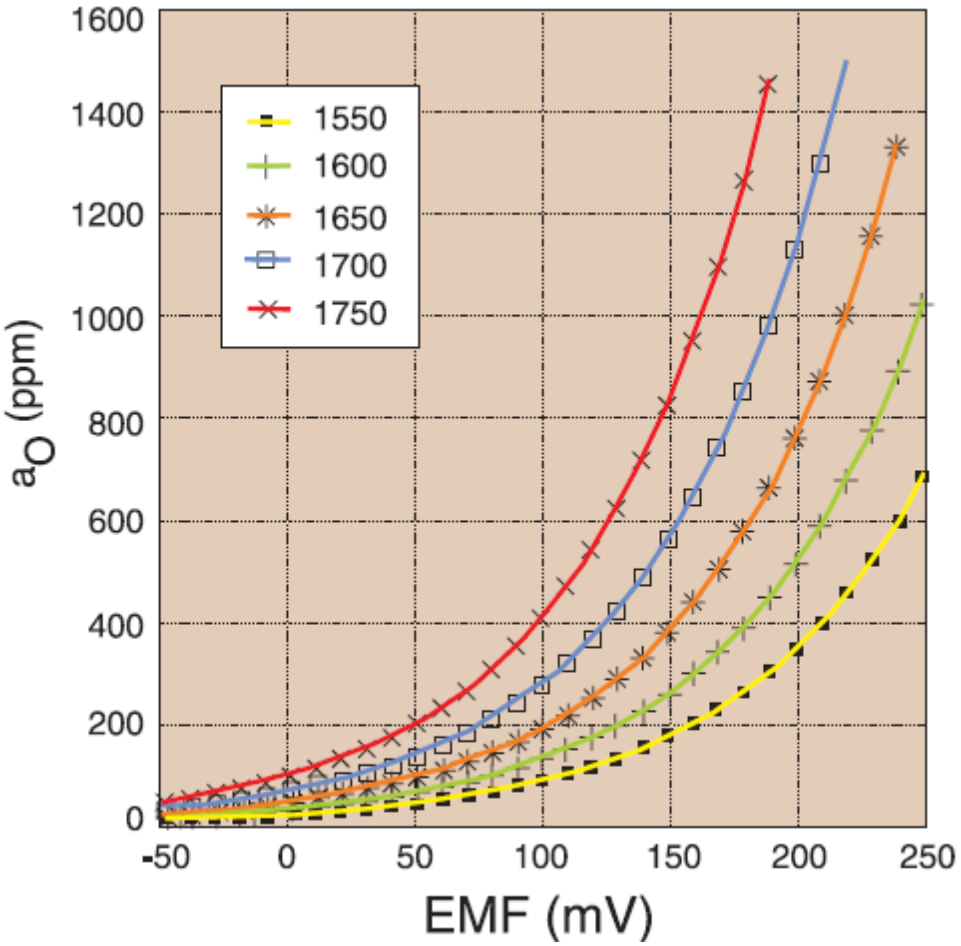

Figure 4.8 This figure indicates that EMF (mV) values change from positive values to negative values depending on pouring temperature and oxygen activity in molten iron. To illustrate, before pouring the molten iron, oxygen (ppm) values can change from 50 to 55 ppm in gray cast iron while it can alter from 0.31 to 0.51 ppm in compacted graphite iron [44].

A linear regression was performed in order to reveal the effect of Mg, S, Mn and pouring temperature on oxygen (ppm) level in the molten iron. Table 4.3 illustrates linear regression results [40].

Table 4.3 The data of 19 different diesel engine block castings is given in this table.

Mg	S	Mn	Pouring Temperature	Oxygen (ppm)	Diesel Engine Code
0,0204	0,019	0,092	1410	0,2181	1
0,016	0,012	0,1	1394	0,2162	2
0,012	0,012	0,1	1417	0,3926	3
0,013	0,016	0,1	1421	0,2286	4
0,014	0,017	0,1	1418	0,1839	5
0,018	0,017	0,2	1441	0,3127	6
0,015	0,015	0,2	1445	0,4522	7
0,015	0,013	0,19	1437	0,405	8
0,015	0,016	0,2	1437	0,3691	9
0,017	0,011	0,19	1404	0,17	16
0,012	0,013	0,19	1413	0,272	17
0,011	0,01	0,18	1426	0,2652	18
0,01	0,013	0,178	1424	0,3196	19
0,013	0,02	0,2	1410	0,1965	12
0,019	0,019	0,22	1392	0,1686	13
0,019	0,019	0,22	1393	0,1109	14
0,017	0,021	0,22	1424	0,384	15
0,011	0,016	0,083	1431	0,4654	10
0,013	0,017	0,084	1449	0,5148	11
0,005332858	-0,251314122	0,345062369	-3,47518189	-7,191002704	
0,001028288	0,318710033	5,826573652	6,878954865	1,489231816	
0,724627138	0,069194915	#N/A	#N/A	#N/A	
9,210039679	14	#N/A	#N/A	#N/A	
0,17638833	0,067031107	#N/A	#N/A	#N/A	

$$y = m_1x_1 + m_2x_2 + m_3x_3 + m_4x_4 + b \tag{4.7}$$

$$y = -3.475x_1 + 0.345x_2 - 0.251x_3 + 0.005x_4 - 7.191 \tag{4.8}$$

Where the dependent y (oxygen ppm) value is a function of the independent x values that are Mg, S, Mn and pouring temperature (T). R – square (correlation coefficient) value of this linear regression is 0.72. Conclusion to be drawn from the final equation is that oxygen (ppm) ratio is highly dependent on 1/T and Mg ratios [44].

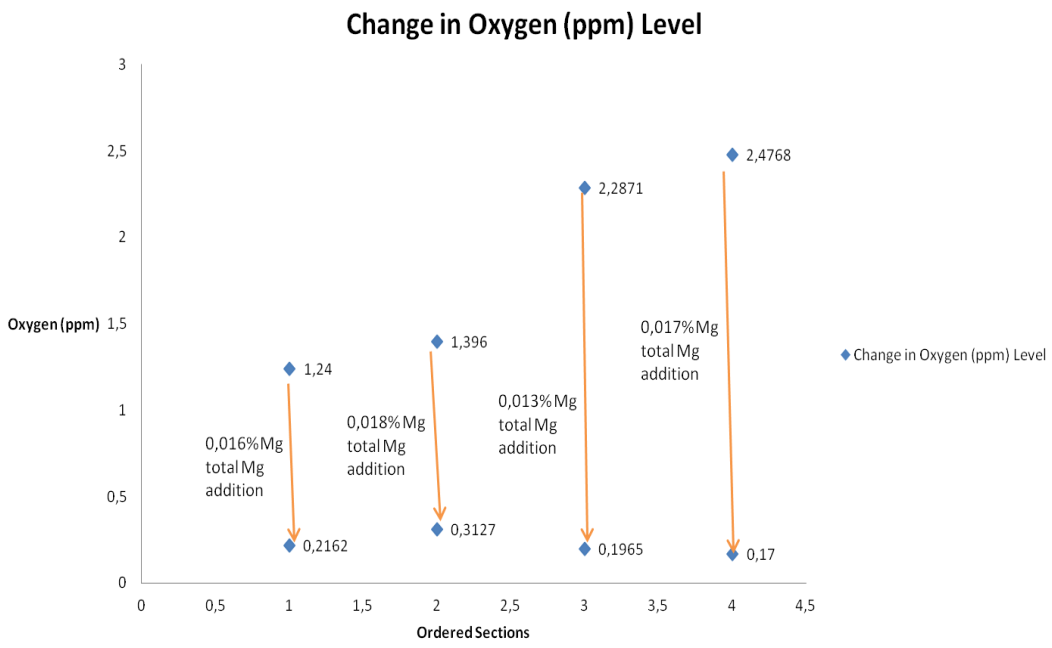

Figure 4.9 Change in oxygen (ppm) values in the molten iron can be noticed with the help of the figure according to added total Mg%. To illustrate, diesel engine block 16 had oxygen level that was 2.4768 ppm in the molten iron. Then oxygen level dropped 0.17 ppm in the molten iron after treatment.

Table 4.4 Total Mg percentages and reacted Mg content with oxygen can be also noticed as shown in this table.

Total Mg %	Amount of Mg Content (gr)	Oxygen Before Treatment (gr)	Oxygen After Treatment (gr)	Reacted Mg with Oxygen (gr)	Diesel Engine Code
0,016	20	0,155	0,0027	0,192	2
0,018	22,5	0,175	0,039	0,204	6
0,013	16,25	0,285	0,0245	0,39	12
0,017	21,25	0,31	0,021	0,433	16

4.1.2.1 Microstructure analysis by optical Microscopy and Image Analysis

If the degree of magnesium is less than sulphur present in molten iron, flake patch microstructure will be generally seen and mechanical properties will drop due to flake – type graphite shape. This ratio is approximately 20 – 30 % in tensile and elastic modulus .When oxygen level that is relevant to Mg, S, Mn and pouring temperature is high such as 0.5148 ppm, microstructure of diesel engine block is composed of fully flake graphite iron. To illustrate, step block casting samples of the diesel engine block 11 can be seen below [2, 32].

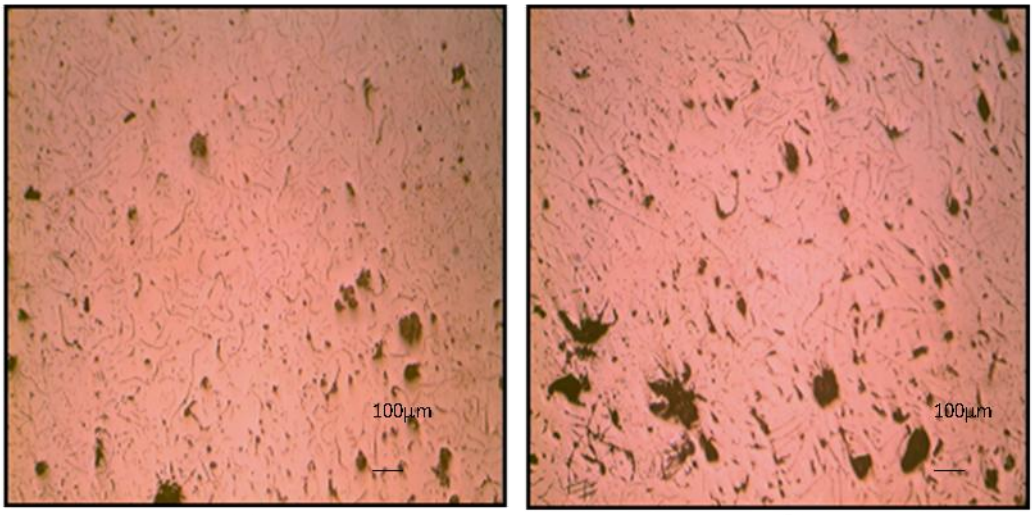

Figure 4.10 (a) The optical micrograph shows microstructure of sample that was cut from 5 mm thickness of the step block casting **(b)** The second figure illustrates microstructure of 9mm thickness of the same step block casting.

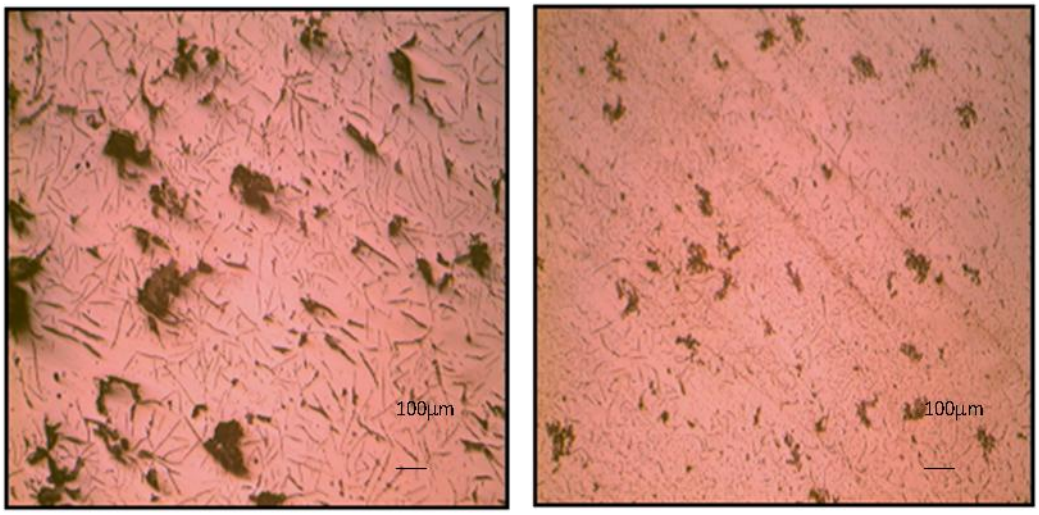

Figure 4.11 (a) The sample was taken from 14 mm thickness of the step block casting section **(b)** The second microstructure shows 26 mm thickness of the sample step block casting. Flake patch microstructure can be noticed if all of the figures are investigated basically.

Nodularity percentage in the diesel engine blocks was strongly related to Magnesium content when Sulphur level was lower than 0.007%. As a matter of fact, changing in Magnesium level such as 0.002 to 0.004% can cause increase in nodularity percentage. Due to the fact that Sulphur level was changed from 0.01 to 0.021% in our experiments, compacted graphite formation was lesser sensitive to Magnesium content than expected. However, higher Magnesium level can easily cause an increase in nodularity percentage since the molten iron does not contain Titanium that reduce the formation of nodular graphite. Hence, magnesium/sulphur level is one of the main factors when chemical composition is considered [24].

As opposed to high oxygen level, high amount of nodular graphite particles are seen in the diesel engine blocks if oxygen level in the molten iron is found to be as a small proportion. Step block casting of the diesel engine block 1 whose oxygen level was 0.2181 can be given as an appropriate example for high nodularity percentage value.

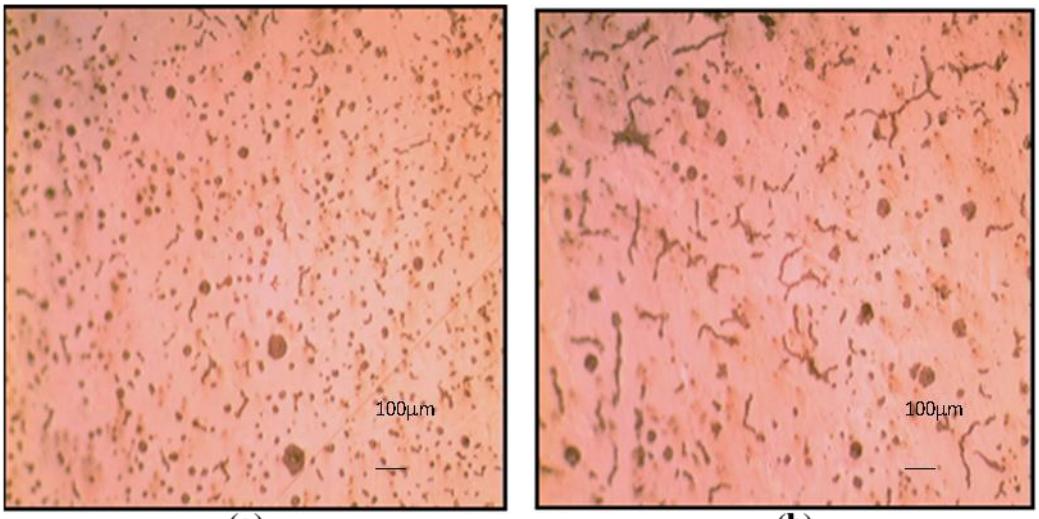

Figure 4.12 (a) Microstructure of the sample that was obtained from 5 mm thickness was almost entirely composed of nodular graphite particles **(b)** Nodular graphite to compacted graphite ratio decreases with increasing thickness of step block casting. This figure belongs to 9 mm thickness of the step block casting.

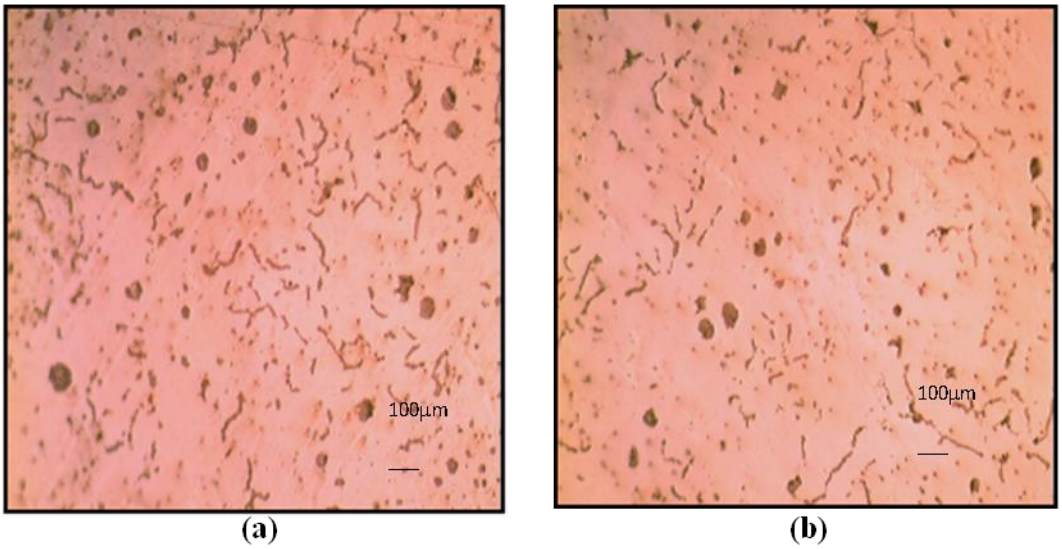

Figure 4.13 (a) Microstructure of 14 mm thickness of step block casting can be noticed **(b)** Microstructure of 26 mm thickness of step block casting can be seen.

The best results were obtained from the diesel engine block 6 whose nodularity percentage values changed from 17 to 31%. Nodularity% values that were between 17 and 23% are suitable for the purpose of the study. Some thin sections of the diesel engine block had higher nodularity percentage values than 25%, but these results are acceptable due to increasing Ultimate Tensile Strength for these thin sections.

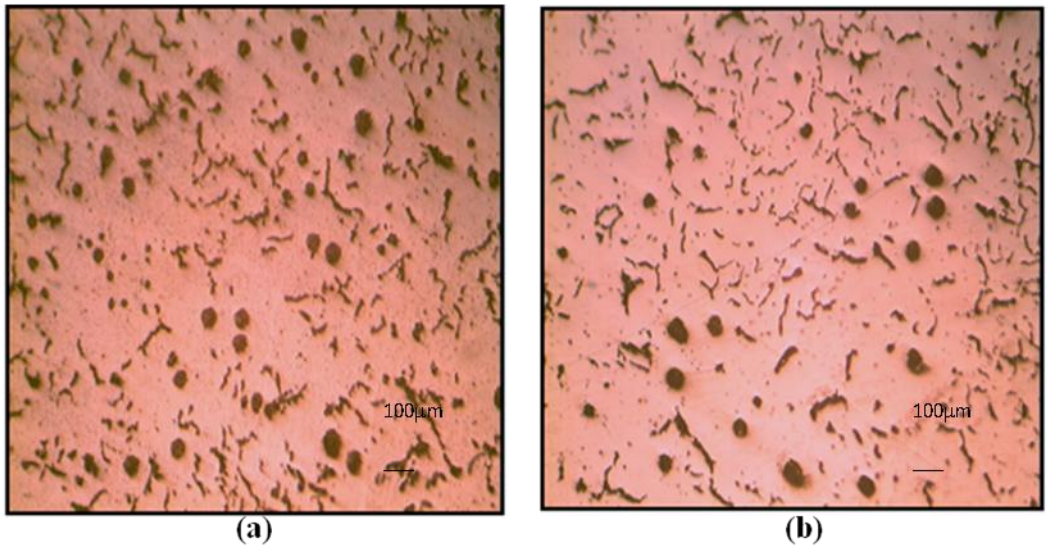

Figure 4.14 (a) The thinnest section of the step block casting included lower nodularity percentage value than the thickest section of step block castings of the other diesel engine blocks. **(b)** Nodularity% value decreases with increasing thickness.

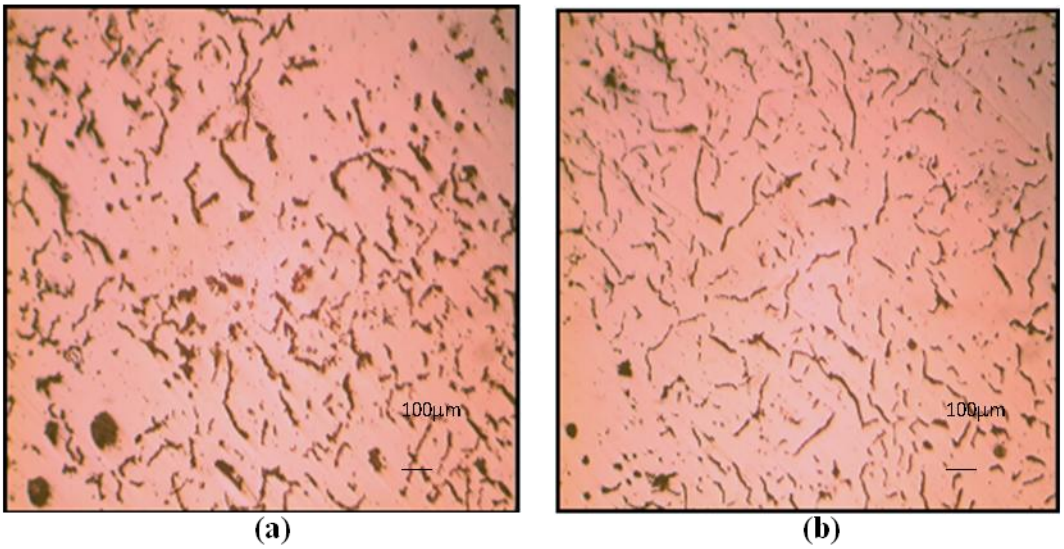

Figure 4.15 An increase in section thickness promotes compacted graphite iron formation due to slow cooling rate.

Chilling tendency of compacted graphite iron increases as nucleation and growth of graphite rate diminish. Thin parts of diesel engine block such as corners and long thin edges were not expected to include chill tendency in our experiments since Spheroidal pig just included approximately 0.74% Silicon and large amount of remaining Silicon that came from inoculants helps to reduce chill tendency at thin sections of diesel engine block due to the fact that Fe – Si dissolved in the molten iron and then dissolved Si leads to an increase in C.E.V. Inoculation that promotes the amount of nuclei and also reduces the required degree of undercooling to initiate a formation of graphite decreased the possibility of chill tendency, and casting that included high carbon equivalent content had less tendency to have chill formation [11].

Diesel engine blocks that were produced at Odöksan A.Ş. did not contain any type of carbides that is critical level as mechanical properties. On account of the fact that the molten iron used for production of diesel engine blocks did not contain carbide stabilizing elements that are usually segregate into the final part of the castings. Cr, when its value is higher than 0,018% and Mn when its value is higher than 0.25%

can be named as carbide forming elements for compacted graphite cast irons. Therefore, Chromium (Cr) content should be retained lower than 0,018% in order to prevent formation of cementite in the castings because presence of approximately 0.2% Cr leads to the formation of chill when thickness of casting sections is less than 5 mm. Pig iron is a source of chromium in our experiments. Minimum inoculation and magnesium treatment processes is another reason for non – carbide presence in our diesel engine blocks during production [2, 11, 25].

4.1.3 Nodularity Percentage Values of the Diesel Engine Blocks

The data presented in this thesis were acquired from 19 different diesel engine block sections that were produced at Odöksan Osmaneli. The base iron was melted in a medium frequency induction furnace. Also, base treatment was introduced by varied chemical Mg treatment alloys such as Mischmetal, CompactMag TM. Diesel engine blocks whose specific details (microstructure and chemical composition) were also given were produced using one and half ton capacity ladle.

Although compacted graphite iron production is too difficult as complexity of product shape and restricted nodularity percentage values, most of the diesel engine blocks that are produced at Odöksan Osmaneli A.Ş. verified the desired result that is between 0 and 25% nodularity [4].

According to literature, high quality of compacted graphite iron should include approximately 0 – 25% nodularity and remaining is compacted graphite iron in the produced engine blocks. In other words, flake – type graphite ought not to be present in the iron matrix. Due to the fact that presence of flake – type graphite in iron matrix leads to decrease in tensile strength and elastic modulus, and this ratio is approximately 20 – 30% [2, 5, 16].

Diesel engine blocks which include different thicknesses are expected to possess nodularity% values that are between 0 and 25%. However, thin sections of the diesel engine blocks that are approximately 10 mm can contain 30 – 40% nodularity and remaining is compacted graphite iron due to fast cooling rate. High nodularity

percentage values promote an increase in strength and stiffness; hence, high nodularity% values for thin sections of diesel engine block can be acceptable to attain requirement of thin sections [16].

While examining each diesel engine block, four or nine different sections from the same sample were evaluated in order to measure all local sections of the same sample. In addition to that, during this process, nodularity percentage values were determined by using optical metallography and an image analysis program. Percent nodularity in other thickness of the diesel engine blocks was alike. However, some thin sections such as section number 6 with 7.99 mm thickness contain higher nodularity values that are about 35% nodularity, and remaining is still compacted graphite iron, which arises from faster cooling rate [2, 9, 18].

Presence of flake graphite at any local area in diesel engine block would cause weak spots. Therefore, 14 different sections of diesel engine blocks were examined by image analyzer to detect presence of flake graphite. In addition to that, the nodularity % value was tried to keep within specific ratio so as to obtain good mechanical properties. The 14 different sections of diesel engine block 6 that have the best results in terms of nodularity percentage value were investigated below.

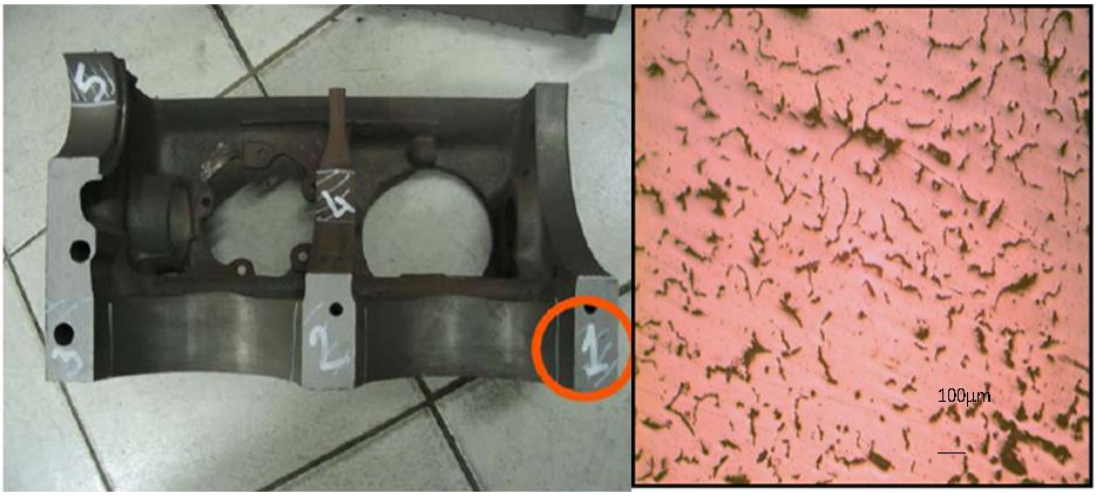

Figure 4.16 Section number 1 having 32.72 mm had 23.68% nodularity. Section 1 was placed near the runner. Moreover, it was one of the thickest sections of the diesel engine block.

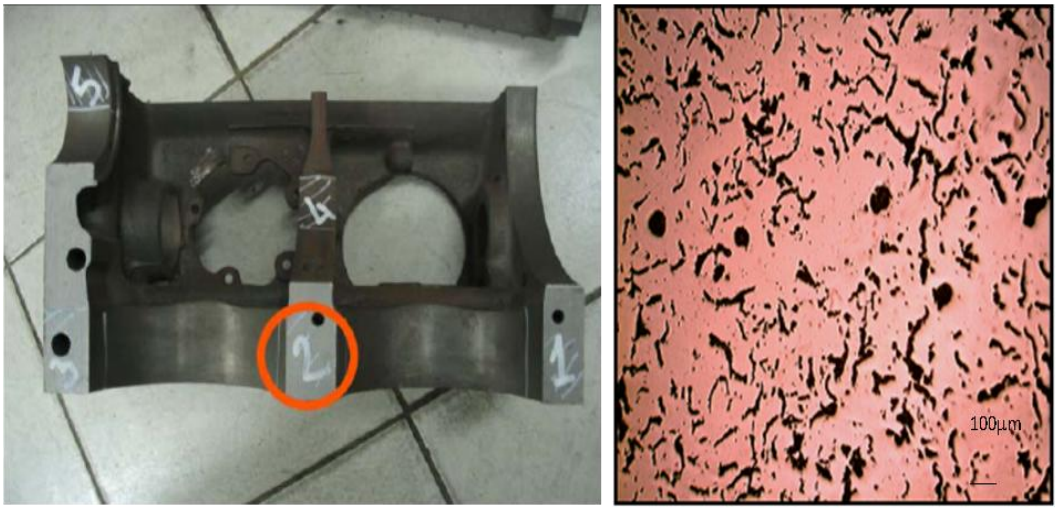

Figure 4.17 Section number 2 with 36.26 mm thickness had 20.82% nodularity. Section 2 was the thickest part among section number 1, 2 and 3.

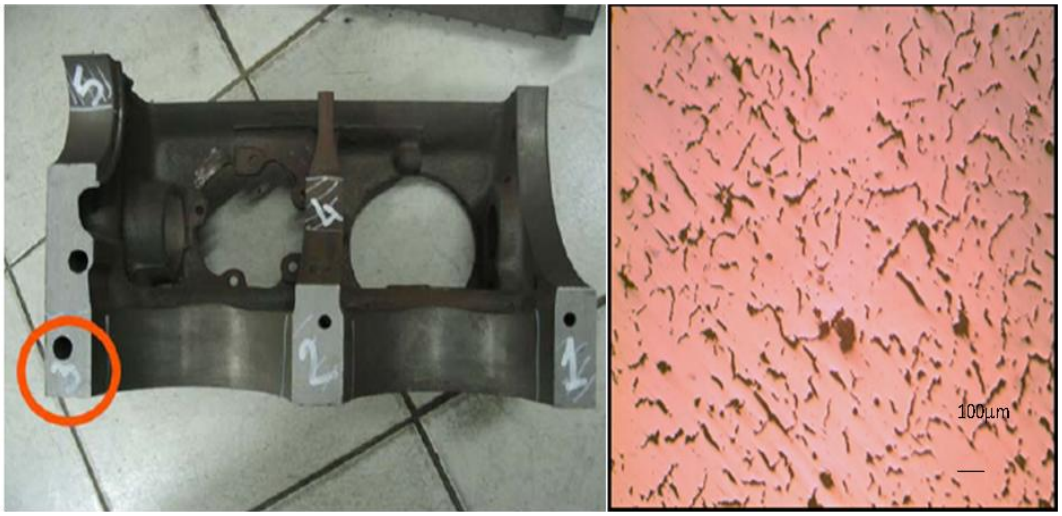

Figure 4.18 Section number 3 having 35.86 mm thickness included 17.65% nodularity. Section 3 was also located near the runner like section number 1.

Section number 1, 2 and 3 generally had the highest compacted graphite iron ratio when compared with the other sections of the diesel engine blocks. Differences in

compacted graphite iron ratio could occur because of the fact that locations in the mold cavity and thicknesses of the sections were different from each other although alloying elements in the diesel engine block were found to be the same ratio. This caused them to have different cooling rates.

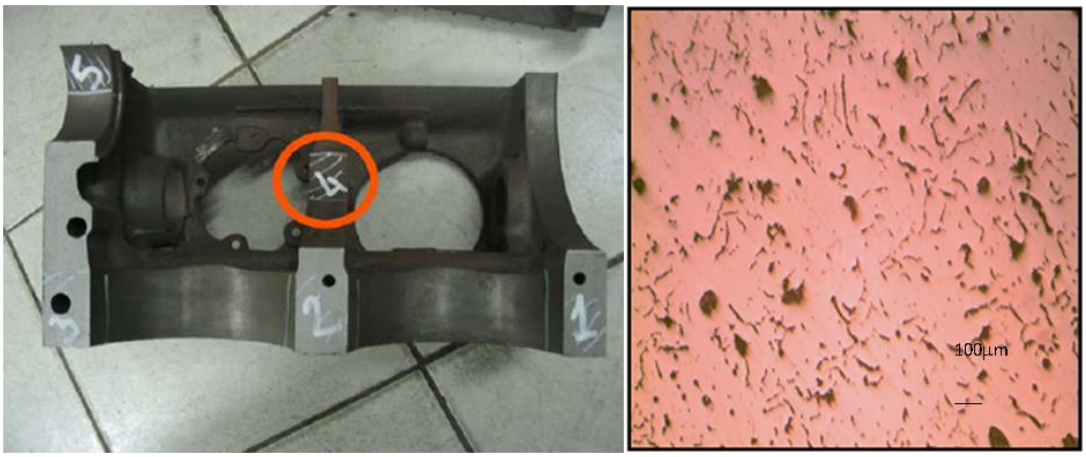

Figure 4.19 Section number 4 with 9.82 mm thickness had 23.52% nodularity. Section 4 was one of the thinnest parts of the diesel engine block. Section number 4 was taken from such a tough place that the point chosen may change from one diesel engine block to another one.

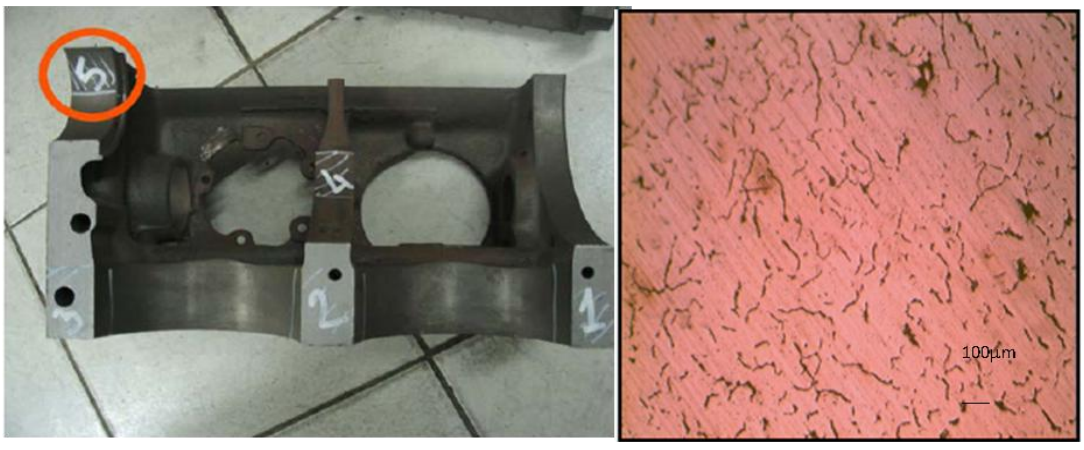

Figure 4.20 Section number 5 having 40.85 mm thickness had 30.13% nodularity. Though section 5 was the thickest section of the diesel engine block, it could include high nodularity% value due to its position in the mold cavity.

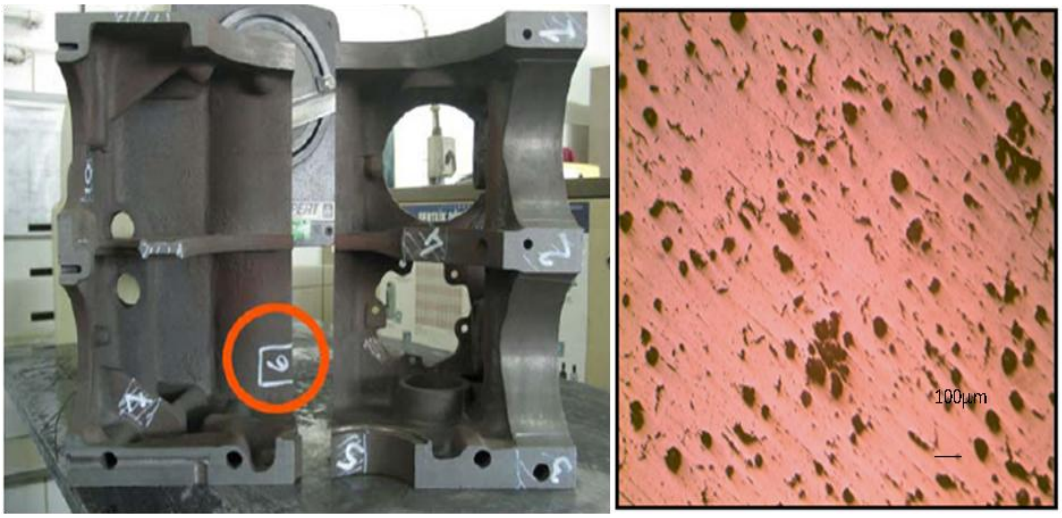

Figure 4.21 Section number 6 with 7.99 mm thickness had 31.18% nodularity. Section 6 had such a high nodularity% value since it was present in the area that liquid metal firstly contacted with cold mold wall at the bottom of mold cavity during liquid iron filling the mold cavity. In addition to that, section 6 was one of the thinnest regions of the diesel engine block.

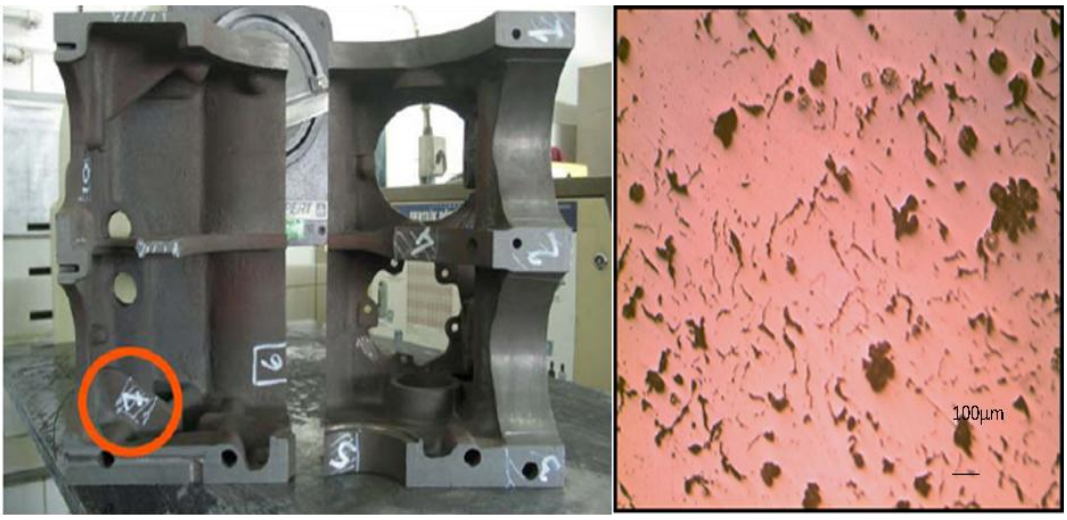

Figure 4.22 Section number 7 having 11.08 mm thickness had 25.39% nodularity. Nodularity values of section number 7 in engine block could be seen to present differences in terms of nodularity values of other sections of the diesel engine blocks.

The main reason of this was the cooling rate difference in the triangle – like – section itself. Nodularity percentage values at the top and bottom of sample 7 were different.

Figure 4.23 Section number 8 with 7.25 mm thickness had 26.33% nodularity. Section 8 generally consisted of higher nodularity percentage value than the other sections of the diesel engine block. This may seem normal due to its thickness.

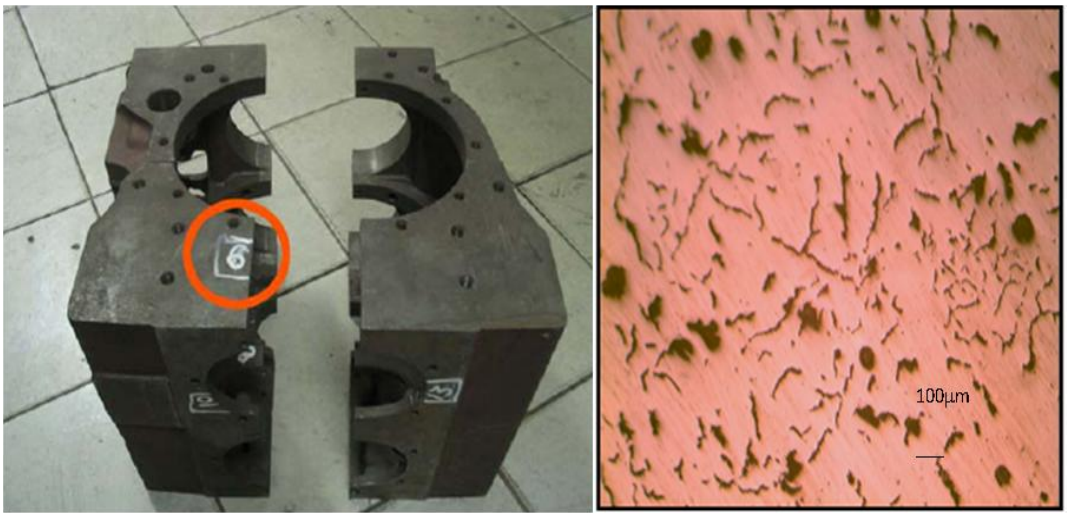

Figure 4.24 Section number 9 having 13.94 mm thickness had 20.88% nodularity. In some engine blocks, nodularity value in section 9 may be high in terms of nodularity values of other sections of the diesel engine blocks. The reason for this is that the

sample which would represent section number 9 was not taken from the area near the gating but was taken from the area far from the gate on the same direction.

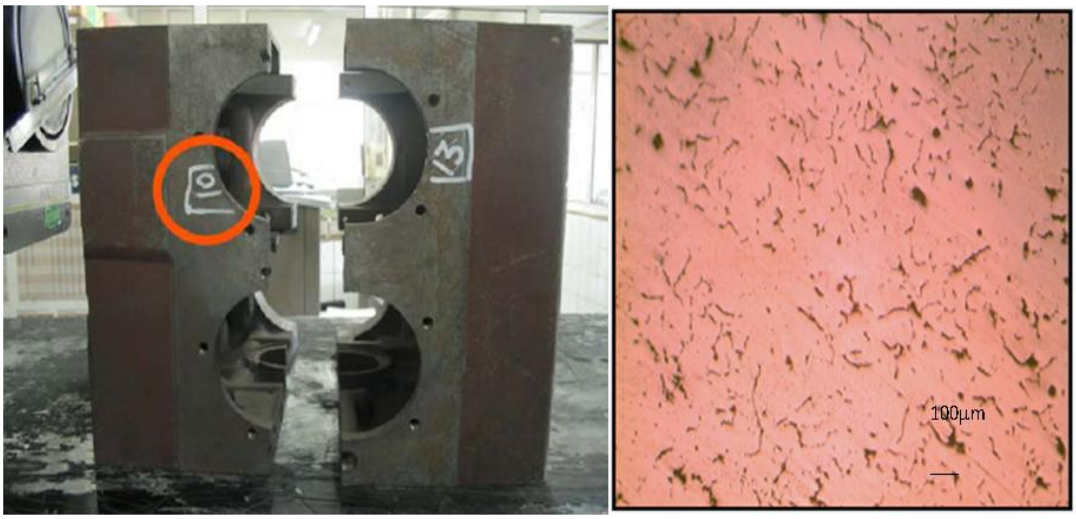

Figure 4.25 Section number 10 with 16.83 mm thickness had 22.89% nodularity. Nodularity value of section 10 may show differences in accordance with obtaining it near the runner or obtaining it far from the runner.

Figure 4.26 Section number 11 having 10.95 mm thickness had 20.39% nodularity. The things that have been told for section number 7 are suitable for section number 11.

Figure 4.27 Section number 12 with 12.71 mm thickness had 27.37% nodularity.

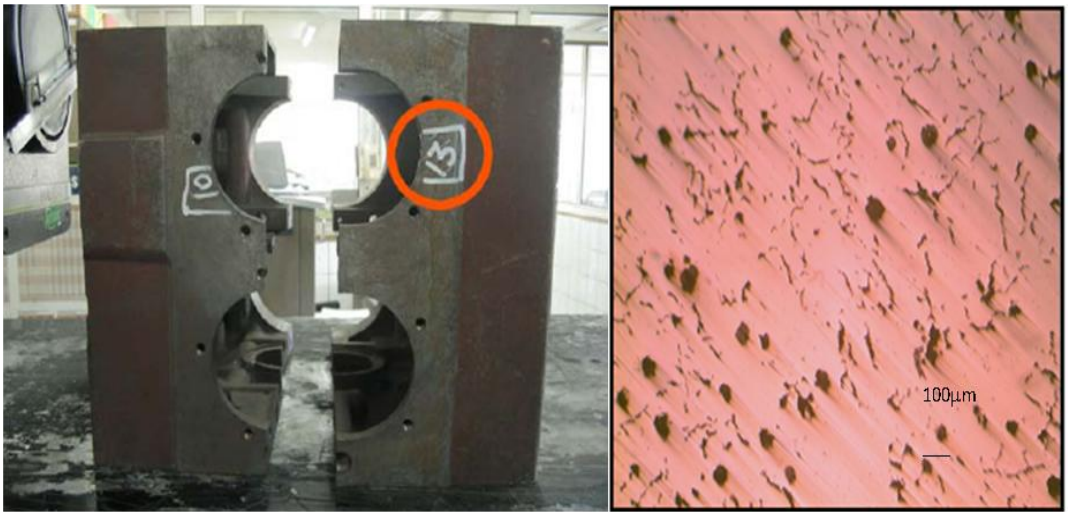

Figure 4.28 Section number 13 having 10.39 mm thickness had 21.42% nodularity. Nodularity value of section 13 was likely to reveal some differences in terms of obtaining it near the gating or far from it.

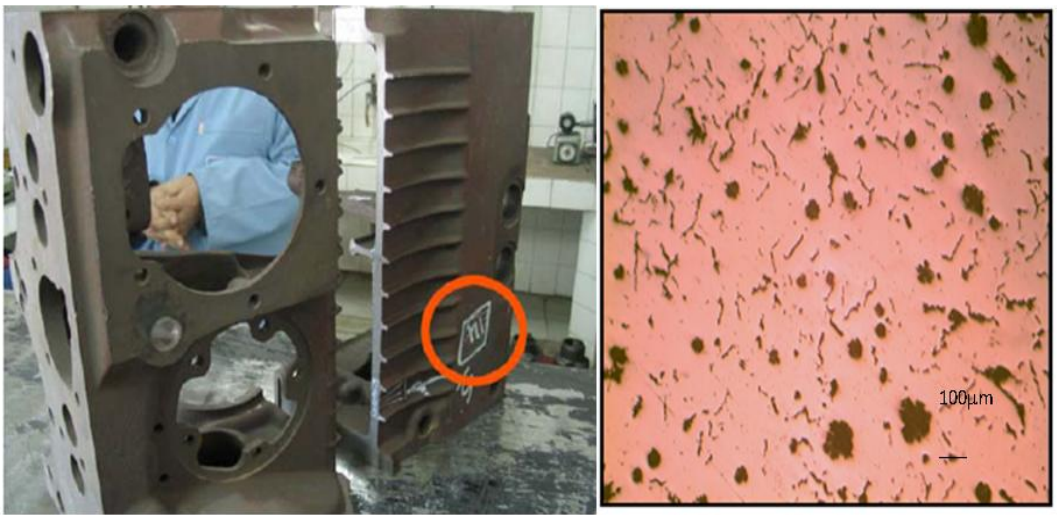

Figure 4.29 Section number 14 with 9.48 mm thickness had 24.11% nodularity. Section 14 was within a critical region. Sections near the area in which liquid iron filled the mold cavity were of enough cooling rate for the formation of compacted graphite iron. As it was moved to the centre of the section, temperature dropped and cooling rate increased. Hence, the nodularity value increased.

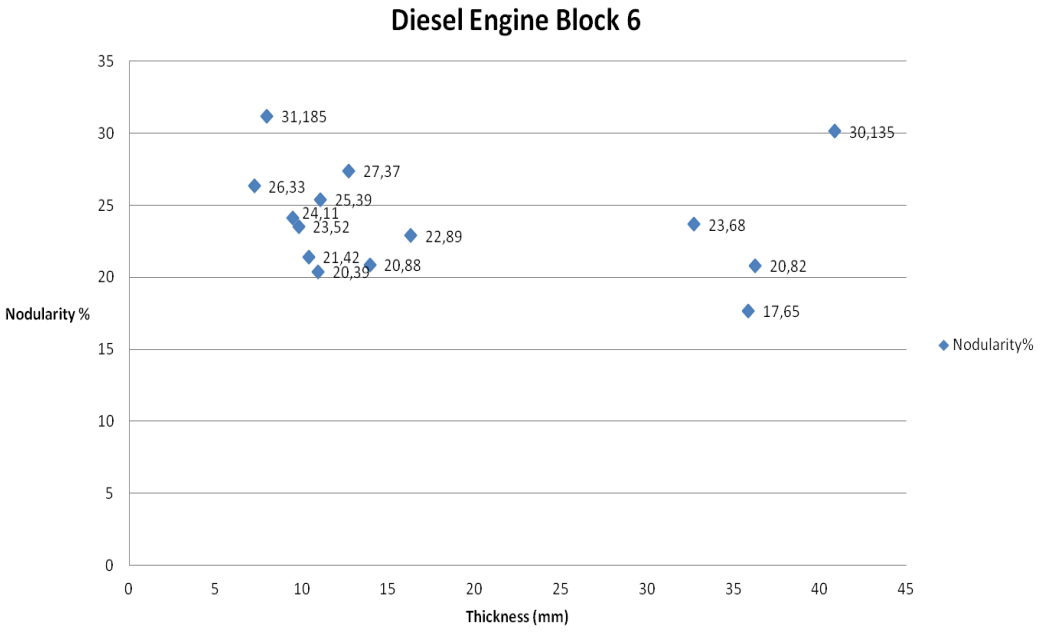

Figure 4.30 Nodularity percentage values of diesel engine block 6 versus thickness (mm) values can be noticed.

4.1.3.1 Linear Regression of the Results Obtained fromDifferent Section Thickness

Excel linear regression code was used to correlate the effect of Mg/S ratio, O_2 (ppm), temperature and C.E.V value on nodularity. Code was exercised on the same 13 different section thicknesses of 16 different diesel engine blocks so as to obtain the most accurate results. Achieved formula for section number 1 with 32.72 mm thickness can be noticed below.

$$y_1 = m_1x_1 + m_2x_2 + m_3x_3 + m_4x_4 + b \quad (4.9)$$

$$y_1 = 1.926x_1 + 12.733x_2 + 4.614x_3 - 0.151x_4 + 212.402 \quad (4.10)$$

Where the dependent variable y (Nodularity% value) is a function of the independent x that can be described as x_1 is a value of C.E.V, x_2 is O_2 (ppm), x_3 is Mg/S and x_4 is temperature (^oC). R – square (correlation coefficient) value of this linear regression is 0.95.

Independent function coefficients x values can be redefined to explain the use of the formula for section number 1 that can be written as fallows.

$$\%Nodular\ Graphite_1 = 1.926C.E.V_1 + 12.733\underline{O}(ppm) + 4.614\frac{Mg}{S}_1 - 0.151T_1 + 212.402 \quad (4.11)$$

Achieved formula for section number 13 and 14 with different thicknesses can be also noticed below. Their R – square (correlation coefficient) values can be respectively given as 0.96 and 0.77.

$$y_{13} = m_1x_1 + m_2x_2 + m_3x_3 + m_4x_4 + b \quad (4.12)$$

$$y_{13} = 9.403x_1 + 4.081x_2 + 2.117x_3 - 0.158x_4 + 183.025 \quad (4.13)$$

$$y_{14} = m_1x_1 + m_2x_2 + m_3x_3 + m_4x_4 + b \quad (4.14)$$

$$y_{14} = 2.489x_1 + 11.308x_2 + 0.253x_3 - 0.078x_4 + 109.094 \quad (4.15)$$

Every factor such as carbon equivalent and temperature did not have equal influence on nodularity%. Although influence of C.E.V, Mg/S, O_2 (ppm) was in the same direction, influence of temperature was in opposite direction. This is the reason for decreasing nodularity percentage value when increasing temperature. This result indicates that there will be a linear plot if nodularity% against Mg/S, C.E.V, O_2 (ppm) and temperature graphics is drawn. Because of five – diamentional graphics cannot be drawn; this linearity can be understood only with the R – square (correlation coefficient) value that was very close to unity 1 [18].

While nodularity percentage value against Mg/S or C.E.V is drawn, linearity cannot be seen logically. However, this linearity can be realized as nodularity percentage value against temperature graphics is drawn.

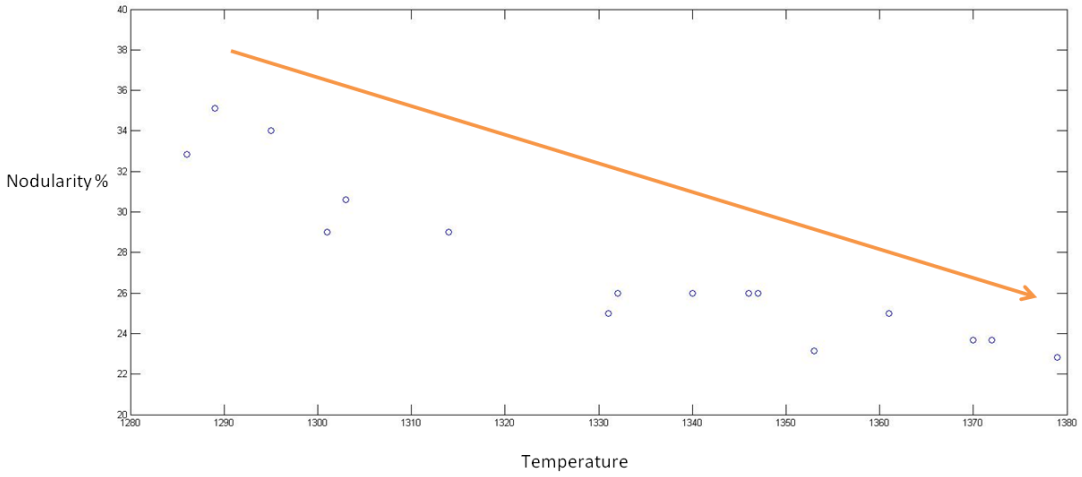

Figure 4.31 Decreasing in nodularity % values of section 1 with increasing temperature can be noticed along the arrow.

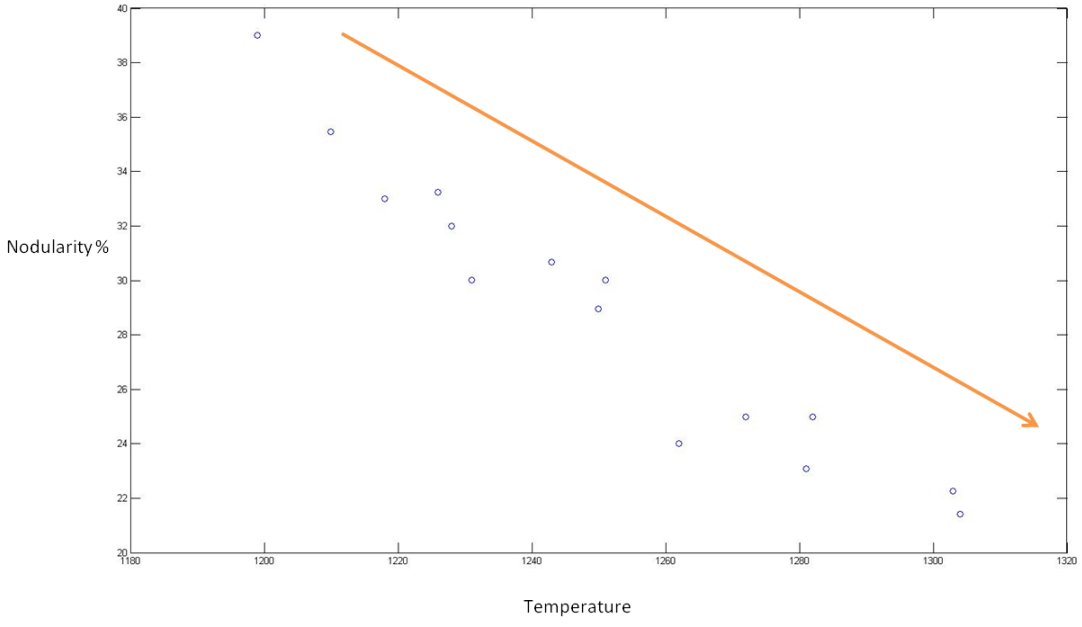

Figure 4.32.Nodularity value of section 13 was reached the top point having 39% nodularity with 1199 ^{o}C which temperature attained the lowest level. The lowest nodularity value of section 13 was obtained when temperature value was 1304 ^{o}C.

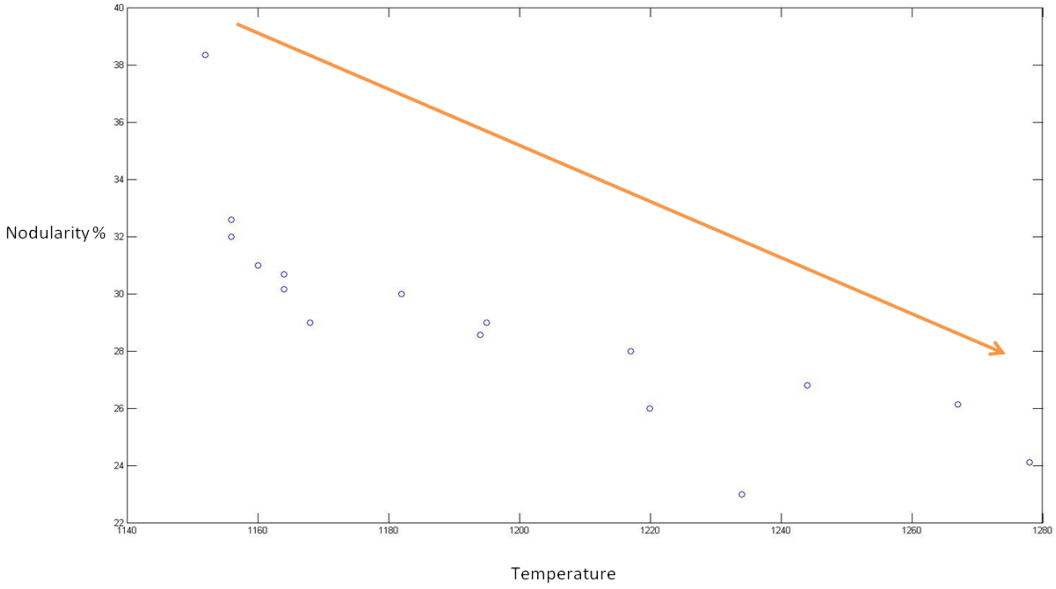

Figure 4.33.As nodularity value – temperature graph of section 14 was investigated, it can be realized that change of nodularity percentage values was highly related to change in temperature.

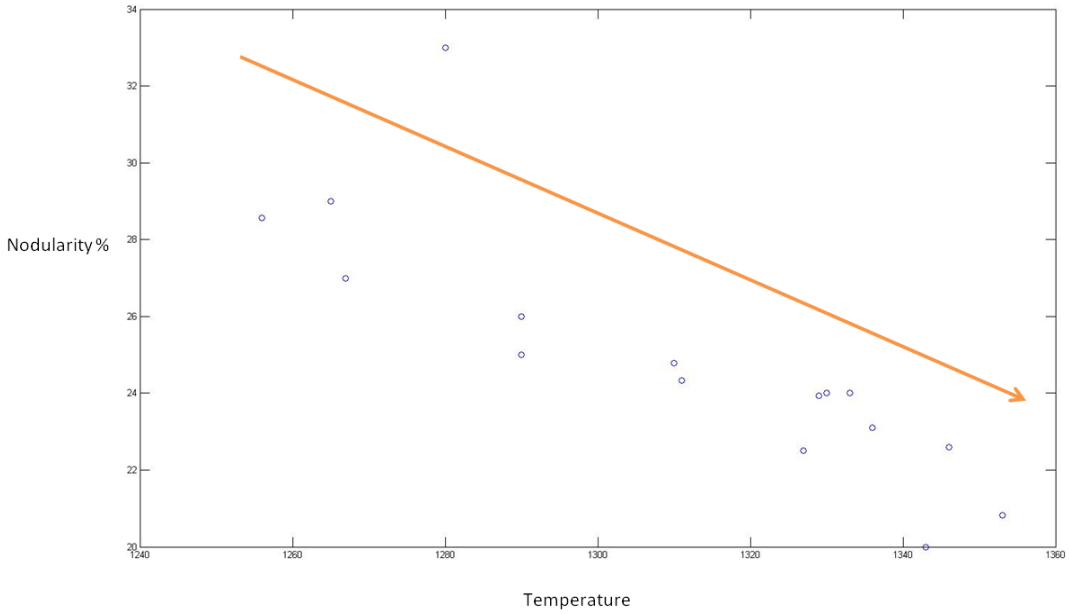

Figure 4.34.If the point which is present above the arrow is neglected, a fine linearity between nodularity values and temperature can be noticed. Data were

obtained by investigating temperature and nodularity values of section 2.

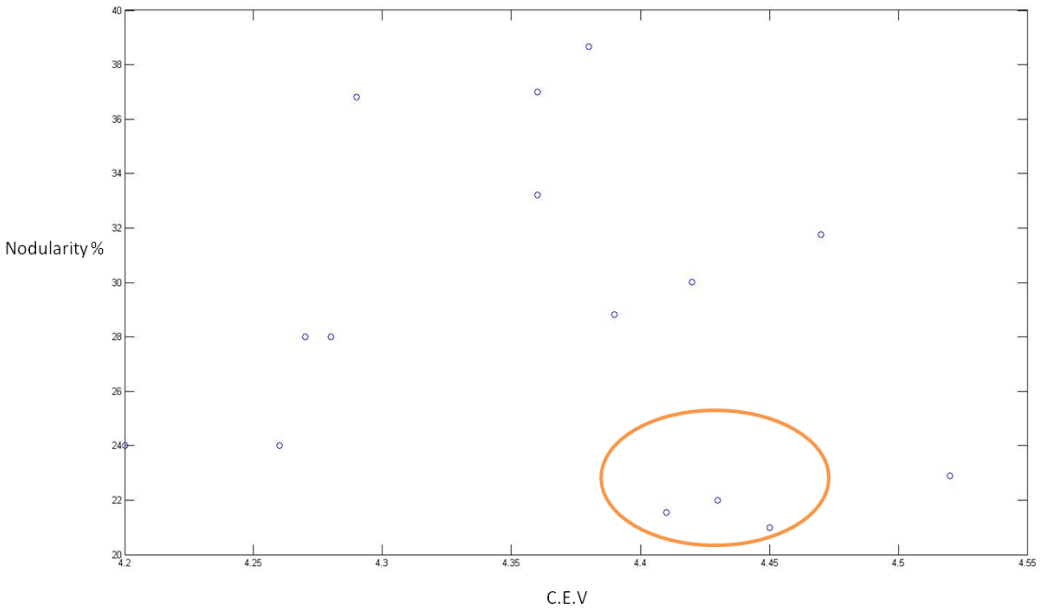

Figure 4.35. It can be seen from graph of C.E.V versus nodularity% value of section 10 that the best nodularity% values usually existed in the area that was between 4.4 and 4.45% C.E.V.

4.1.3.2 Pearlite/Ferrite Content of Diesel Engine Block

The aim of this thesis is to determine nodular graphite to compacted graphite ratio on the target value of different sections of the diesel engine blocks. However, the last diesel engine blocks that is heat 12 – 19 contained strong pearlite stabilizing elements to enhance mechanical properties. Engine blocks that were produced without pearlite stabilizing elements addition were composed of fully ferritic microstructure as shown in figure 4.37. Engine blocks which contained high carbon equivalent values may have approximately 10% pearlite microstructure due to fast cooling rate (figure 4.38). Moreover, heat 12 to 19 including Cu and Sn additions were composed of approximately 70% pearlite phase as shown in figure 4.39.

Ferritizing tendency of compacted graphite iron is too high without pearlite stabilizer elements addition. Since formation of ferrite is more common in compacted graphite iron than spheroidal and flake graphite iron, more pearlite stabilizer elements such as copper and tin (Cu and Sn increase the proportion of the pearlite since these elements drop the carbon diffusion coefficient; thus, carbon cannot attain a graphite region and is expected to react with iron. Consequently, carbon reacts with iron and they produce cementite) were required in compacted graphite iron so as to make sure high pearlite content in the iron matrix [19, 11].

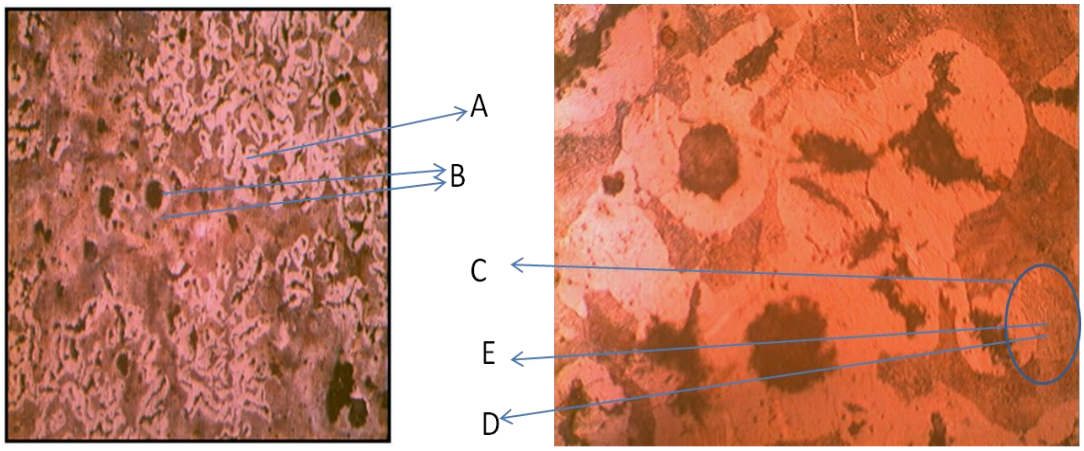

Figure 4.36 A sample was taken from diesel engine block 12. Ferrite phase is marked with a light color (A) pearlite and graphite particles are colored with a dark color at which differences between graphite and pearlite can be easily noticed (B). At higher magnification, pearlite region is seen as finger – print (C) and ferrite areas is light colored (D) between two Fe_3C plates that is dark colored (E). [17].

As magnesium segregation in diesel engine block is considered, present magnesium content that is lower than expected can be lost approximately 0.003% due to fading. This causes the microstructure to be fully D type flake graphite. Since graphite particles are too close to each other in D type flake graphite morphology, carbon atoms cannot diffuse easily, so a ferritic matrix is expected to be seen [4].

Since iron matrix of diesel engine blocks 10 and 11whose chemical compositions did

not include any pearlite – stabilizing elements were composed of fully flake graphite, tendency of ferrite content was expected to be seen in the iron matrix. During our metallographic experiments, it could be seen that samples of diesel engine blocks 10 and 11 did not contain pearlite phase; in other words, structure is composed of approximately fully ferrite phase.

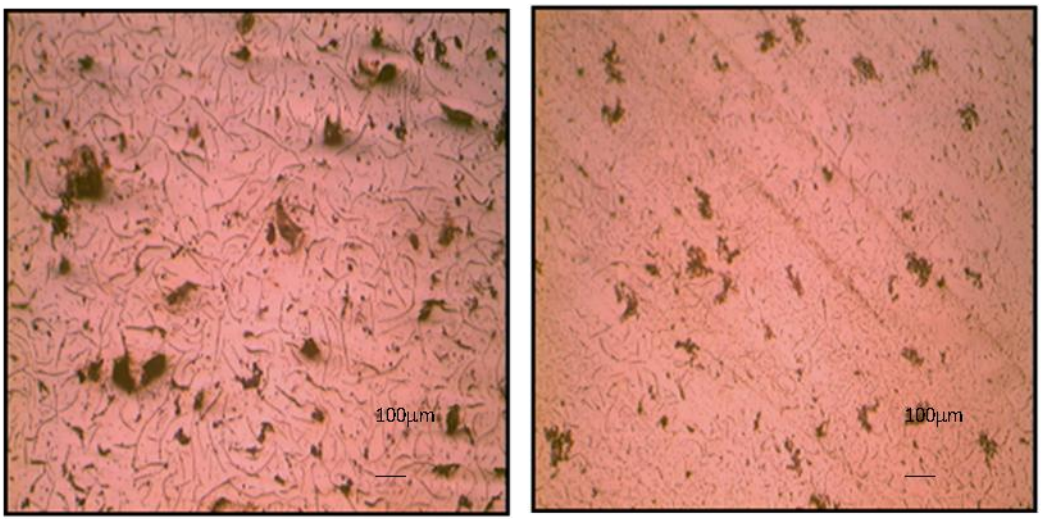

Figure 4.37 (a) A sample was taken from 32.72 mm thickness of the diesel engine block 10 **(b)** Another sample was taken from 26 mm thickness of step block casting which has the same chemical composition with the diesel engine block 10.

Approximately 0.45 – 0.60% copper and 0.05 – 0.08% Sn were added in order to achieve about 70% pearlite matrix. during production of diesel engine blocks 12 – 19 so as to promote the pearlite content in the produced compacted graphite iron diesel engine blocks. Amount of added copper and Tin are based on the shape of the product. The matrix of casting trials for diesel engine blocks without Cu and Sn addition consisted of fully ferritic structure in experiments such as Heat 1 - 11 [5, 40].

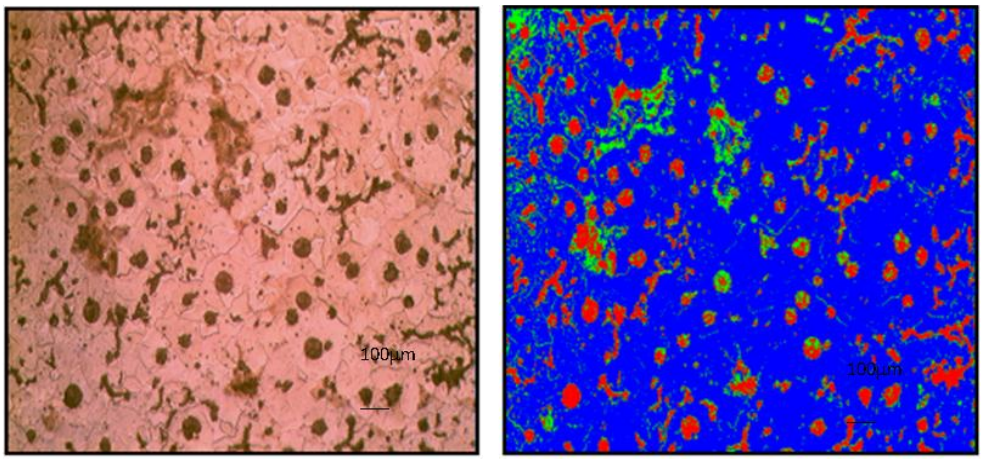

Figure 4.38 A sample was obtained from 26 mm thickness of step block casting diesel engine block 1. Red areas represent graphite, ferrite phase is shown by blue color and pearlite phase is highlighted by yellow color. Microstructure consisted of 10.83% graphite, 10.62% pearlite and 78.53% ferrite phase.

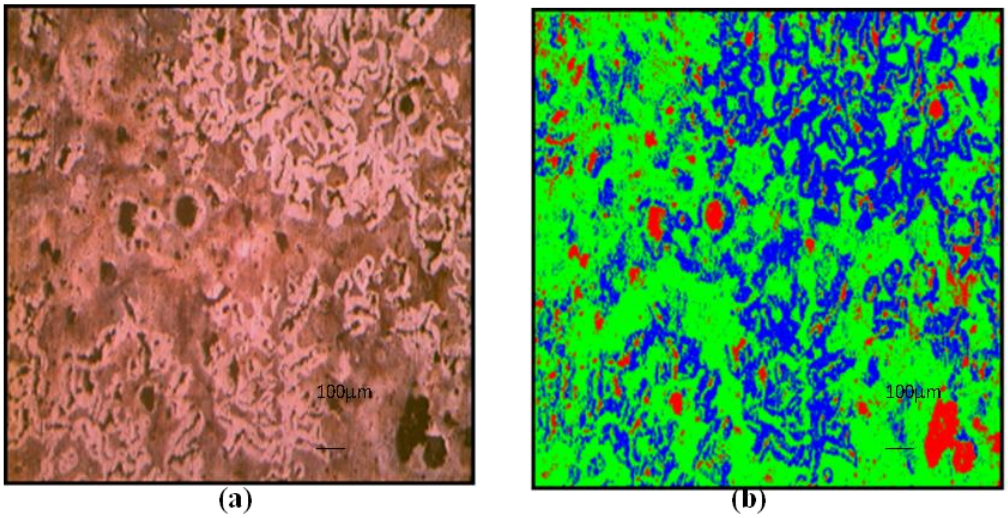

Figure 4.39 A sample was obtained from 32.72 mm thickness of diesel engine block 16. Red areas represent graphite, ferrite phase is shown by blue color and pearlite phase is highlighted by yellow color. Microstructure consisted of 7.42% graphite, 62% pearlite and 30.52% ferrite phase.

4.1.4 Ultrasonic Test Results of Diesel Engine Block

The Compacted graphite iron engine blocks produced as a requirement of the research project (TEYDEB) were tested by ultrasonic device to correlate microstructure details such as compacted graphite to spheroidal graphite ratio.

Step block castings of diesel engine block 2 – 5 were tested by using USM 35 flow sensor test machine at METU. In order to determine velocity (m/s) against the percentage of the different compacted graphite iron obtained, ultrasonic tests were done on 4 different step block casting and diesel engine blocks without cutting and obtaining the samples. The points of nodularity % values in the thickness of step block casing of diesel engine block 2 – 5 had been obtained before.

Table 4.5 Ultrasonic test results which were obtained from step block casting of diesel engine block 2 – 5 are shown below

Diesel Engine Code	Thickness (mm)	Average sound velocity (m/s)
2	27,1	5332
2	27,8	5284
3	29,7	5327
3	26,9	5216
4	28,4	5026
4	28,5	5018
5	27,2	5305
5	28,1	5200

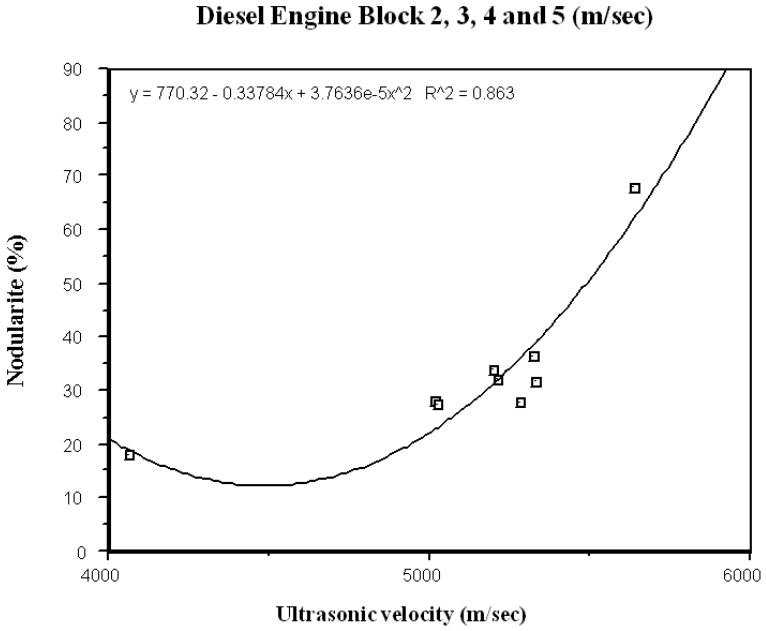

Figure 4.40 Ultrasonic test results of side by side step block castings and these values were used in order to get a velocity – average nodularity variation.

Nodular graphite % versus velocity (m/s) curve can be seen in figure 4.40. After examination of the results, it can be noticed that there is a good correlation with the data which was produced for cast iron given in literature. Therefore, it can be seen that when spheroidal graphite% increases with ultrasonic velocity (m/s) [8].

The reason for increasing nodularity% values when increasing velocity is that increasing velocity is strongly dependent on increasing young modulus. This conclusion can be understood from the equation given below.

$$Velocity = [E(1-v)/p(1+v)(1-2v)]^{0.5} \quad (4.16)$$

Here E is young modulus, p is poisson ratio and it is an independent factor of cast iron of matrix, v is density (g/cc). This ratio is similar for compacted graphite iron and spheroidal graphite iron such as 7.01 and 7.06. Young modulus of spheroidal graphite iron is approximately 168 GPa and 138 GPa for compacted graphite iron [8].

CHAPTER 5

CONCLUSIONS

In the present study concerning the production of compacted graphite iron on diesel engine blocks via Mg treatment alloy, the following major conclusions have been drawn:

1. The compacted graphite volume percent observed at different sections of the diesel engine blocks were found to be a function of cooling rate, which depends on the design of mold.

2. The cooling rates were found to be dependent on the section thickness but there are also exceptions in the filling and liquid metal flow sequence altering the cooling conditions.

3. Thin sections consisted of more nodular graphite structures but there are exceptions in arising from variation of local filling velocities and liquid metal flow losing its sensible heat transferring more heat to the interior thin sections

4. The nodularity values were measured by destructive technique. Specimens cut and prepared for optical microscope and then analyzed by image analyzer yielded a directly increasing trend. Nodularity was found to be increasing with ultrasonic velocity. This diagram can be used to examine as cast and machined blocks without removing specimens form sections.

5. Optimum results are achieved when C.E.V values are between 4.40 and 4.50% and corresponding Mg/S ratios are approximately 1. During experiments, C.E.V values were tried to keep lower than 4.55.

6. In order to avoid formation of flake and excessive nodular graphite, oxygen (ppm) level should be kept between 0.31 and 0.40. This is due to a small increase in oxygen level in terms of ppm can markedly decrease surface energy of liquid gas interface.

7. In parts with same thicknesses, the regions that are closer to the runner have higher ratio of compacted graphite compared to the other ones.

8. To obtain engine blocks with 80% compacted graphite microstructure in sections that are thicker than 10 mm, C.E.V, Mg/S ratio, $\underline{O}$ (ppm) and temperature values should be optimized.

9. Although they had same thicknesses, section 6(7.99 mm) at the bottom of the cavity and 8(7.25 mm) in the middle of cavity had different compacted graphite ratios in the same engine block casting. This result shows that variations in filling sequence affects compacted graphite ratio.

10. After analysis performed and obtained 13 formulas acquired by linear regression revealed that this technique is useful in making estimation of nodular graphite percentage in considered sections of the evaluated engine block without casting process application, but just by placing the related carbon equivalent, Mg/S ratio, $\underline{O}$ (ppm) and temperature values on the formulas for that engine block.

11. The last engine blocks being heat 12 to 19 were produced by means of addition Cu and Sn in order to obtain approximately 70% pearlitic microstructure.

12. After examination of linear regression results, it can be noticed that of pouring

temperature and sulphur level in the molten iron had .an influence to increase oxygen (ppm) level in the molten. As opposed to sulphur and pouring temperature, Mn and Mg ratio in the molten iron had the opposite effect on oxygen activity in the molten iron.

13. Oxygen levels of liquid metal taken from furnace were compared with oxygen level of molten iron taken from ladle after treatment. After treatment, the changes in Mg level of molten iron samples from four different ladles were in the range of 0.013% to 0.018%. The values for four heats 0.018%, 0.017%, 0.016% and 0.013% corresponding oxygen values in the molten iron dropped from 1.392 to 0.3117 ppm, 2.4768 to 0.17ppm, 1.24 to 0.2162 ppm and 2.2871 to 0.1965 ppm respectively.

REFERENCES

1. Sugwen Kim, "Mechanical, Wear and Heat Expesure Properties of Compacted Graphite Cast Iron at Elevated Temperature", 2009, Journel of Alloy and Compounds.

2. C.R. Farais, J. Benavente, T. Schroeder, S. Dawson, "Compacted Graphite Iron Production at Cifunsa Using a Process Control System", AFS Transactions: pp. 947 - 949.

3. M. Gorny, "Castability of Ductile Iron in Thin Wall Castings (TWDI)", 2008, Archives of Foundry Engineering (AFE), Volume 8 Issue 3: pp. 59 - 63.

4. Dr. Steve Dawson, "Process Control for the Production of Compacted Graphite Iron", 2002, AFS Casting Congress Kansas: pp. 1 - 11.

5. W. Guesser, T. Schroeder, S. Dawson, "Production Experience with Compacted graphite Iron Automotive Components", 2001, American Foundry Society: pp. 1061 - 1069.

6. J. Y. Chen, D. H. Wu, P. C. Liu, C. R. Loper, "Liquid Metal Channel Formation in Compacted Graphite Cast Iron Solidfication", 1986, AFS Transactions: pp. 537 - 544.

7. Heine P. W., Loper C. R., Rosenthall P. C., "Principles of Metal Casting", 1967, Mc Graw Hill New York.

8. C H Gür and B Aydınmakina, " Microstructural Characterisation of Ductile Irons by Measuring Melocity and Opponent Attenuation of Ultrasonic Waves ", 2001:pp. 730 - 733.

9. NovaCast and Elkem, "Process Cotrol Technology for Production of Castings in Compacted Graphite Iron", PQ-CGI, NovaCast AB: pp. 1.

10. "Melting - Large Steel Shell Coreless Furnace",Indoctotherm, Taiwan.

11. "ASM Metals Handbook", Volume 15, Casting: pp. 1445 - 1484.

12. Adrian Udroiu, "Thermal Analysis of Gray Iron and Ductile Iron", 2010, The NovaCast Seminar, Düsseldorf.

13. Mark Ihm, "Introduction to Gray Cast Iron Brake Rotor Metallurgy", TRW Automotive, Seminar.

14. Doç. Dr. Ergin M. Çavuşoğlu, "Döküm Teknolojisi 1": pp. 213 - 332.

15. William F. Smith, "Principles of Materials Science and Engineering", 1995, Mcgraw Hill Collage.

16. X. J. Sun, Y. X. Li, X. Chen, "Controlling Melt Quality of Compacted Graphite Iron", 2007, Material Science and Engineering.

17. U. Reuter and H. Schulz, M. Robbins and J. Daeth, "The Effect of Metallurgical Variables on the Machinability of Compacted Graphite Iron", 2001, Society of Automotive Engineers. Inc.

18. K. E. Metzloff, C. R. Loper, "Effect of Nodularity, Heat Treatment and Cupper on the Elastic Modulus of Ductile and Compacted Graphite Irons", 2001, AFS Transactions: pp. 1121 - 1124.

19. E. N. Pan, C. R. Loper, "Matrix Development in Graphitic Cast Iron", 1999, AFS Transactions: pp. 545 - 553.

20. John Vaccari, "How to Machine Compacted Graphite Iron", 2000, Issue of Machine Shop Guide: pp. 1 - 3.

21. F. Mampaey, "Influence of Compacted Graphite on Solidification Morphology of Cast Iron", 1983, AFS Transactions: pp. 11 - 14.

22. Dr. Steve Dawson, "Compacted Graphite Iron Mechanical and Pysical Properties for Engine Design", 1999, Werkstoff and Automobilantrieb VDI: pp. 1 - 19.

23. Sugwon Kim, S. L. Cockcroft. A. M. Omran, Honam Hwang , "Mechanical, Wear and Heat Exposure Properties of Compacted Graphite Cast Iron at Elevated Temperatures", 2009, Journal of Alloys and Compounds, pp.253 - 256.

24. C. R. Reese, W. J. Evans, "Development of an In the Mold Treatment Process for Compacted Graphite Iron Cylinder Blocks", 1998, AFS Transactions: pp. 673 - 683.

25. J. R. Marks, "Metallography of ductile Iron", 1999, AFS Transactions: pp. 819 - 825.

26. Dipl. Ing. C. Heisser, Dr. Ing. Jörg C. Sturm, "Casting Process Simulation of compacted Graphite Iron", 2003, AFS Transactions: pp. 685 - 689.

27. Primoz Mrvar, Jozef Medved"Kinetics of the Eutectoid Transformation of the as - Cast Mostly Perlitic Spheroidalidal Graphite Cast Iron", 2011, University of Ljubljana.

28. Elkem, "CompactMag TM. Alloy", Elkem ASA, vol 43: pp. 360 - 364.

29. W. Troschel, S. Dawson, "Process Control for the Production of CGI", 2001,

Foundry Trade Journal: pp. 8 - 14.

30. Rikard Kallbom, K. Hamberg, M. Wessen, L-E. Björkegren, "On the Solidification Sequence of Ductile Iron Castings Containing Chunky Graphite", 2005, Materials Science and Engineering: pp. 348 - 350.

31. Per Samuelsson, Peter Vomacka, "Compacted Graphite Iron for High Performance Piston Rings", 2003, Shipping World & Shipbuilder.

32. Rudolf Val. Sillen, "Adjusting Cast Iron Melts Using Active Carbon Equivalents", 2010, Adjusting CEL with ATAS White, NovaCast AB.

33. K. P. Shah, "The Hand Book on Mechanical Maintance", 2009, Cast Irons.

34. Rudolf Sillen, "The PQ-DIT Process. Improving Ductile Iron Production Using Situation Based Additions of Magnesium", NovaCast AB.

35. "Oxygen Activity Measurment in Cast Iron", Heraeus Electro - Nite, Celox Foundry: pp. 1 - 3.

36. K. W. Copi, "Total Oxygen Levels in Induction Furnace Melted Irons - A Preliminary Report", 2001, AFS Transactions: pp. 705 - 706.

37. Rudolf Val. Sillen, "Practical Uses of Experts Systems and Other Artificial Intelligence Technologies for Improving Foundry Process", 2010, AI Technology, NovaCast AB.

38. E. Selçuk, "Kinetics of Grahhitization reaction in White Cast Iron", 1973, The Metals Society London: pp. 36 - 37.

39. O. Elmabrouk, A. Kalkanlı, E. Selçuk and A. Çetin, "Oxygen Potential Values to Produce Compacted Graphite Cast Iron", 2008, Canadian Metallurjical Quarterly Volume 47: pp. 174 - 185.

40. R. Hummer, A. Bührig, "Condition of SG and CG Base Iron Melts Based on Measurements Made with a New Oxygen Sensor", 2009.

41. I. Riposan, M. Chisamera, S. Stan, "Role of Al, Ti, Zr in Gray Cast Iron Preconditioning/Inoculation", Elkem

42. "Standart Test Method for Evaluating the Microstructure of Graphite in Iron Casting ", American Society for Testing and Materials: pp. 1 - 2.

43. NovaCast Foundry Technology, "Cost Effective One-Step Process for Compacted Graphite Iron".

44. F. Mampaey, D. Habets, F. Seutens and J. Plessers," The use of oxygen activity measurment to determine optimal properties of ductile iron during production", 2008,: pp. 1 - 5.

APPENDIX A

SOLIDIFICATION SIMULATION RESULTS

Table A.1 Temperature results of the diesel engine block 2 via NovaCast NovaFlow simulation code.

Section Number	Section Thickness (mm)	Temperature ^{o}C
1	32.72	1289
2	36.26	1256
3	35.86	1292
4	9.82	1249
5	40.85	1252
6	7.99	1153
7	11.08	1185
8	7.25	1193
9	13.94	1244
10	16.30	1225
11	10.95	1184
13	10.39	1199
14	9.48	1156

Table A.2 Temperature results of the diesel engine block 3 via NovaCast NovaFlow simulation code.

Section Number	Section Thickness (mm)	Temperature ^{o}C
1	32.72	1353
2	36.26	1327
3	35.86	1323
4	9.82	1256
5	40.85	1274
6	7.99	1190
7	11.08	1248
8	7.25	1219
9	13.94	1278
10	16.30	1237
11	10.95	1243
13	10.39	1226
14	9.48	1244

Table A.3 Temperature results of the diesel engine block 4 via NovaCast NovaFlow simulation code.

Section Number	Section Thickness (mm)	Temperature ^{o}C
1	32.72	1286
2	36.26	1311
3	35.86	1315
4	9.82	1235
5	40.85	1260
6	7.99	1160
7	11.08	1250
8	7.25	1206
9	13.94	1272
10	16.30	1285
11	10.95	1234
13	10.39	1281
14	9.48	1194

Table A.4 Temperature results of the diesel engine block 5 via NovaCast NovaFlow simulation code.

Section Number	Section Thickness (mm)	Temperature ^{o}C
1	32.72	1303
2	36.26	1310
3	35.86	1274
4	9.82	1235
5	40.85	1231
6	7.99	1163
7	11.08	1301
8	7.25	1185
9	13.94	1257
10	16.30	1237
11	10.95	1299
13	10.39	1210
14	9.48	1164

Table A.5 Temperature results of the diesel engine block 6 via NovaCast NovaFlow simulation code.

Section Number	Section Thickness (mm)	Temperature ^{o}C
1	32.72	1370
2	36.26	1353
3	35.86	1356
4	9.82	1247
5	40.85	1259
6	7.99	1193
7	11.08	1270
8	7.25	1244
9	13.94	1302
10	16.30	1282
11	10.95	1349
13	10.39	1304
14	9.48	1278

Table A.6 Temperature results of the diesel engine block 7 via NovaCast NovaFlow simulation code.

Section Number	Section Thickness (mm)	Temperature ^{o}C
1	32.72	1379
2	36.26	1329
3	35.86	1337
4	9.82	1245
5	40.85	1294
6	7.99	1199
7	11.08	1221
8	7.25	1218
9	13.94	1301
10	16.30	1266
11	10.95	1234
13	10.39	1303
14	9.48	1164

Table A.7 Temperature results of the diesel engine block 8 via NovaCast NovaFlow simulation code.

Section Number	Section Thickness (mm)	Temperature ^{o}C
1	32.72	1372
2	36.26	1336
3	35.86	1336
4	9.82	1252
5	40.85	1281
6	7.99	1197
7	11.08	1287
8	7.25	1231
9	13.94	1268
10	16.30	1261
11	10.95	1230
13	10.39	1250
14	9.48	1267

Table A.8 Temperature results of the diesel engine block 9 via NovaCast NovaFlow simulation code.

Section Number	Section Thickness (mm)	Temperature ^{o}C
1	32.72	1361
2	36.26	1346
3	35.86	1346
4	9.82	1252
5	40.85	1242
6	7.99	1187
7	11.08	1247
8	7.25	1231
9	13.94	1293
10	16.30	1246
11	10.95	1212
13	10.39	1243
14	9.48	1152

Table A.9 Temperature results of the diesel engine block 12 via NovaCast NovaFlow simulation code.

Section Number	Section Thickness (mm)	Temperature ^{o}C
1	32.72	1301
2	36.26	1290
3	35.86	1308
4	9.82	1218
5	40.85	1246
6	7.99	1163
7	11.08	1272
8	7.25	1229
9	13.94	1246
10	16.30	1279
11	10.95	1279
13	10.39	1262
14	9.48	1217

Table A.10 Temperature results of the diesel engine block 13 via NovaCast NovaFlow simulation code.

Section Number	Section Thickness (mm)	Temperature ^{o}C
1	32.72	1332
2	36.26	1290
3	35.86	1330
4	9.82	1222
5	40.85	1258
6	7.99	1173
7	11.08	1181
8	7.25	1201
9	13.94	1220
10	16.30	1270
11	10.95	1252
13	10.39	1251
14	9.48	1234

Table A.11 Temperature results of the diesel engine block 14 via NovaCast NovaFlow simulation code.

Section Number	Section Thickness (mm)	Temperature ^{o}C
1	32.72	1331
2	36.26	1267
3	35.86	1318
4	9.82	1250
5	40.85	1245
6	7.99	1173
7	11.08	1257
8	7.25	1225
9	13.94	1267
10	16.30	1294
11	10.95	1261
13	10.39	1272
14	9.48	1156

Table A.12 Temperature results of the diesel engine block 15 via NovaCast NovaFlow simulation code.

Section Number	Section Thickness (mm)	Temperature ^{o}C
1	32.72	1347
2	36.26	1330
3	35.86	1344
4	9.82	1265
5	40.85	1259
6	7.99	1201
7	11.08	1242
8	7.25	1240
9	13.94	1288
10	16.30	1280
11	10.95	1228
13	10.39	1231
14	9.48	1182

Table A.13 Temperature results of the diesel engine block 16 via NovaCast NovaFlow simulation code.

Section Number	Section Thickness (mm)	Temperature ^{o}C
1	32.72	1346
2	36.26	1265
3	35.86	1313
4	9.82	1222
5	40.85	1260
6	7.99	1175
7	11.08	1296
8	7.25	1218
9	13.94	1277
10	16.30	1263
11	10.95	1209
13	10.39	1218
14	9.48	1220

Table A.14 Temperature results of the diesel engine block 17 via NovaCast NovaFlow simulation code.

Section Number	Section Thickness (mm)	Temperature ^{o}C
1	32.72	1340
2	36.26	1333
3	35.86	1353
4	9.82	1247
5	40.85	1267
6	7.99	1169
7	11.08	1307
8	7.25	1218
9	13.94	1271
10	16.30	1294
11	10.95	1321
13	10.39	1228
14	9.48	1160

Table A.15 Temperature results of the diesel engine block 18 via NovaCast NovaFlow simulation code.

Section Number	Section Thickness (mm)	Temperature ^{o}C
1	32.72	1295
2	36.26	1343
3	35.86	1338
4	9.82	1250
5	40.85	1280
6	7.99	1187
7	11.08	1304
8	7.25	1225
9	13.94	1267
10	16.30	1294
11	10.95	1261
13	10.39	1272
14	9.48	1156

Table A.16 Temperature results of the diesel engine block 19 via NovaCast NovaFlow simulation code.

Section Number	Section Thickness (mm)	Temperature ^{o}C
1	32.72	1314
2	36.26	1280
3	35.86	1327
4	9.82	1249
5	40.85	1259
6	7.99	1168
7	11.08	1242
8	7.25	1240
9	13.94	1277
10	16.30	1280
11	10.95	1228
13	10.39	1231
14	9.48	1182

APPENDIX B

REPORT SHEETS OF THE DIESEL ENGINE BLOCKS

Table B.1 After treatment, chemical composition and pouring temperature of the diesel engine block 1 is given below.

ANALYSİS. :

CHEMİCAL ANALYSIS	FURNACE	AFTER TREATMENT	AFTER CASTING	RESULTS OF TEMPERATURE		
					T(^{0}C)	b(O) (ppm)
	C	C 3,870	C			
	Si	Si 2,180	Si			
	S	S 0,019	S			
	P	P 0,053	P			
	Mn	Mn 0,092	Mn	AFTER FURNACE	1472	1,4266
	Ni	Ni -	Ni			
	Cr	Cr 0,010	Cr			
	Mo	Mo -	Mo			
	V	V -	V	LADLE		
	Cu	Cu 0,010	Cu			
	W	W -	W			
	Sn	Sn 0,006	Sn			
	Al	Al -	Al	AFTER TREATMENT	1410,4	0,2181
	Pb	Pb -	Pb			
	Mg -	Mg 0,0204	Mg			

Table B.2 After treatment, chemical composition and pouring temperature of the diesel engine block 2 is given below.

ANALYSİS. :								
		RESULTS				RESULTS OF TEMPERATURE		
CHEMİCAL ANALYSİS	FURNACE	AFTER TREATMENT		AFTER CASTING		T(^{0}C)	b(O) (ppm)	
	C	C	3,710	C				
	Si	Si	2,250	Si				
	S	S	0,012	S				
	P	P	0,041	P				
	Mn	Mn	0,100	Mn		AFTER FURNACE	1469,2	1,24
	Ni	Ni	-	Ni				
	Cr	Cr	0,016	Cr				
	Mo	Mo	-	Mo				
	V	V	-	V		LADLE		
	Cu	Cu	0,008	Cu				
	W	W	-	W				
	Sn	Sn	0,003	Sn				
	Al	Al	-	Al		AFTER TREATMENT	1394	0,2162
	Pb	Pb	-	Pb				
	Mg	Mg	0,016	Mg				

Table B.3 After treatment, chemical composition and pouring temperature of the diesel engine block 3 is given below.

ANALYSİS. :

CHEMİCAL ANALYSIS			RESULTS		RESULTS OF TEMPERATURE		
						T(^{0}C)	b(O) (ppm)
	FURNACE	C	C 3,620	C			
		Si	Si 2,240	Si			
		S	S 0,012	S			
		P	P 0,042	P			
		Mn	Mn 0,100	Mn	AFTER FURNACE		
		Ni	Ni -	Ni			
		Cr	Cr 0,016	Cr			
		Mo	Mo -	Mo			
		V	V -	V	LADLE		
		Cu	Cu 0,007	Cu			
		W	W -	W			
		Sn	Sn 0,003	Sn			
		Al	Al -	Al	AFTER TREATMENT	1417,3	0,3926
		Pb	Pb -	Pb			
		Mg	Mg 0,012	Mg			

Table B.4 After treatment, chemical composition and pouring temperature of the diesel engine block 4 is given below.

ANALYSİS. :								
		RESULTS				RESULTS OF TEMPERATURE		
CHEMİCAL ANALYSIS	FURNACE		AFTER TREATMENT		AFTER CASTING		T(^{0}C)	b(O) (ppm)
		C	C	3,650	C			
		Si	Si	2,240	Si			
		S	S	0,016	S			
		P	P	0,040	P			
		Mn	Mn	0,100	Mn	AFTER FURNACE		
		Ni	Ni	-	Ni			
		Cr	Cr	0,016	Cr			
		Mo	Mo	-	Mo			
		V	V	-	V	LADLE		
		Cu	Cu	0,008	Cu			
		W	W	-	W			
		Sn	Sn	0,003	Sn			
		Al	Al	-	Al	AFTER TREATMENT	1421,8	0,2286
		Pb	Pb	-	Pb			
		Mg	Mg	0,013	Mg			

Table B.5 After treatment, chemical composition and pouring temperature of the diesel engine block 5 is given below.

ANALYSİS. :

CHEMİCAL ANALYSIS			RESULTS			RESULTS OF TEMPERATURE		
	FURNACE		AFTER TREATMENT		AFTER CASTING		T(^{0}C)	b(O) (ppm)
		C	C 3,630		C			
		Si	Si 2,260		Si			
		S	S 0,017		S			
		P	P 0,041		P			
		Mn	Mn 0,100		Mn	AFTER FURNACE		
		Ni	Ni -		Ni			
		Cr	Cr 0,016		Cr			
		Mo	Mo -		Mo			
		V	V -		V	LADLE		
		Cu	Cu 0,008		Cu			
		W	W -		W			
		Sn	Sn 0,003		Sn			
		Al	Al -		Al	AFTER TREATMENT	1418	0,1839
		Pb	Pb -		Pb			
		Mg	Mg 0,014		Mg			

Table B.6 After treatment, chemical composition and pouring temperature of the diesel engine block 6 is given below.

ANALYSİS. :

CHEMİCAL ANALYSIS			RESULTS		RESULTS OF TEMPERATURE		
	FURNACE	AFTER TREATMENT		AFTER CASTING		T(^{0}C)	b(O) (ppm)
	C	C	3,800	C			
	Si	Si	2,120	Si			
	S	S	0,017	S			
	P	P	0,040	P			
	Mn	Mn	0,210	Mn	AFTER FURNACE	1455,4	1,396
	Ni	Ni		Ni			
	Cr	Cr	0,015	Cr			
	Mo	Mo		Mo			
	V	V		V	LADLE		
	Cu	Cu	0,030	Cu			
	W	W	0,008	W			
	Sn	Sn		Sn			
	Al	Al		Al	AFTER TREATMENT	1441,7	0,3127
	Pb	Pb		Pb			
	Mg	Mg	0,018	Mg			

Table B.7 After treatment, chemical composition and pouring temperature of the diesel engine block 7 is given below.

ANALYSİS. :

CHEMİCAL ANALYSIS						RESULTS OF TEMPERATURE		
	FURNACE		AFTER TREATMENT		AFTER CASTING		T(^{0}C)	b(O) (ppm)
		C		C 3,580				
		Si		Si 2,100				
		S		S 0,015				
		P		P 0,040				
		Mn		Mn 0,200		AFTER FURNACE		
		Ni		Ni				
		Cr		Cr 0,015				
		Mo		Mo				
		V		V		LADLE		
		Cu		Cu 0,030				
		W		W				
		Sn		Sn 0,007				
		Al		Al		AFTER TREATMENT	1445	0,4522
		Pb		Pb				
		Mg		Mg 0,015				

Table B.8 After treatment, chemical composition and pouring temperature of the diesel engine block 8 is given below.

ANALYSİS. :

RESULTS – CHEMİCAL ANALYSİS

Element	FURNACE	AFTER TREATMENT	AFTER CASTING
C		3,650	
Si		2,080	
S		0,013	
P		0,040	
Mn		0,190	
Ni			
Cr		0,015	
Mo			
V			
Cu		0,030	
W			
Sn		0,007	
Al			
Pb			
Mg		0,015	

RESULTS OF TEMPERATURE

	T(^{0}C)	b(O) (ppm)
AFTER FURNACE		
LADLE		
AFTER TREATMENT	1437,9	0,405

Table B.9 After treatment, chemical composition and pouring temperature of the diesel engine block 9 is given below.

ANALYSİS. :

CHEMİCAL ANALYSIS			RESULTS		RESULTS OF TEMPERATURE		
	FURNACE	AFTER TREATMENT		AFTER CASTING		T(^{0}C)	b(O) (ppm)
	C	C	3,650	C			
	Si	Si	2,100	Si			
	S	S	0,016	S			
	P	P	0,040	P			
	Mn	Mn	0,200	Mn	AFTER FURNACE	1456	5,9976
	Ni	Ni		Ni			
	Cr	Cr	0,015	Cr			
	Mo	Mo		Mo			
	V	V		V	LADLE		
	Cu	Cu	0,030	Cu			
	W	W		W			
	Sn	Sn	0,007	Sn			
	Al	Al	0,001	Al	AFTER TREATMENT	1437,1	0,3691
	Pb	Pb		Pb			
	Mg	Mg	0,015	Mg			

Table B.10 After treatment, chemical composition and pouring temperature of the diesel engine block 10 is given below.

ANALYSİS. :								
		RESULTS				RESULTS OF TEMPERATURE		
CHEMİCAL ANALYSİS	FURNACE		AFTER TREATMENT		AFTER CASTING		T(^{0}C)	b(O) (ppm)
		C	C 3,600		C			
		Si	Si 2,100		Si			
		S	S 0,016		S			
		P	P 0,043		P			
		Mn	Mn 0,084		Mn	AFTER FURNACE		
		Ni	Ni		Ni			
		Cr	Cr 0,012		Cr			
		Mo	Mo		Mo			
		V	V		V	LADLE		
		Cu	Cu 0,018		Cu			
		W	W		W			
		Sn	Sn 0,007		Sn			
		Al	Al 0,007		Al	AFTER TREATMENT	1431,2	0,4654
		Pb	Pb		Pb			
		Mg	Mg 0,011		Mg			

Table B.11 After treatment, chemical composition and pouring temperature of the diesel engine block 11 is given below.

ANALYSİS. :

CHEMİCAL ANALYSIS			RESULTS		RESULTS OF TEMPERATURE		
						T(^{0}C)	b(O) (ppm)
	FURNACE	AFTER TREATMENT		AFTER CASTING			
	C	C	3,580	C			
	Si	Si	2,100	Si			
	S	S	0,017	S			
	P	P	0,045	P			
	Mn	Mn	0,083	Mn	AFTER FURNACE		
	Ni	Ni		Ni			
	Cr	Cr	0,012	Cr			
	Mo	Mo		Mo			
	V	V		V	LADLE		
	Cu	Cu	0,017	Cu			
	W	W		W			
	Sn	Sn	0,007	Sn			
	Al	Al	0,007	Al	AFTER TREATMENT	1449	0,5148
	Pb	Pb		Pb			
	Mg	Mg	0,013	Mg			

Table B.12 After treatment, chemical composition and pouring temperature of the diesel engine block 12 is given below.

ANALYSİS. :

CHEMİCAL ANALYSIS						RESULTS OF TEMPERATURE		
	FURNACE		AFTER TREATMENT		AFTER CASTING		T(^{0}C)	b(O) (ppm)
		C		C 3,640				
		Si		Si 1,960				
		S		S 0,020				
		P		P 0,060				
		Mn		Mn 0,200		AFTER FURNACE	1505,6	2,2871
		Ni		Ni -				
		Cr		Cr -				
		Mo		Mo -				
		V		V -		LADLE		
		Cu		Cu 0,420				
		W		W -				
		Sn		Sn 0,010				
		Al		Al -		AFTER TREATMENT	1410,4	0,1965
		Pb		Pb -				
		Mg		Mg 0,013				

Table B.13 After treatment, chemical composition and pouring temperature of the diesel engine block 13 is given below.

ANALYSİS. :							
RESULTS					RESULTS OF TEMPERATURE		
CHEMİCAL ANALYSİS	FURNACE	AFTER TREATMENT		AFTER CASTING		T(⁰C)	b(O) (ppm)
	C	C	3,750	C			
	Si	Si	2,050	Si			
	S	S	0,019	S			
	P	P	0,062	P			
	Mn	Mn	0,220	Mn	AFTER FURNACE		
	Ni	Ni	-	Ni			
	Cr	Cr	-	Cr			
	Mo	Mo	-	Mo			
	V	V	-	V	LADLE		
	Cu	Cu	0,550	Cu			
	W	W	-	W			
	Sn	Sn	0,011	Sn			
	Al	Al	-	Al	AFTER TREATMENT	1392,5	0,1686
	Pb	Pb	-	Pb			
	Mg	Mg	0,019	Mg			

Table B.14 After treatment, chemical composition and pouring temperature of the diesel engine block 14 is given below.

ANALYSİS. :

CHEMİCAL ANALYSIS		RESULTS				RESULTS OF TEMPERATURE		
							T(^{0}C)	b(O) (ppm)
	C		C	3,710	C			
	Si		Si	2,060	Si			
	S		S	0,019	S			
	P		P	0,062	P			
	Mn		Mn	0,220	Mn	AFTER FURNACE		
	Ni		Ni	-	Ni			
	Cr		Cr	-	Cr			
	Mo		Mo	-	Mo			
	V		V	-	V	LADLE		
	Cu		Cu	0,550	Cu			
	W		W	-	W			
	Sn		Sn	0,011	Sn			
	Al		Al	-	Al	AFTER TREATMENT	1393,8	0,1109
	Pb		Pb	-	Pb			
	Mg		Mg	0,019	Mg			

Table B.15 After treatment, chemical composition and pouring temperature of the diesel engine block 15 is given below.

ANALYSİS. :

CHEMİCAL ANALYSIS			RESULTS		RESULTS OF TEMPERATURE		
						T(^{0}C)	b(O) (ppm)
	C		C 3,730				
	Si		Si 2,050				
	S		S 0,021				
	P		P 0,063				
	Mn		Mn 0,220		AFTER FURNACE		
	Ni		Ni -				
	Cr		Cr -				
	Mo		Mo -				
	V		V -		LADLE		
	Cu		Cu 0,570				
	W		W -				
	Sn		Sn 0,012				
	Al		Al -		AFTER TREATMENT	1424	0,384
	Pb		Pb -				
	Mg		Mg 0,017				

Table B.16 After treatment, chemical composition and pouring temperature of the diesel engine block 16 is given below.

ANALYSİS. :									
		RESULTS				RESULTS OF TEMPERATURE			
CHEMİCAL ANALYSİS	FURNACE		AFTER TREATMENT		AFTER CASTING		T(^{0}C)	b(O) (ppm)	
	C		C 3,640		C				
	Si		Si 1,850		Si				
	S		S 0,011		S				
	P		P 0,045		P				
	Mn		Mn 0,190		Mn	AFTER FURNACE	1520,1	2,4768	
	Ni		Ni -		Ni				
	Cr		Cr 0,032		Cr				
	Mo		Mo 0,003		Mo				
	V		V -		V	LADLE			
	Cu		Cu 0,557		Cu				
	W		W -		W				
	Sn		Sn 0,007		Sn				
	Al		Al 0,009		Al	AFTER TREATMENT	1404,3	0,17	
	Pb		Pb -		Pb				
	Mg		Mg 0,017		Mg				

Table B.17 After treatment, chemical composition and pouring temperature of the diesel engine block 17 is given below.

ANALYSİS. :

CHEMİCAL ANALYSIS			RESULTS			RESULTS OF TEMPERATURE		
							T(^{0}C)	b(O) (ppm)
	FURNACE	C	AFTER TREATMENT C 3,570	AFTER CASTING C				
		Si	Si 1,830	Si				
		S	S 0,013	S				
		P	P 0,046	P				
		Mn	Mn 0,190	Mn		AFTER FURNACE		
		Ni	Ni -	Ni				
		Cr	Cr 0,032	Cr				
		Mo	Mo 0,003	Mo				
		V	V -	V		LADLE		
		Cu	Cu 0,725	Cu				
		W	W -	W				
		Sn	Sn 0,007	Sn				
		Al	Al 0,007	Al		AFTER TREATMENT	1413,4	0,272
		Pb	Pb -	Pb				
		Mg	Mg 0,012	Mg				

Table B.18 After treatment, chemical composition and pouring temperature of the diesel engine block 18 is given below.

ANALYSİS. :								
		RESULTS				RESULTS OF TEMPERATURE		
CHEMİCAL ANALYSIS	FURNACE		AFTER TREATMENT		AFTER CASTING		T(^{0}C)	b(O) (ppm)
		C	C 3,620		C			
		Si	Si 1,860		Si			
		S	S 0,010		S			
		P	P 0,045		P			
		Mn	Mn 0,180		Mn	AFTER FURNACE		
		Ni	Ni -		Ni			
		Cr	Cr 0,032		Cr			
		Mo	Mo 0,003		Mo			
		V	V -		V	LADLE		
		Cu	Cu 0,642		Cu			
		W	W -		W			
		Sn	Sn 0,007		Sn			
		Al	Al 0,007		Al	AFTER TREATMENT	1426,1	0,2652
		Pb	Pb -		Pb			
		Mg	Mg 0,011		Mg			

Table B.19 After treatment, chemical composition and pouring temperature of the diesel engine block 19 is given below.

ANALYSİS. :

CHEMİCAL ANALYSIS						RESULTS OF TEMPERATURE		
							T(^{0}C)	b(O) (ppm)
	FURNACE	C	AFTER TREATMENT C 3,680	AFTER CASTING C				
		Si	Si 1,770	Si				
		S	S 0,013	S				
		P	P 0,044	P				
		Mn	Mn 0,178	Mn		AFTER FURNACE		
		Ni	Ni -	Ni				
		Cr	Cr 0,032	Cr				
		Mo	Mo 0,003	Mo				
		V	V -	V		LADLE		
		Cu	Cu 0,575	Cu				
		W	W -	W				
		Sn	Sn 0,006	Sn				
		Al	Al 0,006	Al		AFTER TREATMENT	1424	0,3196
		Pb	Pb -	Pb				
		Mg	Mg 0,010	Mg				

APPENDIX C

LINEER REGRESSION RESULTS

Table C.1 Lineer regression result of thickness section 1 with 32.72 mm, which was obtained by means of excel linest code.

C.E.V	O ppm	Mg/S	Temp.	Nod %	Diesel Engine Code
4,52	0,3127	1,05	1370	23,68	6
4,29	0,4522	1	1379	22,82	7
4,36	0,405	1,15	1372	23,68	8
4,36	0,369	0,93	1361	25	9
4,27	0,1965	0,65	1301	29	12
4,45	0,1686	1	1332	26	13
4,42	0,1109	1	1331	25	14
4,43	0,384	0,8	1347	26	15
4,27	0,17	1,54	1346	26	16
4,2	0,272	0,92	1340	26	17
4,26	0,2652	1,1	1295	34	18
4,28	0,3196	0,76	1314	29	19
4,47	0,2162	1,33	1289	35,115	2
4,38	0,3926	1	1353	23,15	3
4,41	0,2286	0,81	1286	32,844	4
4,39	0,1839	0,82	1303	30,59	5
-0,151262461	4,614333484	12,73303376	1,926565878	212,4024405	
0,011854415	1,298555525	3,578933891	2,992288487	18,52351265	
0,950289282	1,028500523	#N/A	#N/A	#N/A	
52,57006219	11	#N/A	#N/A	#N/A	
222,4372493	11,63594659	#N/A	#N/A	#N/A	
X4	X3	X2	X1	b	
y=m1*x1+m2*x2+m3*x3+m4*x4+b					
y=1,926*x1+12,733*x2+4,614*x3-0,151x4+212,402					

Table C.2 Lineer regression result of thickness section 2 with 36.26 mm, which was obtained by means of excel linest code.

C.E.V.	O (ppm)	Mg/S	Temp.	Nod. %	Diesel Engine Code
4,52	0,3127	1,05	1353	20,82	6
4,29	0,4522	1	1329	23,93	7
4,36	0,405	1,15	1336	23,11	8
4,36	0,369	0,93	1346	22,6	9
4,27	0,1965	0,65	1290	26	12
4,45	0,1686	1	1290	25	13
4,42	0,1109	1	1267	27	14
4,43	0,384	0,8	1330	24	15
4,27	0,17	1,54	1265	29	16
4,2	0,272	0,92	1333	24	17
4,26	0,2652	1,1	1343	20	18
4,28	0,3196	0,76	1280	33	19
4,47	0,2162	1,33	1256	28,57	2
4,38	0,3926	1	1327	22,51	3
4,41	0,2286	0,81	1311	24,326	4
4,39	0,1839	0,82	1310	24,79	5
-0,120227973	-2,644722066	12,65481	-5,439982539	205,2823878	
0,01668985	1,764628411	5,058792	4,205222377	27,54128309	
0,854108283	1,453447786	#N/A	#N/A	#N/A	
16,09959654	11	#N/A	#N/A	#N/A	
136,0422649	23,23761514	#N/A	#N/A	#N/A	
X4	X3	X2	X1	b	
y=m1*x1+m2*x2+m3*x3+m4*x4+b					
y=-5,439*x1+12,654*x2-2,644*x3-0,12*x4+205,282					

Table C.3 Lineer regression result of thickness section 3 with 35.86 mm, which was obtained by means of excel linest code.

C.E.V.	O (ppm)	Mg/S	Temp.	Nod. %	Diesel Engine Code
4,52	0,3127	1,05	1356	17,65	6
4,29	0,4522	1	1337	25,49	7
4,36	0,405	1,15	1336	22,88	8
4,36	0,369	0,93	1346	21,78	9
4,27	0,1965	0,65	1308	25	12
4,45	0,1686	1	1330	17	13
4,42	0,1109	1	1318	23	14
4,43	0,384	0,8	1344	23	15
4,27	0,17	1,54	1313	26	16
4,2	0,272	0,92	1353	20	17
4,26	0,2652	1,1	1338	22	18
4,28	0,3196	0,76	1327	24	19
4,47	0,2162	1,33	1292	27,485	2
4,38	0,3926	1	1323	26,974	3
4,41	0,2286	0,81	1315	23,312	4
4,39	0,1839	0,82	1274	30,14	5
-0,176210091	1,598233589	19,84575073	-9,233777167	290,229581	
0,018282516	1,52453005	3,967546186	3,75212277	29,85579757	
0,89745918	1,293891897	#N/A	#N/A	#N/A	
24,06858784	11	#N/A	#N/A	#N/A	
161,1783063	18,41571866	#N/A	#N/A	#N/A	
X4	X3	X2	X1	b	
y=m1*x1+m2*x2+m3*x3+m4*x4+b					
y=-9,233*x1+19,845*x2-1,598*x3-0,176*x4+290,229					

Table C.4 Lineer regression result of thickness section 4 with 9.82 mm, which was obtained by means of excel linest code.

C.E.V.	O (ppm)	Mg/S	Temp.	Nod. %	Diesel Engine Code
4,52	0,3127	1,05	1247	23,52	6
4,29	0,4522	1	1245	34,616	7
4,36	0,405	1,15	1252	29,05	8
4,36	0,369	0,93	1252	26,14	9
4,27	0,1965	0,65	1218	28	12
4,45	0,1686	1	1222	25	13
4,42	0,1109	1	1201	29	14
4,43	0,384	0,8	1265	23	15
4,27	0,17	1,54	1222	25	16
4,2	0,272	0,92	1247	25	17
4,26	0,2652	1,1	1250	23	18
4,28	0,3196	0,76	1249	27	19
4,47	0,2162	1,33	1202	35,442	2
4,38	0,3926	1	1256	27,754	3
4,39	0,1839	0,82	1235	20,13	5
-0,351157956	0,145135956	61,92679486	-8,01929549	478,722787	
0,025846837	1,326478829	4,669774898	3,108031112	36,5127178	
0,955283486	1,04099305	#N/A	#N/A	#N/A	
53,40775753	10	#N/A	#N/A	#N/A	
231,5047971	10,8366653	#N/A	#N/A	#N/A	
X4	X3	X2	X1	b	
y=m1*x1+m2*x2+m3*x3+m4*x4+b					
y=-8,019*x1+61,926*x2+0,145*x3-0,351*x4+428,722					

Table C.5 Lineer regression result of thickness section 5 with 40.85 mm, which was obtained by means of excel linest code.

C.E.V.	O (ppm)	Mg/S	Temp.	Nod. %	Diesel Engine Code
4,52	0,3127	1,05	1259	30,135	6
4,29	0,4522	1	1294	20,72	7
4,36	0,405	1,15	1281	26,79	8
4,36	0,369	0,93	1242	41,8	9
4,27	0,1965	0,65	1246	26	12
4,45	0,1686	1	1258	23	13
4,42	0,1109	1	1245	27	14
4,43	0,384	0,8	1259	23	15
4,2	0,272	0,92	1267	27	17
4,26	0,2652	1,1	1280	21	18
4,28	0,3196	0,76	1259	25	19
4,47	0,2162	1,33	1252	39,824	2
4,38	0,3926	1	1274	21,298	3
4,41	0,2286	0,81	1260	21,714	5
4,39	0,1839	0,82	1231	35,102	17
-0,581394514	32,31153565	41,20556855	-27,1636024	836,1211	
0,056126295	4,323456402	7,679506871	8,090195427	89,70225	
0,925788014	2,163324079	#N/A	#N/A	#N/A	
31,18728046	10	#N/A	#N/A	#N/A	
583,8222817	46,79971073	#N/A	#N/A	#N/A	
X4	X3	X2	X1	b	
y=m1*x1+m2*x2+m3*x3+m4*x4+b					
y=-27,163*x1+41,205*x2+32,311*x3-0,581*x4+836,121					

Table C.6 Lineer regression result of thickness section 6 with 7.99 mm, which was obtained by means of excel linest code.

C.E.V.	O (ppm)	Mg/S	Temp.	Nod. %	Diesel Engine Code
4,52	0,3127	1,05	1193	31,185	6
4,29	0,4522	1	1199	27,02	7
4,36	0,405	1,15	1197	30,22	8
4,36	0,369	0,93	1187	31,13	9
4,27	0,1965	0,65	1163	24	12
4,45	0,1686	1	1173	22	13
4,42	0,1109	1	1173	21	14
4,43	0,384	0,8	1201	22	15
4,27	0,17	1,54	1175	28	16
4,2	0,272	0,92	1169	31	17
4,26	0,2652	1,1	1187	24	18
4,28	0,3196	0,76	1188	23	19
4,47	0,2162	1,33	1153	33,892	2
4,38	0,3926	1	1190	28,972	3
4,41	0,2286	0,81	1160	28,26	4
4,39	0,1839	0,82	1163	25,67	5
-0,282954864	9,90952737	48,08309396	5,844230311	312,0191	
0,065774636	2,789985753	9,925814957	6,795933218	79,11056	
0,743835263	2,347600961	#N/A	#N/A	#N/A	
7,985279318	11	#N/A	#N/A	#N/A	
176,0348524	60,623533	#N/A	#N/A	#N/A	
X4	X3	X2	X1	b	
y=m1*x1+m2*x2+m3*x3+m4*x4+b					
y=5,844*x1+48,083*x2+9,909*x3-0,282*x4+312,019					

Table C.7 Lineer regression result of thickness section 7 with 11.08 mm, which was obtained by means of excel linest code.

C.E.V.	O (ppm)	Mg/S	Temp.	Nod. %	Diesel Engine Code
4,52	0,3127	1,05	1270	25,39	6
4,29	0,4522	1	1221	34,2	7
4,36	0,405	1,15	1287	21,62	8
4,36	0,369	0,93	1247	28,46	9
4,27	0,1965	0,65	1272	25	12
4,45	0,1686	1	1181	38	13
4,42	0,1109	1	1257	25	14
4,43	0,384	0,8	1242	29	15
4,27	0,17	1,54	1296	25	16
4,2	0,272	0,92	1307	25	17
4,26	0,2652	1,1	1304	23	18
4,28	0,3196	0,76	1242	30	19
4,47	0,2162	1,33	1185	34,878	2
4,38	0,3926	1	1248	28,44	3
4,41	0,2286	0,81	1250	28,856	4
4,39	0,1839	0,82	1301	22,07	5
-0,13032051	0,808242935	0,08953879	-13,0079	247,4294	
0,011600258	1,73985205	3,816966643	5,007144	32,12508	
0,928268501	1,476969224	#N/A	#N/A	#N/A	
35,5874114	11	#N/A	#N/A	#N/A	
310,5269388	23,99581897	#N/A	#N/A	#N/A	
X4	X3	X2	X1	b	
y=m1*x1+m2*x2+m3*x3+m4*x4+b					
y=-13,007*x1+0,089*x2+0,808*x3-0,13*x4+247,429					

Table C.8 Lineer regression result of thickness section 8 with 7.25 mm, which was obtained by means of excel linest code.

C.E.V.	O (ppm)	Mg/S	Temp.	Nod. %	Diesel Engine Code
4,52	0,3127	1,05	1244	26,33	6
4,29	0,4522	1	1218	40,09	7
4,36	0,405	1,15	1231	27,448	8
4,36	0,369	0,93	1231	26,76	9
4,27	0,1965	0,65	1229	26	12
4,45	0,1686	1	1201	32	13
4,42	0,1109	1	1214	29	14
4,43	0,384	0,8	1240	23	15
4,27	0,17	1,54	1218	32	16
4,2	0,272	0,92	1218	31	17
4,26	0,2652	1,1	1225	30	18
4,28	0,3196	0,76	1203	38	19
4,47	0,2162	1,33	1193	35,025	2
4,38	0,3926	1	1219	33,552	3
4,41	0,2286	0,81	1206	31,616	4
4,39	0,1839	0,82	1185	38,104	5
-0,29583408	3,079604466	22,77740788	-11,2559	431,0234	
0,043939407	2,866211955	7,158468395	7,028802	60,66164	
0,815482164	2,432099081	#N/A	#N/A	#N/A	
12,15370828	11	#N/A	#N/A	#N/A	
287,5618881	65,06616531	#N/A	#N/A	#N/A	
X4	X3	X2	X1	b	
y=m1*x1+m2*x2+m3*x3+m4*x4+b					
y=-12,515*x1+23,029*x2+3,036*x3-0,303*x4+445,304					

Table C.9 Lineer regression result of thickness section 9 with 7.25 mm, which was obtained by means of excel linest code.

C.E.V.	O (ppm)	Mg/S	Temp.	Nod. %	Diesel Engine Code
4,52	0,3127	1,05	1302	20,88	6
4,29	0,4522	1	1301	21,78	7
4,36	0,405	1,15	1268	28,65	8
4,36	0,369	0,93	1293	24,53	9
4,27	0,1965	0,65	1246	28	12
4,45	0,1686	1	1220	32	13
4,42	0,1109	1	1260	25	14
4,43	0,384	0,8	1288	23	15
4,27	0,17	1,54	1277	23	16
4,2	0,272	0,92	1271	26	17
4,26	0,2652	1,1	1267	28	18
4,28	0,3196	0,76	1277	26	19
4,47	0,2162	1,33	1244	27,874	2
4,38	0,3926	1	1278	26,25	3
4,41	0,2286	0,81	1272	25,745	4
4,39	0,1839	0,82	1257	28,95	5
-0,15513397	-0,94852721	10,86988991	-2,86198	233,4058	
0,01981496	1,430732321	4,243725359	3,493075	29,26558	
0,87527451	1,20726281	#N/A	#N/A	#N/A	
19,29842012	11	#N/A	#N/A	#N/A	
112,508515	16,03231842	#N/A	#N/A	#N/A	
X4	X3	X2	X1	b	
y=m1*x1+m2*x2+m3*x3+m4*x4+b					
y=-2,861*x1+10,869*x2-0,948*x3-0,155*x4+233,406					

Table C.10 Lineer regression result of thickness section 10 with 7.25 mm, which was obtained by means of excel linest code.

C.E.V	O ppm	Mg/S	Temp.	Nod. %	Diesel Engine Code
4,52	0,3127	1,05	1282	22,89	6
4,29	0,4522	1	1266	36,81	7
4,36	0,405	1,15	1261	33,22	8
4,36	0,369	0,93	1246	36,99	9
4,27	0,1965	0,65	1279	28	12
4,45	0,1686	1	1270	21	13
4,42	0,1109	1	1220	30	14
4,43	0,384	0,8	1290	22	15
4,27	0,17	1,54	1263	28	16
4,2	0,272	0,92	1294	24	17
4,26	0,2652	1,1	1294	24	18
4,28	0,3196	0,76	1280	28	19
4,47	0,2162	1,33	1225	31,772	2
4,38	0,3926	1	1237	38,66	3
4,41	0,2286	0,81	1285	21,56	4
4,39	0,1839	0,82	1237	28,82	5
-0,221961018	-0,042496209	34,75712075	-27,321	418,6119	
0,020153559	2,044710912	4,336289188	5,173127	40,11924	
0,938870634	1,665380395	#N/A	#N/A	#N/A	
42,23656199	11	#N/A	#N/A	#N/A	
468,5710433	30,50841045	#N/A	#N/A	#N/A	
X4	X3	X2	X1	b	
y=m1*x1+m2*x2+m3*x3+m4*x4+b					
y=-27,321*x1+34,757*x2-0,042*x3-0,221*x4+418,612					

Table C.11 Lineer regression result of thickness section 11 with 7.25 mm, which was obtained by means of excel linest code.

C.E.V	O ppm	Mg/S	Temp.	Nod. %	Diesel Engine Code
4,52	0,3127	1,05	1349	20,39	6
4,29	0,4522	1	1234	32,64	7
4,36	0,405	1,15	1230	33,68	8
4,36	0,369	0,93	1212	37,92	9
4,27	0,1965	0,65	1279	29	12
4,45	0,1686	1	1252	26	13
4,42	0,1109	1	1228	29	14
4,43	0,384	0,8	1279	27	15
4,27	0,17	1,54	1209	31	16
4,2	0,272	0,92	1321	22	17
4,26	0,2652	1,1	1261	27	18
4,28	0,3196	0,76	1228	34	19
4,47	0,2162	1,33	1184	33,85	2
4,38	0,3926	1	1243	32,036	3
4,41	0,2286	0,81	1234	30,76	4
4,39	0,1839	0,82	1299	23,68	5
-0,10719965	-4,356105699	14,7439471	-2,80504	176,1033	
0,009538873	1,890758861	3,739136191	4,21877	21,88676	
0,932423057	1,457466489	#N/A	#N/A	#N/A	
37,94435324	11	#N/A	#N/A	#N/A	
322,4068808	23,36629423	#N/A	#N/A	#N/A	
X4	X3	X2	X1	b	
y=m1*x1+m2*x2+m3*x3+m4*x4+b					
y=-2,805*x1+14,743*x2-4,356*x3-0,107*x4+176,103					

Table C.12 Lineer regression result of thickness section 13 with 10.39 mm, which was obtained by means of excel linest code.

C.E.V	O ppm	Mg/S	Temp.	Nod. %	Diesel Engine Code
4,52	0,3127	1,05	1304	21,42	6
4,29	0,4522	1	1303	22,26	7
4,36	0,405	1,15	1250	28,96	8
4,36	0,369	0,93	1243	30,668	9
4,27	0,1965	0,65	1262	24	12
4,45	0,1686	1	1251	30	13
4,42	0,1109	1	1251	30	14
4,43	0,384	0,8	1282	25	15
4,27	0,17	1,54	1218	33	16
4,2	0,272	0,92	1228	32	17
4,26	0,2652	1,1	1272	25	18
4,28	0,3196	0,76	1231	30	19
4,47	0,2162	1,33	1199	39,016	2
4,38	0,3926	1	1226	33,236	3
4,41	0,2286	0,81	1281	23,088	4
4,39	0,1839	0,82	1210	35,46	5
-0,15856442	2,117765515	4,08162219	9,40362288	183,0253	
0,00991326	1,305882275	2,92617022	3,13867812	16,43893	
0,96797021	1,059570107	#N/A	#N/A	#N/A	
83,107583	11	#N/A	#N/A	#N/A	
373,215814	12,34957692	#N/A	#N/A	#N/A	
X4	X3	X2	X1	b	
y=m1*x1+m2*x2+m3*x3+m4*x4+b					
y=9,403*x1+4,081*x2+2,117*x3-0,158*x4+183,025					

Table C.13 Lineer regression result of thickness section 14 with 9.48 mm, which was obtained by means of excel linest code.

C.E.V	O ppm	Mg/S	Temp.	Nod. %	Diesel Engine Code
4,52	0,3127	1,05	1278	24,11	6
4,29	0,4522	1	1164	30,16	7
4,36	0,405	1,15	1267	26,12	8
4,36	0,369	0,93	1152	38,34	9
4,27	0,1965	0,65	1217	28	12
4,45	0,1686	1	1234	23	13
4,42	0,1109	1	1168	29	14
4,43	0,384	0,8	1195	29	15
4,27	0,17	1,54	1220	26	16
4,2	0,272	0,92	1160	31	17
4,26	0,2652	1,1	1156	32	18
4,28	0,3196	0,76	1182	30	19
4,47	0,2162	1,33	1156	32,59	2
4,38	0,3926	1	1244	26,798	3
4,41	0,2286	0,81	1194	28,568	4
4,39	0,1839	0,82	1164	30,682	5
-0,078747116	0,253577411	11,3084794	2,489191	109,0936	
0,013948196	2,436982302	5,371076762	6,340987	26,63488	
0,771379849	2,046048194	#N/A	#N/A	#N/A	
9,278685972	11	#N/A	#N/A	#N/A	
155,3739427	46,04944532	#N/A	#N/A	#N/A	
X4	X3	X2	X1	b	
y=m1*x1+m2*x2+m3*x3+m4*x4+b					
y=2,489*x1+11,308*x2+0,253*x3-0,078*x4+109,094					